

AD-A100 334

PURDUE UNIV LAFAYETTE IND SCHOOL OF AERONAUTICS AND --ETC F/6 26/4  
FLUTTER ANALYSIS OF TWO-DIMENSIONAL AND TWO-DEGREE-OF-FREEDOM M--ETC(U)  
MAR 81 T Y YANG, A G STRIZ, P GURUSWAMY AFOSR-78-3523

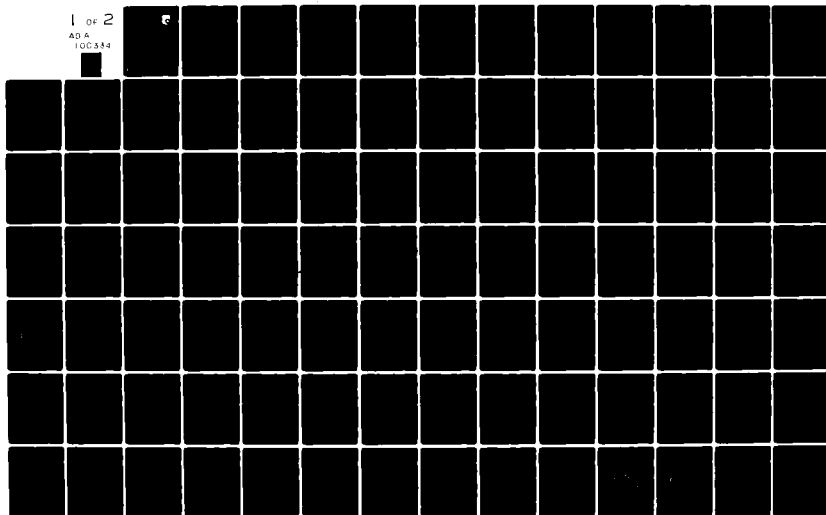
UNCLASSIFIED

AFWAL-TR-81-3004

NL

1 OF 2

AD A  
100334



AD A100334

AFWAL-TR-81-3004



FLUTTER ANALYSIS OF TWO-DIMENSIONAL AND TWO-DEGREE-OF-FREEDOM MBB A-3, CAST 7, AND TF-8A SUPERCRITICAL AIRFOILS IN SMALL-DISTURBANCE UNSTEADY TRANSONIC FLOW

T. Y. Yang  
A. G. Striz  
P. Guruswamy

Purdue University  
West Lafayette, Indiana 47907

March 1981

Final Report for period November 1979 - October 1980

Approved for public release; distribution unlimited.

FLIGHT DYNAMICS LABORATORY  
AIR FORCE WRIGHT AERONAUTICAL LABORATORIES  
AIR FORCE SYSTEMS COMMAND  
WRIGHT-PATTERSON AIR FORCE BASE, OHIO 45433

DTIC FILE COPY

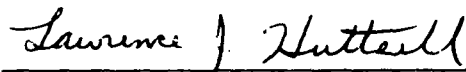
81 6 16 12P

NOTICE

When Government drawings, specifications, or other data are used for any purpose other than in connection with a definitely related Government procurement operation, the United States Government thereby incurs no responsibility nor any obligation whatsoever; and the fact that the government may have formulated, furnished, or in any way supplied the said drawings, specifications, or other data, is not to be regarded by implication or otherwise as in any manner licensing the holder or any other person or corporation, or conveying any rights or permission to manufacture use, or sell any patented invention that may in any way be related thereto.

This report has been reviewed by the Office of Public Affairs (ASD/PA) and is releasable to the National Technical Information Service (NTIS). At NTIS, it will be available to the general public, including foreign nations.

This technical report has been reviewed and is approved for publication.



LAWRENCE J. HUTTSELL  
Aerospace Engineer  
Aeroelastic Group



FREDERICK A. PICCHIONI, Lt Col, USAF  
Chief, Analysis & Optimization Branch  
Structures & Dynamics Division

FOR THE COMMANDER



RALPH KUSTER  
CHIEF

"If your address has changed, if you wish to be removed from our mailing list, or if the addressee is no longer employed by your organization please notify AFWAL/FIBRC, W-PAFB, OH 45433 to help us maintain a current mailing list".

Copies of this report should not be returned unless return is required by security considerations, contractual obligations, or notice on a specific document.

19 REPORT DOCUMENTATION PAGE		READ INSTRUCTIONS BEFORE COMPLETING FORM
1. REPORT NUMBER AFWAL-TR-81-3004	2. GOVT ACCESSION NO. AD-A200	3. RECIPIENT'S CATALOG NUMBER 334
4. TITLE (and Subtitle) Flutter Analysis of Two-Dimensional and Two-Degree-of-Freedom MBB A-3, CAST 7, and TF-8A Supercritical Airfoils in Small-Disturbance Unsteady Transonic Flow		5. TYPE OF REPORT & PERIOD COVERED 9 Final Report November 1979-October 1980
7. AUTHOR(s) T. Y. Yang, A. G. Striz, P. Guruswamy		6. PERFORMING ORG. REPORT NUMBER
9. PERFORMING ORGANIZATION NAME AND ADDRESS School of Aeronautics and Astronautics Purdue University West Lafayette, Indiana 47907		8. CONTRACT OR GRANT NUMBER(s) AFOSR-78-3523
11. CONTROLLING OFFICE NAME AND ADDRESS Air Force Wright Aeronautical Laboratories (FIBR) Wright-Patterson AFB, Ohio 45433		10. PROGRAM ELEMENT, PROJECT, TASK AREA & WORK UNIT NUMBERS PE 61102 F 239/N5/11
14. MONITORING AGENCY NAME & ADDRESS (if different from Controlling Office)		12. REPORT DATE 11 March 1981
		13. NUMBER OF PAGES 102
		15. SECURITY CLASS. (of this report) Unclassified
16. DISTRIBUTION STATEMENT (of this Report) Approved for public release, distribution unlimited.		15a. DECLASSIFICATION DOWNGRADING SCHEDULE
17. DISTRIBUTION STATEMENT (of the abstract entered in Block 20, if different from Report)		
18. SUPPLEMENTARY NOTES		
19. KEY WORDS (Continue on reverse side if necessary and identify by block number) Airfoils Flutter Supercritical Transonic Unsteady Aerodynamics		
20. ABSTRACT (Continue on reverse side if necessary and identify by block number) Flutter analyses at transonic Mach numbers are performed for three supercritical airfoils: (1) MBB A-3; (2) CAST 7; and (3) TF-8A wing section at the 65.3% semispan station. For all airfoils, two degrees of freedom, pitching and plunging, are considered. The unsteady aerodynamic data are obtained by using two separate transonic aerodynamic computational codes: (1) LTRAN2 based on the time integration method and (2) STRANS2 and UTRANS2 based on the harmonic analysis method.		

The steady aerodynamic results are shown in the form of upper and lower surface pressure curves. The unsteady aerodynamic coefficients are obtained for various values of low reduced frequencies by pitching the airfoils about the quarter chord axis. Unsteady results are presented as plots of unsteady coefficients versus angle of attack for the MBB A-3 airfoil and versus Mach number for the CAST 7 and TF-8A airfoils..

At design Mach number of 0.765, aerodynamic and corresponding flutter results are obtained for the MBB A-3 airfoil by both programs at various angles of attack. The angles of attack considered when using LTRAN2 are  $-0.2^\circ$ ,  $0.0^\circ$ ,  $0.2^\circ$ ,  $0.42^\circ$ ,  $0.6^\circ$ , and  $0.8^\circ$ , respectively, and those considered when using STRANS2/UTRANS2 are  $-0.4^\circ$ ,  $0.0^\circ$ ,  $0.42^\circ$ ,  $0.75^\circ$ ,  $1.0^\circ$ ,  $1.2^\circ$ , and  $1.3^\circ$ , respectively. Results are presented as curves of flutter speed and corresponding reduced frequency versus angle of attack for selected values of aeroelastic parameters. The effects of angle of attack on flutter speed obtained by the two programs are compared and discussed.

For the CAST 7 supercritical airfoil, aerodynamic and corresponding flutter results are obtained at zero mean angle of attack for various Mach numbers by using LTRAN2. The Mach numbers considered are 0.6, 0.625, 0.650, 0.675, 0.70, 0.71, and 0.72, respectively. Results are presented as curves of flutter speed and the corresponding reduced frequency versus Mach number for selected values of aeroelastic parameters. The transonic dip phenomenon is observed in all curves. The effect of each aeroelastic parameter on the curves is studied.

For the TF-8A wing section at 65.3% semispan, aerodynamic and corresponding flutter results are obtained at  $0.0^\circ$  and  $-3.0^\circ$  angle of attack for various Mach numbers by STRANS2/UTRANS2. The angle of attack  $-3.0^\circ$  of the present wing section corresponds to zero mean angle of attack of the zero-twist section of the wing in the wind tunnel experiment conducted by NASA. The Mach numbers considered are 0.70, 0.74, 0.76, 0.77, 0.78, 0.79, and 0.80, for  $\alpha = -3.0^\circ$ , and 0.70, 0.72, 0.74, 0.76, and 0.78 for  $\alpha = 0.0^\circ$ , respectively. Flutter results are presented in the form of curves of flutter speed and the corresponding reduced frequency versus Mach number for selected values of the aeroelastic parameters. The transonic dip phenomenon is more pronounced in the curves for  $-3.0^\circ$  local angle of attack. The effect of each aeroelastic parameter on the curves is studied and discussed.

# FOREWORD

This report was prepared by Professor T. Y. Yang of the School of Aeronautics and Astronautics of Purdue University under AFOSR Grant 78-3523 , "Application of Time-Accurate Transonic Aerodynamics to Aero-elastic Problems". The research was administered by Lawrence J. Huttshell of the Structures and Dynamics Division, Flight Dynamics Laboratory, Air Force Wright Aeronautical Laboratories, Wright-Patterson Air Force Base, Ohio.

The report covers work conducted from November 1979 to October 1980. T. Y. Yang was the principal investigator. P. Guruswamy and Alfred G. Striz were the graduate research assistants.

Accession	
NTIS	X
DTIC	
Uncl	
Spec	
Dist	
Dist	
Availability Codes	
Dist	Avail and/or Special
A	

## TABLE OF CONTENTS

SECTION	PAGE
I INTRODUCTION . . . . .	1
1. Development of Supercritical Airfoils . . . . .	1
2. Wind Tunnel Studies on Supercritical Airfoils . . . . .	4
3. Developments in Unsteady Transonic Aerodynamics . . . . .	6
4. Developments in Transonic Aeroelasticity of Supercritical Airfoils . . . . .	8
5. Scope of the Present Study . . . . .	10
a. Flutter Analysis of a MBB A-3 Supercritical Airfoil . . . . .	10
b. Flutter Analysis of a CAST 7 Supercritical Airfoil . . . . .	11
c. Flutter Analysis of a TF-8A Wing Section at the 65.3% Semispan Station . . . . .	12
II TRANSONIC FLOW EQUATIONS AND TWO COMPUTATIONAL METHODS . . . .	14
1. Unsteady Two-Dimensional Flow Equation for Transonic Flow . . . . .	14
2. Harmonic Method . . . . .	15
3. Time Integration Method . . . . .	16
4. Procedures for Obtaining Aerodynamic Data . . . . .	17
III AEROELASTIC AND TRANSFORMATION EQUATIONS . . . . .	19
1. Aeroelastic Equations of Motion . . . . .	19
2. Transformation of Aerodynamic Coefficients . . . . .	22
IV FLUTTER ANALYSIS OF A MBB A-3 SUPERCRITICAL AIRFOIL . . . . .	23
1. Airfoil Configuration . . . . .	23
2. Results based on LTRAN2 . . . . .	24
a. Steady Pressure Curves . . . . .	26

# TABLE OF CONTENTS (Continued)

SECTION	PAGE
b. Unsteady Aerodynamic Coefficients . . . . .	26
c. Flutter Results . . . . .	29
3. Results based on STRANS2/UTRANS2 . . . . .	38
a. Steady Pressure Curves . . . . .	40
b. Unsteady Aerodynamic Coefficients . . . . .	40
c. Flutter Results . . . . .	48
V FLUTTER ANALYSIS OF A CAST 7 SUPERCRITICAL AIRFOIL . . . . .	55
1. Airfoil Configuration . . . . .	55
2. Steady Pressure Curves . . . . .	57
3. Unsteady Aerodynamic Coefficients . . . . .	60
4. Flutter Results . . . . .	65
VI FLUTTER ANALYSIS OF A TF-8A WING SECTION . . . . .	74
1. Airfoil Configuration . . . . .	74
2. Steady Pressure Curves . . . . .	75
3. Unsteady Aerodynamic Coefficients . . . . .	78
4. Flutter Results . . . . .	87
VII CONCLUDING REMARKS . . . . .	97
REFERENCES . . . . .	100



# LIST OF ILLUSTRATIONS

FIGURE		PAGE
1	Definition of Parameters for Two-D.O.F. Aeroelastic System . . .	20
2	Airfoil Configuration for MBB A-3 . . . . .	25
3	Effect of Angle of Attack on Steady Pressure Curves for MBB A-3 Airfoil by LTRAN2 . . . . .	27
4	Effect of Angle of Attack on Lift Coefficient due to Plunging for MBB A-3 Airfoil by LTRAN2 . . . . .	30
5	Effect of Angle of Attack on Lift Coefficient due to Pitching for MBB A-3 Airfoil by LTRAN2 . . . . .	31
6	Effect of Angle of Attack on Moment Coefficient due to Plunging for MBB A-3 Airfoil by LTRAN2 . . . . .	32
7	Effect of Angle of Attack on Moment Coefficient due to Pitching for MBB A-3 Airfoil by LTRAN 2 . . . . .	33
8	Effect of Angle of Attack on Flutter Speed for Five Positions of Mass Center for MBB A-3 Airfoil by LTRAN2 . . . . .	35
9	Effect of Angle of Attack on Flutter Speed for Three Values of Airfoil-Air Mass Density Ratio for MBB A-3 Airfoil by LTRAN2 . . . . .	36
10	Effect of Angle of Attack on Flutter Speed for Two Values of Plunge-to-Pitch Frequency Ratio for MBB A-3 Airfoil by LTRAN2 . . . . .	37
11	Effect of Angle of Attack on Flutter Speed for Three Positions of Elastic Axis for MBB A-3 Airfoil by LTRAN2 . . . . .	39

# LIST OF ILLUSTRATIONS (Continued)

FIGURE		PAGE
12	Effect of Angle of Attack on Steady Pressure Curves for MBB A-3 Airfoil by STRANS2 . . . . .	41
13	Effect of Angle of Attack on Lift Coefficient due to Plunging for MBB A-3 Airfoil by UTRANS2 . . . . .	44
14	Effect of Angle of Attack on Lift Coefficient due to Pitching for MBB A-3 Airfoil by UTRANS2 . . . . .	45
15	Effect of Angle of Attack on Moment Coefficient due to Plunging for MBB A-3 Airfoil by UTRANS2 . . . . .	46
16	Effect of Angle of Attack on Moment Coefficient due to Pitching for MBB A-3 Airfoil by UTRANS2 . . . . .	47
17	Effect of Angle of Attack on Flutter Speed for Six Positions of Mass Center for MBB A-3 Airfoil by STRANS2/UTRANS2 . . . . .	49
18	Effect of Angle of Attack on Flutter Speed for Three Values of Airfoil-Air Mass Density Ratio for MBB A-3 Airfoil by STRANS2/UTRANS2 . . . . .	50
19	Effect of Angle of Attack on Flutter Speed for Two Values of Plunge-to-Pitch Frequency Ratio for MBB A-3 Airfoil by STRANS2/UTRANS2 . . . . .	52
20	Effect of Angle of Attack on Flutter Speed for Two Positions of Elastic Axis for MBB A-3 Airfoil by STRAN2/UTRANS2 . . . . .	53
21	Airfoil Configuration for CAST 7 . . . . .	56
22	Comparison between Steady Pressure Curves by LTRAN2 and Experiment for CAST 7 Airfoil . . . . .	58

# LIST OF ILLUSTRATIONS (Continued)

FIGURE		PAGE
23	Effect of Mach Number on Steady Pressure Curves for CAST 7 Airfoil by LTRAN2 . . . . .	59
24	Effect of Mach Number on Lift Coefficient due to Plunging for CAST 7 Airfoil by LTRAN2 . . . . .	62
25	Effect of Mach Number on Lift Coefficient due to Pitching for CAST 7 Airfoil by LTRAN2 . . . . .	63
26	Effect of Mach Number on Moment Coefficient due to Plunging for CAST 7 Airfoil by LTRAN2 . . . . .	64
27	Effect of Mach Number on Moment Coefficient due to Pitching for CAST 7 Airfoil by LTRAN2 . . . . .	65
28	Effect of Mach Number on Flutter Speed for Three Positions of Mass Center for CAST 7 Airfoil by LTRAN2 . . . . .	67
29	Effect of Mach Number on Flutter Speed for Three Values of Airfoil-Air Mass Density Ratio for CAST 7 Airfoil by LTRAN2 . . .	69
30	Effect of Mach Number on Flutter Speed for Two Values of Plunge-to-Pitch Frequency Ratio for CAST 7 Airfoil by LTRAN2 . . .	70
31	Effect of Mach Number on Flutter Speed for Two Positions of Elastic Axis for CAST 7 Airfoil by LTRAN2 . . . . .	71
32	Compensating Effects of $Re (C_{\ell\alpha})$ and the Position of Center of Pressure on Flutter Speed for CAST 7 Airfoil by LTRAN2 . . . .	73
33	Airfoil Configuration for TF-8A Wing Section at 65.3% Semispan Station . . . . .	76
34	Comparison between Steady Pressure Curves by STRANS2 and Experiment for TF-8A Airfoil . . . . .	77

# LIST OF ILLUSTRATIONS (Continued)

FIGURE		PAGE
35	Effect of Mach Number on Steady Pressure Curves for TF-8A Airfoil at $\alpha = -3.0^\circ$ by STRANS2 . . . . .	79
36	Effect of Mach Number on Steady Pressure Curves for TF-8A Airfoil at $\alpha = 0.0^\circ$ by STRANS2 . . . . .	80
37	Effect of Mach Number on Lift Coefficient due to Plunging for TF-8A Airfoil by UTRANS2 . . . . .	84
38	Effect of Mach Number on Lift Coefficient due to Pitching for TF-8A Airfoil by UTRANS2 . . . . .	85
39	Effect of Mach Number on Moment Coefficient due to Plunging for TF-8A Airfoil by UTRANS2 . . . . .	86
40	Effect of Mach Number on Moment Coefficient due to Pitching for TF-8A Airfoil by UTRANS2 . . . . .	87
41	Effect of Mach Number on Flutter Speed for Four Positions of Mass Center for TF-8A Airfoil by STRANS2/UTRANS2 . . . . .	89
42	Effect of Mach Number on Flutter Speed for Three Values of Airfoil - Air Mass Density Ratio for TF-8A Airfoil by STRANS2/ UTRANS2 . . . . .	91
43	Effect of Mach Number on Flutter Speed for Two Values of Plunge-to-Pitch Frequency Ratio for TF-8A Airfoil by STRANS2/ UTRANS2 . . . . .	92
44	Effect of Mach Number on Flutter Speed for Two Positions of Elastic Axis for TF-8A Airfoil by STRANS2/UTRANS2 . . . . .	94
45	Compensating Effects of $Re (C_{l\alpha})$ and the Position of Center of Pressure on Flutter Speed for TF-8A Airfoil by STRANS2/ UTRANS2 . . . . .	95

# LIST OF TABLES

TABLE		PAGE
1	Aerodynamic Coefficients for MBB A-3 Airfoil for Various Angles of Attack at $M = 0.765$ by LTRAN2 . . . . .	28
2	Aerodynamic Coefficients for MBB A-3 Airfoil for Various Angles of Attack at $M = 0.765$ by UTRANS2 . . . . .	43
3	Aerodynamic Coefficients for CAST 7 Airfoil for Various Mach Numbers at $\alpha = 0.0^\circ$ by LTRAN2 . . . . .	61
4	Aerodynamic Coefficients for TF-8A Airfoil for Various Mach Numbers at $\alpha = -3.0^\circ$ by UTRANS2 . . . . .	82
5	Aerodynamic Coefficients for TF-8A Airfoil for Various Mach Numbers at $\alpha = 0.0^\circ$ by UTRANS2 . . . . .	83

# NOMENCLATURE

$a_h$	- Distance between mid-chord and elastic axis in semi-chords, positive toward the trailing edge
[A]	- aerodynamic matrix
b	- semi-chord of the airfoil
c	- full chord of the airfoil
$C_l$	- steady lift coefficient
$C_m$	- steady moment coefficient
$C_{l_\delta}$	- lift coefficient due to plunging, positive upward
$C_{l_\alpha}$	- lift coefficient due to pitching, positive upward
$C_{m_\delta}$	- moment coefficient due to plunging, positive nose-up
$C_{m_\alpha}$	- moment coefficient due to pitching, positive nose-up
e	- position of center of pressure measured in chords from leading edge
$\eta$	- structural damping coefficient
$g_h$	- damping coefficient for plunging mode
$g_\alpha$	- damping coefficient for pitching mode
h	- plunging degree of freedom, positive downward
$I_\alpha$	- polar moment of inertia about elastic axis
$k_b$	- $\omega b/U$ , reduced frequency with respect to semi-chord length b
$k_c$	- $\omega c/U$ , reduced frequency with respect to full chord length c
$k_h$	- bending stiffness coefficient corresponding to plunging displacement
$k_\alpha$	- torsional stiffness coefficient corresponding to pitching rotation
[K]	- matrix of stiffness coefficients
m	- mass of airfoil per unit span
M or $M_\infty$	- free stream Mach number
[M]	- mass matrix
$Q_h$	- total aerodynamic lifting force
$Q_\alpha$	- total aerodynamic moment about pitching axis

# NOMENCLATURE (Continued)

$r_\alpha$	- $(I_\alpha/mb^2)^{1/2}$ , radius of gyration about elastic axis
$s$	- $(a_h - x_p)/2$
$S$	- airfoil static moment about elastic axis
$U$	- free stream velocity
$x_p$	- distance between mid-chord and pitching axis in semi-chords positive toward the trailing edge
$x_\alpha$	- $S/mb$ , distance between elastic axis and center of mass in semi-chords, positive toward the trailing edge
$\alpha$	- pitching degree of freedom, positive in nose-up direction
$\theta_1$	- phase angle between lift force and plunging displacement
$\theta_2$	- phase angle between lift force and pitching rotation
$\theta_3$	- phase angle between moment and plunging displacement
$\theta_4$	- phase angle between moment and pitching rotation
$\alpha_i$	- induced angle of attack
$\gamma$	- ratio of specific heats
$\delta$	- $h/c$
$\epsilon$	- unsteady perturbation parameter
$\lambda$	- flutter eigenvalue
$\mu$	- $m/\pi \rho b^2$ , airfoil-air mass density ratio
$\xi$	- $h/b$
$\rho$	- free stream air density
$\tau$	- ratio of airfoil thickness to chord length
$\phi$	- disturbance velocity potential
$\omega$	- flutter frequency of harmonic oscillation
$\omega_h$	- $(k_h/m)^{1/2}$ , uncoupled plunging frequency
$\omega_\alpha$	- $(k_\alpha/I_\alpha)^{1/2}$ , uncoupled pitching frequency
$\omega_r$	- reference frequency set equal to unity

## SECTION I

### INTRODUCTION

Over the last decade, one of the major emphasis of the research in airfoil technology has been on the analysis and design of supercritical airfoils. Such airfoils have proven to be more efficient than conventional airfoils, particularly in the transonic regime. In general, supercritical airfoils have higher drag rise Mach numbers and higher lift coefficients when compared to equivalent conventional airfoils.

Extensive theoretical and experimental studies have been conducted to prove that supercritical airfoils are aerodynamically more efficient than conventional airfoils. However, comparisons between the performance of these two types of airfoils based on aeroelastic studies have begun only recently. The purpose of this report is to study the flutter characteristics of supercritical airfoils in the transonic regime.

In this study, three supercritical airfoils were considered: (1) MBB A-3 airfoil designed by Messerschmitt-Bölkow-Blohm of the Federal Republic of Germany; (2) CAST 7 airfoil designed by Dornier GmbH of the Federal Republic of Germany; and (3) TF-8A wing section at the 65.3% semispan station designed by NASA.

#### 1. Development of Supercritical Airfoils

Early literature regarding the development of the concept of supercritical airfoils can be found in References 1 and 2. A brief report on



a recent flutter analysis of supercritical airfoils is given in Reference 3.

In Reference 4, Whitcomb discussed research conducted on supercritical airfoils at NASA. The salient aerodynamic features of supercritical airfoils were pointed out. Major advantages of these airfoils over the conventional airfoils were illustrated. Methods of incorporating supercritical airfoils in swept wings were discussed.

In Reference 5, Whitcomb discussed flight correlations for the F-8 supercritical wing configurations developed by NASA. Reasons for the differences between the flight and wind tunnel results for pitching moment, drag polars, drag rise, and pressure distribution for the F-8 wing were discussed. The primary differences were attributed to Reynolds number effects and wind tunnel-wall interference. It was stated that wall interference particularly influenced the transonic drag rise.

In Reference 6, Yu presented a transonic shock-free wing redesign procedure by using a fictitious gas method. The method was based on the full potential equation and local redesign of the wing surface geometry beneath the supersonic region to produce a shock-free flow. Results for a redesigned non-lifting rectangular wing and for a redesigned lifting wing of ONERA M6 planform were presented. A supercritical wing configuration obtained by this method showed significant drag reduction and improved lift-drag characteristics.

A detailed description of the design and analysis of supercritical wing sections was given by Bauer, Garabedian, and Korn in References 7, 8, and 9 with Jameson being another author in Reference 8. In Reference 7.

the authors presented a mathematical theory based on the finite difference scheme for the design of supercritical wing sections. They presented a computer program for the analysis and also illustrated the method by examples. Several shockless airfoils were designed and tested in the wind tunnel. Their theoretical results established satisfactory agreement with the experimental results.

In Reference 8, the work carried out in Reference 7 was modified and was presented in a more definitive form. The authors improved the design of the trailing edge by which a lift increase of 15 to 20 percent was obtained. The improved method had provision to handle supersonic as well as subsonic free stream Mach numbers, and to capture the shock wave as far back on an airfoil as required. Moreover, the method led to an effective three-dimensional program for the computation of transonic flows past an oblique wing. Detailed comparisons were made with experimental data. The comparisons were favorable.

The work presented in Reference 9 was a sequel to the two earlier References (7 and 8). New mathematical techniques for the design and analysis of a supercritical airfoil were incorporated into the computer code. The advanced mathematical approach made it possible to assign the pressure as a function of the arc length and then obtain a shockless airfoil that nearly achieves the desired distribution of pressure. This tool enabled them to design families of transonic airfoils more easily both for airplane wings and for compressor blades in cascades.

The iterative process employed in Reference 9 can be summarized as follows: (1) The airfoil is prescribed and mapped onto the unit circle. The free stream Mach number is specified and either the coefficient of lift

or the angle of attack can be prescribed; (2) The flow calculations are executed for a fixed number of cycles; (3) A boundary layer correction is computed and added to the original airfoil to give a new profile; and (4) The profile is mapped onto the unit circle. Steps 2 through 4 are repeated till a satisfactory profile is obtained. The authors illustrated the method with examples. Results compare well with those obtained from experiment.

## 2. Wind Tunnel Studies on Supercritical Airfoils

Many of the supercritical airfoils designed have been tested in the wind tunnel for aerodynamic performance. Some of these wind tunnel tests are discussed in this section.

In Reference 10, Bucciantini, Oggiano, and Onorato conducted wind tunnel tests on the MBB A-3 supercritical airfoil. Steady state surface pressure distributions, wake and boundary layer measurements were obtained in two different wind tunnels by using the same model. The chord length and span of the model were equal to 0.127 meters and 0.203 meters, respectively. Several Mach numbers between 0.751 and 0.855 and several angles of attack between  $1.12^\circ$  and  $4.18^\circ$  were considered. Results were presented in the form of steady pressure distributions. Measured values of the lift and moment coefficients about the quarter chord axis were also presented. These results can serve as an experimental data base for comparison with computational results for the MBB A-3 airfoil.

In Reference 11, Stanewsky, Puffert, Müller, and Bateman presented wind tunnel test results for the CAST 7 supercritical airfoil. Steady state surface pressure distributions, wake and boundary layer measurements were obtained in three independent wind tunnels. Several Mach numbers

between 0.4 and 0.8 and several angles of attack between  $-2.0^\circ$  and  $+5.0^\circ$  were considered. Results were presented in the form of steady pressure curves. Measured values of drag, lift and moment coefficients, and boundary layer thickness were also given. These results can serve as an experimental data base for comparison with computational results for the CAST 7 airfoil.

In Reference 12, Harris and Bartlett conducted wind tunnel experiments on a NASA supercritical wing research airplane model. Experiments were conducted at the NASA-Langley 8-foot transonic pressure tunnel with Mach numbers ranging from 0.25 to 1.00. They measured the steady aerodynamic load distributions over the wing and rear fuselage of the model with and without fuselage area-rule additions. Pressure measurements over the surface of the area-rule additions at sideslip angles of approximately  $-5^\circ$ ,  $0^\circ$ , and  $5^\circ$  were also included.

In Reference 13, Davis and Malcolm obtained experimental unsteady aerodynamic results for a conventional and a supercritical airfoil. The two airfoils were NACA 64A010, a 10% thick airfoil of conventional shape, and NLR 7301, a 16.5% thick supercritical airfoil. Results were obtained for four conditions: (1) conventional airfoil in transonic flow with weak normal shock; (2) conventional airfoil in transonic flow with stronger shock; (3) supercritical airfoil at experimentally determined shock-free design condition; and (4) supercritical airfoil at off-design condition with stronger shock. Measured chordwise unsteady pressure time-histories for the four conditions were compared. It was concluded that although an oscillating supercritical airfoil excites more harmonics, the strength of the airfoil shock is the more important parameter governing

the complexity of the unsteady flow. Whether they are conventional or supercritical, it was found that airfoils which support weak shocks induce unsteady loads that are qualitatively predictable with classical theories. It was also found that flows with strong shocks are sensitive to details of the shock and boundary-layer interaction and cannot be adequately predicted. Results presented can provide as a comparative basis for those obtained by the new generation of Navier-Stokes-type codes.

### 3. Developments in Unsteady Transonic Aerodynamics

Due to the fast growth of digital computers, advances in the numerical computational methods of a transonic flow field around oscillating two-dimensional airfoils have been extensive. Many computer programs have been developed based on these methods. A bibliography of these developments was given by Borland in Reference 14. It was observed in References 15 and 3 that both the computer programs STRANS2 and UTRANS2 developed by Traci, Albano, and Farr (Reference 16) and the LTRAN2 developed by Ballhaus and Goorjian (Reference 17) can be efficiently used to obtain unsteady transonic aerodynamic data for conventional and supercritical airfoils.

The computer programs STRANS2 and UTRANS2 use a harmonic analysis method to solve the two-dimensional, moderate-frequency, small-disturbance transonic equations. The unsteady aerodynamic equations are linearized with respect to time. Thus, the unsteady solution is treated as a small linear perturbation over a nonlinear steady state solution. The position of the shock is fixed at the steady state position throughout the analysis. In these programs, both steady and unsteady aerodynamic equations are solved by a mixed differencing line relaxation procedure.

On the other hand, the computer program LTRAN2 is based on the time integration method. This program solves the two-dimensional, low-frequency, small-disturbance transonic equation. The solution for the steady part is obtained by successive line over-relaxation method (SLOR). The solution for the unsteady part is obtained by an alternating-direction implicit finite difference algorithm. In this program, the shock is allowed to move during the unsteady analysis.

In Reference 18, Houwink and Van der Vooren modified LTRAN2 by extending the program for high frequency computations. High frequency terms were added to boundary conditions and pressure computations. However, the same basic low frequency potential equation used in LTRAN2 was again considered. Modifications showed improvements on the results obtained for a flat plate at  $M = 0.7$ . For the case of the harmonic pitching oscillation of a NACA 64A006 airfoil and a reduced frequency of 0.8 based on full chord, they found significant differences relative to the LTRAN2 results. However, these results have not been compared with other transonic codes.

Recently, Rizzetta and Yoshihara (Reference 19) developed an unsteady transonic code ExTRAN2 which does not have any low frequency assumptions. High frequency terms were retained in potential equation, boundary conditions, and pressure computations. Viscous effects were incorporated in the program by using a viscous ramp method. Unsteady pressure and coefficients were computed for a NACA 64A010 airfoil at  $M = 0.80$ . It was shown that these results compared favorably with those reported in Reference 18. Also the boundary conditions play a more important role than does the differential equation in obtaining unsteady aerodynamic coefficients. In addition, viscous interaction was found to have the expected important effects.

#### 4. Developments in Transonic Aeroelasticity of Supercritical Airfoils

Based on the steady aerodynamic data, the supercritical airfoils have proven to be more efficient than conventional airfoils in the transonic regime. However, it is of more practical interest to compare the unsteady aerodynamic data between the two types of airfoils. In that case, aeroelastic characteristics of the two types of airfoils can be studied and compared and more useful conclusions can be drawn. Studies of the aeroelastic characteristics of supercritical airfoils have begun recently. A short review of the work of Farmer and Hanson (Reference 20), McGrew et al. (Reference 21), and Ashley (Reference 22) was given by the authors in Reference 23.

In Reference 3 and 23, the present authors have investigated the flutter characteristics of a MBB A-3 supercritical airfoil. This airfoil is one of the AGARD standard airfoils suggested for aeroelastic applications of transonic unsteady aerodynamics (Reference 24). Results presented in References 3 and 23 are briefly discussed here.

The steady aerodynamic results were obtained by both STRANS2 and LTRAN2 in the form of pressure plots on upper and lower surfaces. The unsteady results were obtained by UTRANS2 (harmonic method) and LTRAN2 (time integration method) in the form of lift and moment aerodynamic coefficients at various values of reduced frequency.

The study was first conducted by considering a case at design Mach number of 0.765 and zero mean angle of attack. Two parallel sets of results for steady pressure distributions, unsteady aerodynamic coefficients, and

flutter speed curves were obtained by simultaneously using the two separate computer programs. The two sets of results were in good agreement.

The design conditions of the MBB A-3 supercritical airfoil are:  $M = 0.765$ , angle of attack  $\alpha = 1.3^\circ$ , and steady lift coefficient  $C_L = 0.58$ . From the steady pressure computations, it was found that at the design Mach number of 0.765 the angles of attack required to produce the design lift coefficient of 0.58 were  $0.75^\circ$  and  $0.42^\circ$  by STRANS2 and LTRAN2, respectively. Hence, flutter analyses were performed separately by using angles of attack of  $0.75^\circ$  and  $0.42^\circ$  for the two respective computer programs. Results were obtained and discussed in a fashion similar to that performed in the case of zero mean angle of attack. Based on the specific values assumed for the aeroelastic parameters, it was concluded that the MBB A-3 supercritical aeroelastic system is, in general, more stable at the equivalent design angles of attack than at zero angle of attack.

In order to study the effect of camber on flutter results, a MBB A-3 airfoil without camber was considered. Flutter analyses were performed for design Mach number of 0.765 and at angles of attack of  $0.75^\circ$  and  $0.42^\circ$  for STRANS2/UTRANS2 and LTRAN2, respectively. The results showed that the camber has a beneficial effect in increasing the flutter speeds.

A parallel set of results was also obtained for a NACA 64A010 conventional airfoil scaled down to the same maximum thickness-to-chord ratio (8.9%) as that of the MBB A-3 supercritical airfoil. The aerodynamic and flutter results were compared with those obtained for the MBB A-3 supercritical airfoil, with and without camber. It was found that the scaled down NACA 64A010 airfoil gives aerodynamic and flutter results almost identical to those for the MBB A-3 airfoil without camber.



In order to investigate the effect of Mach number, flutter analysis was also carried out for the MBB A-3 supercritical airfoil at five different Mach numbers: 0.7, 0.72, 0.74, 0.765, and 0.78. The angle of attack was assumed to be zero. Flutter curves were presented as plots of flutter speed and the corresponding reduced frequency versus Mach number for various values of different aeroelastic parameters. The "transonic dip" phenomenon was observed and the comparisons of the curves by the two computer programs were favorable.

## 5. Scope of the Present Study

In this study, flutter analysis was conducted for three supercritical airfoils: (1) MBB A-3; (2) CAST 7; and (3) TF-8A. Aerodynamic computations for MBB A-3 were carried out by both the STRANS2/UTRANS2 and LTRAN2 transonic codes simultaneously. On the other hand, aerodynamic computations for CAST 7 and TF-8A were carried out separately by LTRAN2 and STRANS2/UTRANS2, respectively. For all the airfoils, two degrees of freedom, pitching and plunging, were considered.

Four aeroelastic parameters were considered in this analysis: (1) airfoil-air mass density ratio; (2) plunge-to-pitch frequency ratio; (3) position of the mass center; and (4) position of the elastic axis.

### a. Flutter Analysis of a MBB A-3 Supercritical Airfoil

This study is a sequel to the study reported by the authors in Reference 3. Here, the effect of angle of attack on flutter speed was studied.

7

The steady aerodynamic results were obtained by both STRANS2 and LTRAN2 in the form of pressure plots on upper and lower surfaces. The unsteady results were obtained by UTRANS2 and LTRAN2 in the form of lift and moment coefficients at various values of reduced frequency.

Because of the different limitations of the two programs, separate values of angle of attack were considered for the two programs. For LTRAN2, six angles of attack between  $-0.2^\circ$  and  $0.8^\circ$  were considered, whereas for STRANS2/UTRANS2, seven angles of attack between  $-0.4^\circ$  and  $1.3^\circ$  were considered.

Based on the two sets of aerodynamic coefficients obtained for various angles of attack, flutter analyses of the MBB A-3 airfoil were conducted. The effect of angle of attack on flutter speed was studied for various values of the four aeroelastic parameters. Results obtained by the two programs are compared and discussed.

#### b. Flutter Analysis of a CAST 7 Supercritical Airfoil

The purpose of this study was to investigate the flutter characteristics of a CAST 7 supercritical airfoil. This configuration is one of the AGARD standard airfoils suggested for aeroelastic applications of transonic unsteady aerodynamics (Reference 24).

The steady and unsteady aerodynamic results were obtained by LTRAN2. Seven Mach numbers between 0.6 and 0.72 were considered at zero angle of attack. The steady results are presented in the form of plots of pressure curves on upper and lower surfaces. The unsteady results are presented as plots of the magnitudes of the unsteady coefficients and the corresponding phase angles versus Mach number.

Based on the unsteady aerodynamic coefficients obtained for various Mach numbers, flutter analysis of the CAST 7 airfoil was conducted. The effect of Mach number on flutter speed was studied for various values of the four aeroelastic parameters. Curves of flutter speed versus Mach number were plotted. The transonic dip phenomenon similar to that obtained for the NACA 64A006 airfoil (Reference 25) and the MBB A-3 airfoil (Reference 3) was observed.

c. Flutter Analysis of a TF-8A Wing Section at the 65.3% Semispan Station

The purpose of this study was to investigate flutter characteristics of a TF-8A wing section at the 65.3% semispan station. This wing was designed by NASA and its configuration was given in Reference 26. Based on experimental data, transonic flutter studies on this wing were carried out in References 20, 21, and 22.

During wind tunnel tests on the TF-8A wing (Reference 26) it was noticed that because of twist, the angle of attack at the 65.3% semispan station was  $-3.0^\circ$ . This corresponded to a zero angle of attack of the zero-twist section of the wing. Based on the wind tunnel data given in Reference 26, the transonic dip phenomenon was found for the TF-8A wing section in Reference 22. Hence, the present flutter analysis for the TF-8A wing section was performed at a mean angle of attack equal to  $-3.0^\circ$  as well as zero degrees.

The steady and unsteady aerodynamic data were obtained by STRANS2 and UTRANS2, respectively. Seven Mach numbers between 0.70 and 0.80 were considered for the airfoil at  $-3.0^\circ$  mean angle of attack and five Mach numbers

7

between 0.70 and 0.78 were considered for the airfoil at zero mean angle of attack. Steady state results are presented in the form of pressure curves on the upper and lower surfaces. Unsteady results are presented as plots of magnitudes of unsteady coefficients and corresponding phase angles versus Mach numbers.

Based on the unsteady aerodynamic coefficients obtained for these Mach numbers at the two angles of attack, flutter analysis of the TF-8A wing section was conducted. The effect of Mach number on flutter speed was studied for various values of the four aeroelastic parameters. Curves of flutter speed and corresponding reduced frequency versus Mach number were plotted. The transonic dip phenomenon was observed.

## SECTION II

### TRANSONIC FLOW EQUATIONS AND TWO COMPUTATIONAL METHODS

Developments of numerical procedures for obtaining practical solutions for the unsteady flow around two-dimensional airfoils have been extensive. A number of solution procedures have led to successful transonic codes. The computer codes based on time integration method and harmonic method are two among them. In this section the aerodynamic equations employed in the two codes are discussed.

#### 1. Unsteady Two-Dimensional Flow Equation for Transonic Flow

The simplified basic aerodynamic equation, following the assumptions that the flow is two-dimensional, inviscid, transonic ( $M_\infty \approx 1$ ), and that the velocity disturbances are small compared to the free stream velocity  $U$ , can be deduced from the general equation of continuity of gas dynamics as

$$k_c^2 M_\infty^2 \phi_{tt} + 2k_c M_\infty^2 \phi_{xt} = V_c \phi_{xx} + \phi_{yy} \quad (1)$$

where  $k_c = \omega c/U$  is the reduced frequency;  $M_\infty$  is the free stream Mach number;  $\phi$  is the disturbance velocity potential;  $V_c = 1 - M_\infty^2 - (\gamma + 1)M_\infty^m \phi_x$ ;  $m$  is a function of  $M_\infty$ ; and  $\gamma$  is the ratio of specific heats.

In deriving the above equation, the coordinate system is fixed with respect to the airfoil, and  $x$  is aligned with the free stream direction. The flow is defined as locally subsonic or supersonic, relative to the fixed

coordinate system, for  $V_c > 0$  or  $V_c < 0$ , respectively. A measure of the degree of unsteadiness is given by the reduced frequency  $k_c$  when the airfoil is oscillating periodically with a frequency  $\omega$ .

Several numerical approaches have been developed for the solution of transonic flow fields governed by Equation 1.

## 2. Harmonic Method

In the harmonic method it is assumed that the flow field for some sinusoidal body motion of frequency  $\omega$  can be expressed in the form

$$\phi(x,y,t) = \phi_0(x,y) + \epsilon \phi_1(x,y)e^{i\omega t} + \epsilon^2 \phi_2(x,y)e^{i\omega t} + \text{higher-order terms} \quad (2)$$

where  $\phi$  is the disturbance velocity potential, and  $\epsilon$  is related to the amplitude of body motion. For purely subsonic or supersonic flows, the sinusoidal motion produces a sinusoidal response  $\phi$  at the same frequency and all higher-order terms are zero. This is not true in the transonic case, in which a higher harmonic content in  $\phi$  results because the governing equations are nonlinear. However, if the amplitudes of motion are assumed to be very small ( $\epsilon \ll 1$ ), terms of order  $\epsilon^2$  or higher can still be neglected. Hence, Equation 2 can be simplified as

$$\phi(x,y,t) = \phi_0(x,y) + \epsilon \phi_1(x,y)e^{i\omega t} \quad (3)$$

In Equation 3, the solution for  $\phi_1$  depends on the mean steady-state solution  $\phi_0$ . In this equation, it is implied that the unsteady solution is a small linear perturbation about some nonlinear steady state solution. In other words, the unsteady solution is linearized with respect to time.

Equation 3 has the advantage that  $\phi_1$  can be computed using essentially the same well-known finite-difference relaxation algorithms used to compute the mean steady state solution  $\phi_0$ . Based on this approach, Traci et al. (Reference 16) developed computer programs STRANS2 and UTRANS2 that can solve the steady and unsteady aerodynamic equations, respectively. Because of the elliptic/hyperbolic characteristic of the governing equations for the steady and unsteady perturbation velocity potentials, the mixed differencing line relaxation procedure of Murman and Cole was used for steady and unsteady computations. These programs are used in the present report to compute aerodynamic data for flutter analysis.

### 3. Time Integration Method

In the harmonic method, a time linearized assumption is used to obtain the unsteady solution. Such method constrains the shock wave to its steady-state position. As an alternative and more complete solution, Ballhaus and Goorjian (Reference 17) proposed to use the time integration method to obtain an unsteady transonic solution. In this method, the shock movements can accurately be treated. Also, there is no need to linearize the aerodynamic equations with respect to time in the unsteady part.

As a further simplification of Equation 1, the frequency of the transonic flow can be assumed as low so that  $k_c \approx 1 - M_\infty^2 \approx \tau^{2/3} \ll 1$ . Equation 1 may then be reduced to

$$2k_c M_\infty^2 \phi_{xt} = V_c \phi_{xx} + \phi_{yy} \quad (4)$$

where  $\tau$  is the thickness-chord ratio of the airfoil.

Equation 4 is suitable for the time integration approach. This approach is based on the finite-difference scheme that integrates Equation 2 in time for harmonic aerodynamic motions until the transient states in the solution disappear and the forces become periodic.

Several numerical procedures are available to solve Equation 4. Among them the procedure developed by Ballhaus and Goorjian (Reference 17) based on the alternate-direction implicit algorithm has been proven to be computationally efficient and is being widely used. This procedure uses a conservative, implicit finite-difference scheme to time-accurately integrate the nonlinear, low-frequency, transonic small-disturbance equation as defined in Equation 4. A computer code LTRAN2 was developed based on this procedure. This code can be used to find the flow field solutions for airfoils with arbitrary combinations of pitch, plunge, and flap deflections.

In order to comply with the low-frequency approximation of LTRAN2, the unsteady aerodynamic coefficients were computed for a reduced frequency range  $k_c \leq 0.2$ .

Although UTRANS2 retains the  $\phi_{tt}$ -term, it experiences numerical instability difficulty at higher reduced frequencies. Hence, in this study the reduced frequencies considered for UTRANS2 were also limited to the range  $k_c \leq 0.2$ .

#### 4. Procedures for Obtaining Aerodynamic Data

A description of the procedures for obtaining steady and unsteady aerodynamic data by using both LTRAN2 and STRANS2/UTRANS2 was given in detail in Section IV of Reference 3. The reader is thus referred to that reference.

In that section, the sizes and patterns of the finite difference meshes at various stages of computation, distributions of gridpoints near airfoils,



size and number of time steps required for convergence in integration method, relaxation parameters and convergence tolerances in relaxation method, and relevance of all these parameters to computer capacity, computing time, and accuracy were discussed in detail.

### SECTION III

#### AEROELASTIC AND TRANSFORMATION EQUATIONS

In the present flutter analysis, the airfoil is assumed to oscillate about the elastic axis with two degrees of freedom, plunge and pitch. The necessary aeroelastic equations of motion and the transformation equations for aerodynamic coefficients are discussed in this section.

##### 1. Aeroelastic Equations of Motion

The parameters and sign conventions for a typical airfoil oscillating with pitching and plunging degrees of freedom are defined in Figure 1. The following assumptions are made in deriving the equations:

- a. The displacement  $h$  and rotation  $\alpha$  are measured with respect to the mean position defined by the steady state conditions.
- b. The airfoil is rigid.
- c. The amplitudes of oscillation are small.
- d. The principle of superposition for aerodynamic forces is valid even in the presence of shocks. Discussion and justification of this assumption were given in References 27 and 28.

Assuming harmonic oscillations with flutter frequency  $\omega$ , the final eigenvalue equations for flutter analysis are

$$[\mu k_b^2 [M] - [A]] \begin{Bmatrix} \xi_0 \\ \alpha_0 \end{Bmatrix} = \lambda [K] \begin{Bmatrix} \xi_0 \\ \alpha_0 \end{Bmatrix} \quad (5)$$

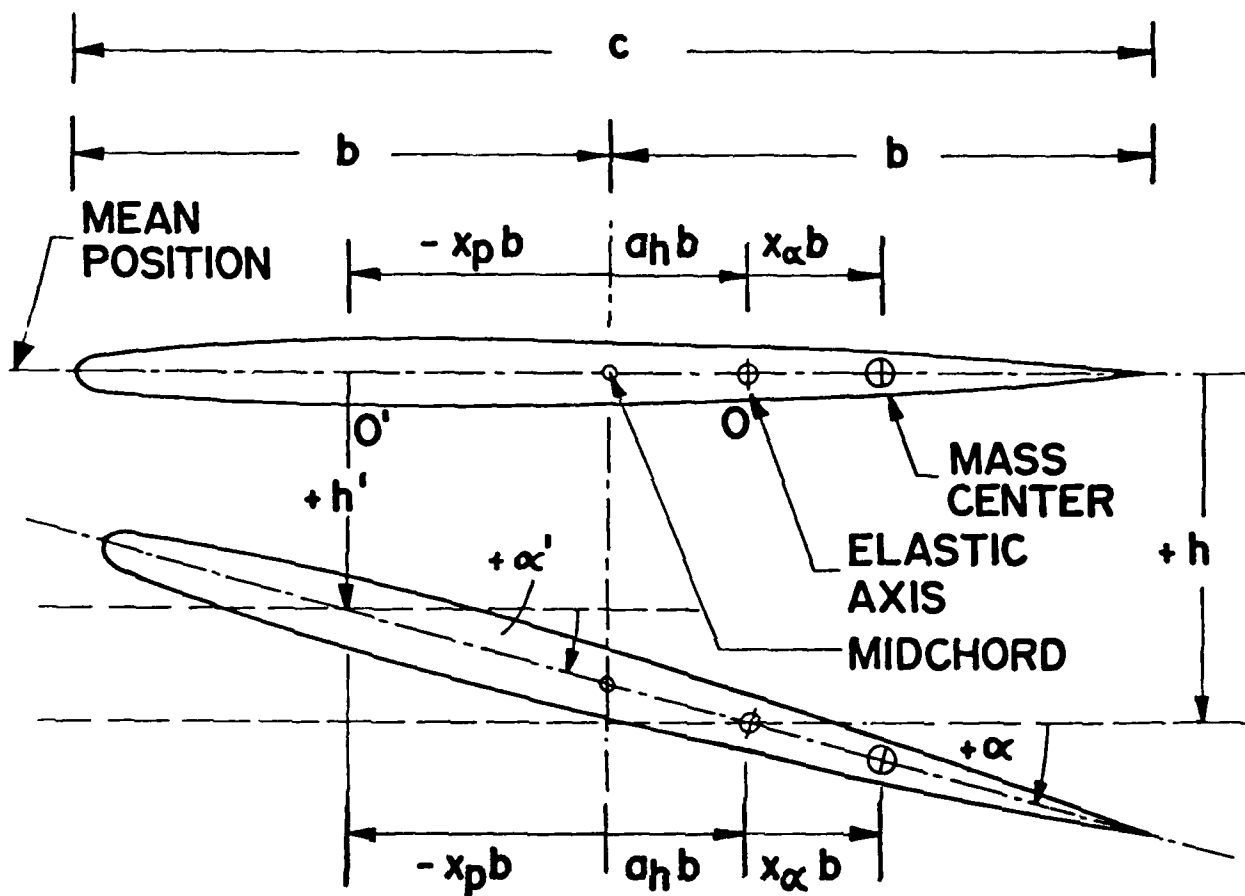


Figure 1. Definition of Parameters for Two-D.O.F. Aeroelastic System.

where  $\xi_0$  and  $\alpha_0$  are the nondimensional amplitudes in plunge and pitch oscillations, respectively;  $\mu = m/\pi\rho b^2$ , the airfoil-air mass density ratio;  $k_b = \omega b/U$ , the reduced frequency.

The matrices  $[M]$ ,  $[A]$ , and  $[K]$  are defined as

$$[M] = \left[ \begin{array}{c|c} 1 & x_\alpha \\ \hline x_\alpha & r_\alpha^2 \end{array} \right] \quad (6a)$$

$$[A] = \frac{1}{\pi} \left[ \begin{array}{c|c} C_{\ell\delta}/2 & C_{\ell\alpha} \\ \hline -C_{m\delta} & -2C_{m\alpha} \end{array} \right] \quad (6b)$$

$$[K] = \left[ \begin{array}{c|c} (\omega_h/\omega_r)^2 & 0 \\ \hline 0 & r_\alpha^2 (\omega_\alpha/\omega_r)^2 \end{array} \right] \quad (6c)$$

The eigenvalue  $\lambda$  is a complex number defined as

$$\lambda = \mu(1 + ig)\omega_r^2 b^2 / U^2 \quad (7)$$

where  $g = g_h = g_\alpha$  is the structural damping coefficient which is assumed to be small and of the same order for both plunging and pitching modes.

The flutter solution is obtained when  $g$  is found to be zero. In the transonic flutter analysis, to compute the aerodynamic coefficients for Equation 6b comprises the essential task.

## 2. Transformation of Aerodynamic Coefficients

In some situations, the aerodynamic coefficients originally obtained with reference to a pitching axis need to be transformed to those with reference to the elastic axis for aeroelastic analysis. The transformation relations can be derived by using the principle of superposition of airloads.

Let it be assumed that the aerodynamic coefficients  $C'_{\ell\delta}$ ,  $C'_{\ell\alpha}$ ,  $C'_{m\delta}$ , and  $C'_{m\alpha}$  for point  $O'$  (see Figure 1) due to pitching about  $O'$  have been obtained. It is desired to transform these coefficients to be  $C_{\ell\delta}$ ,  $C_{\ell\alpha}$ ,  $C_{m\delta}$ , and  $C_{m\alpha}$  for another pitching axis (elastic axis)  $O$ .

Assuming rigid airfoil and small amplitude of oscillations, the transformation relationships may be written as

$$\begin{aligned}C_{\ell\delta} &= C'_{\ell\delta} \\C_{\ell\alpha} &= C'_{\ell\alpha} - (sC'_{\ell\delta}) \\C_{m\delta} &= C'_{m\delta} + sC'_{\ell\delta} \\C_{m\alpha} &= C'_{m\alpha} + sC'_{\ell\alpha} - (sC'_{m\delta}) - (s^2C'_{\ell\delta})\end{aligned}\tag{8}$$

where  $s = (a_h - x_p)/2$ . The three terms in the parentheses are relatively small when compared with the other terms. If they are neglected, Equations 8 are in the form as those given previously by Traci et al. in Reference 16.

## SECTION IV

### FLUTTER ANALYSIS OF A MBB A-3 SUPERCRITICAL AIRFOIL

This study is a sequel to the investigation reported by the authors in Reference 3. The effect of angle of attack on flutter speed of the MBB A-3 supercritical airfoil was studied at design Mach number 0.765.

Aerodynamic data were obtained by both LTRAN2 and STRANS2/UTRANS2. The airfoil was assumed to oscillate with two degrees of freedom, plunge and pitch, about the elastic axis.

Because of the different limitations of the two programs, separate values of angle of attack were considered, respectively. For LTRAN2, six angles of attack between  $-0.2^\circ$  and  $0.8^\circ$  were considered. For STRANS2/UTRANS2, seven angles of attack between  $-0.4^\circ$  and  $1.3^\circ$  were considered.

Based on the two sets of aerodynamic data obtained, flutter analysis of the MBB A-3 airfoil was conducted. The effect of angle of attack on flutter speed was studied for selected values of four different aeroelastic parameters. Results obtained by the two programs are compared and discussed.

Throughout this study, the values for radius of gyration  $r_\alpha$  and reference frequency  $\omega_p$  were assumed as 0.5 and 1.0, respectively.

#### 1. Airfoil Configuration

In order to perform accurate aerodynamic computations, it is necessary to use accurate data for the airfoil configurations, especially in the region of

the leading edge. The equations for one-segment fitting of eight AGARD/SMP standard airfoil configurations were provided by Dr. J. J. Olsen of the Flight Dynamics Laboratory (Reference 24).

$$\begin{aligned}
 Z_u(x) &= c(x) + 0.5 t(x) \\
 Z_l(x) &= c(x) - 0.5 t(x) \\
 t(x) &= a_0 \sqrt{x} + a_1 + a_2 x + a_3 x^2 + a_4 x^3 + a_5 x^4 \\
 c(x) &= b_1 + b_2 x + b_3 x^2 + b_4 x^3 + b_5 x^4
 \end{aligned} \tag{9}$$

where  $Z_u(x)$  and  $Z_l(x)$  are the equations for the upper and lower surfaces, respectively;  $x$  is the nondimensional axis with leading edge at  $x = 0$  and trailing edge at  $x = 1$ ;  $c(x)$  is the camber; and  $t(x)$  is the thickness. Reference 24 also gives two-segment fitting functions which would be necessary for more precise description of the geometry.

The coefficients for the thickness function for the MBB A-3 airfoil are:  $a_0 = 0.2457807$ ;  $a_1 = 0$ ;  $a_2 = -0.2470393$ ;  $a_3 = 0.5556936$ ;  $a_4 = -1.1377743$ ; and  $a_5 = 0.5833393$ . The coefficients for the camber function are:  $b_1 = 0$ ;  $b_2 = 0.1294408$ ;  $b_3 = -0.4206819$ ;  $b_4 = 0.5516741$ ; and  $b_5 = -0.2604330$ . A plot of this configuration is given in Figure 2.

The maximum thickness-to-chord ratio of this airfoil is 8.9%. It has a blunter nose than equivalent conventional airfoils (Reference 3).

## 2. Results Based on LTRAN2

Aerodynamic data were obtained by the time integration program LTRAN2 for the MBB A-3 airfoil at design Mach number 0.765. The values for mean

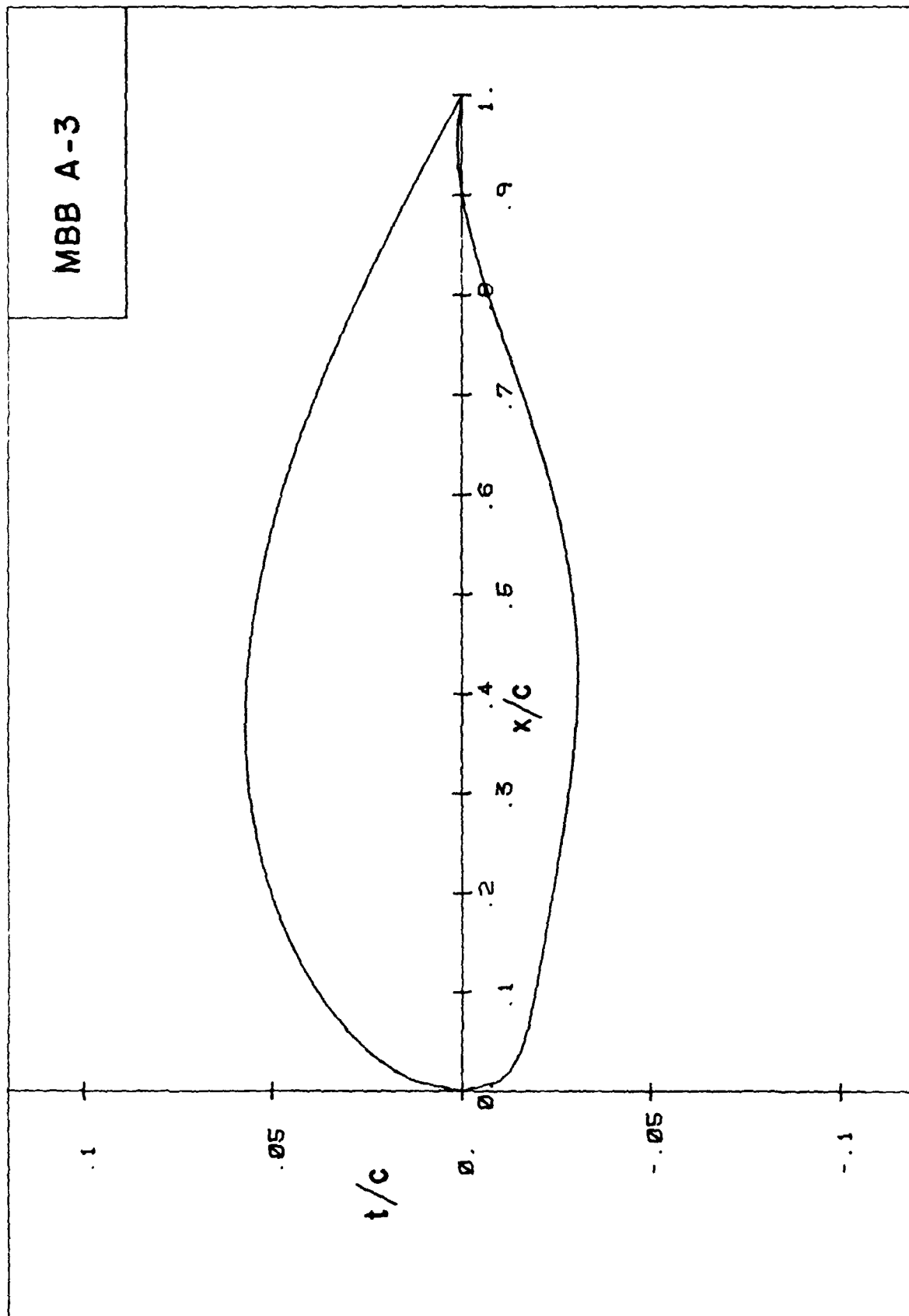


Figure 2. Airfoil Configuration for MBB A-3.



angle of attack considered were  $-0.2^\circ$ ,  $0.0^\circ$ ,  $0.2^\circ$ ,  $0.42^\circ$ ,  $0.6^\circ$ , and  $0.8^\circ$ , respectively, where  $0.42^\circ$  corresponds to the equivalent design angle of attack that yields the design lift coefficient of 0.58 (Reference 3).

#### a. Steady Pressure Curves

Figure 3 shows the steady pressure distributions on the upper and lower surfaces for the MBB A-3 airfoil for seven mean angles of attack obtained by the successive line over relaxation method of LTRAN2.

The pressure curves of the upper surface are seen to move upward with the increase in angle of attack whereas the pressure curves of the lower surface move downward with the increase in angle of attack. Shocks are seen to exist for all angles of attack. The shock moves toward the trailing edge with increasing strength as the angle of attack is increased.

From the nature of the changes in the steady pressure curves it can be expected that both lift and moment coefficients increase as the angle of attack increases.

#### b. Unsteady Aerodynamic Coefficients

Four unsteady aerodynamic coefficients,  $C_{l\delta}$ ,  $C_{l\alpha}$ ,  $C_{m\delta}$ , and  $C_{m\alpha}$ , were obtained by pitching the airfoil about the quarter chord axis at  $M = 0.765$ . The angles of attack considered were  $-0.2^\circ$ ,  $0.0^\circ$ ,  $0.2^\circ$ ,  $0.42^\circ$ ,  $0.6^\circ$ , and  $0.8^\circ$ . For LTRAN2,  $0.8^\circ$  was practically the highest angle of attack that could be considered for this airfoil. Reduced frequencies considered were 0.05, 0.10, 0.15, and 0.20, respectively. The results are given in Table 1.

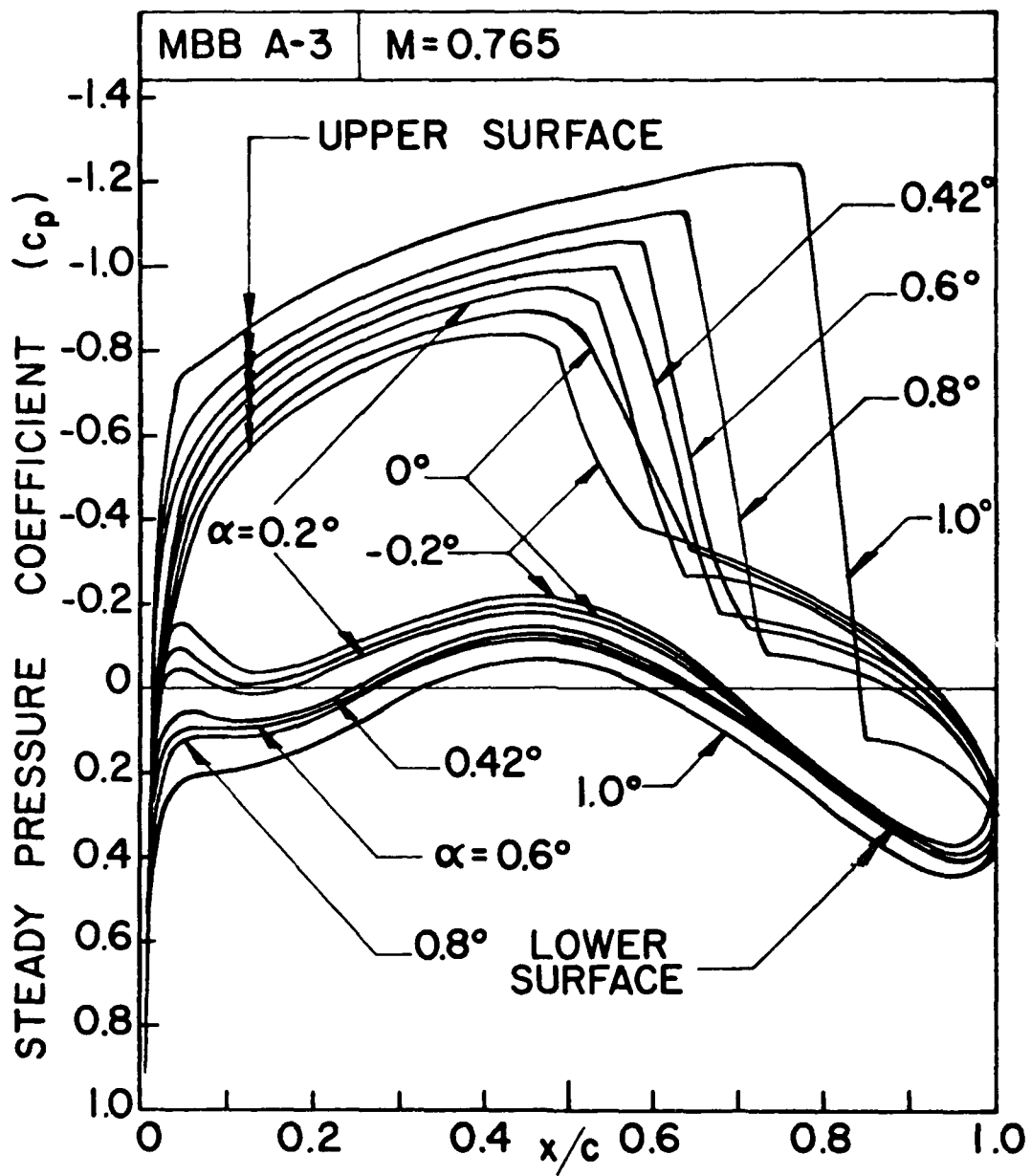


Figure 3. Effect of Angle of Attack on Steady Pressure Curves for MBB A-3 Airfoil by LTRAN2.

Table 1. Aerodynamic Coefficients for MBB A-3 Airfoil for Various Angles of Attack at M = 0.765 by LTRAN2

	Angle of Attack	Reduced Frequency ( $k_c$ )							
		0.05		0.10		0.15		0.20	
		Real	Imag.	Real	Imag.	Real	Imag.	Real	Imag.
$C_z$	-0.2°	0.160	0.598	0.429	1.036	0.694	1.362	0.977	1.595
	0.0°	0.171	0.636	0.422	1.100	0.724	1.420	0.881	1.728
	0.2°	0.238	0.671	0.595	1.095	0.900	1.386	1.199	1.563
	0.42°	0.324	0.728	0.734	1.130	1.058	1.379	1.355	1.505
	0.6°	0.452	0.783	0.917	1.133	1.247	1.314	1.493	1.417
	0.8°	0.709	0.830	1.165	1.105	1.441	1.231	1.619	1.311
$C_{z\alpha}$	-0.2°	11.965	-3.206	10.356	-4.290	9.078	-4.625	7.974	-4.886
	0.0°	12.724	-3.409	11.001	-4.223	9.469	-4.825	8.642	-4.403
	0.2°	13.419	-4.752	10.952	-5.946	9.237	-5.999	7.815	-5.997
	0.42°	14.555	-6.480	11.303	-7.340	9.195	-7.055	7.524	-6.775
	0.6°	15.662	-9.043	11.329	-9.174	8.763	-8.316	7.086	-7.467
	0.8°	16.604	-14.18	11.053	-11.65	8.205	-9.607	6.554	-8.093
$C_{m_z}$	-0.2°	-0.005	-0.026	-0.031	-0.049	-0.022	-0.073	-0.030	-0.100
	0.0°	-0.008	-0.038	-0.015	-0.071	-0.022	-0.103	-0.029	-0.136
	0.2°	-0.021	-0.054	-0.052	-0.089	-0.077	-0.118	-0.107	-0.140
	0.42°	-0.043	-0.085	-0.092	-0.127	-0.137	-0.152	-0.180	-0.162
	0.6°	-0.078	-0.120	-0.158	-0.158	-0.215	-0.174	-0.268	-0.164
	0.8°	-0.171	-0.171	-0.280	-0.182	-0.346	-0.176	-0.385	-0.171
$C_{m_{z\alpha}}$	-0.2°	-0.511	0.109	-0.489	0.131	-0.489	0.145	-0.502	0.149
	0.0°	-0.763	0.162	-0.706	0.150	-0.686	0.146	-0.680	0.145
	0.2°	-1.084	0.416	-0.892	0.515	-0.790	0.513	-0.699	0.537
	0.42°	-1.704	0.868	-1.272	0.924	-1.014	0.913	-0.811	0.901
	0.6°	-2.391	1.553	-1.579	1.579	-1.158	1.430	-0.820	1.338
	0.8°	-3.409	3.409	-1.820	2.803	-1.175	2.306	-0.857	1.924

The unsteady coefficients  $C_{\ell\delta}$ ,  $C_{\ell\alpha}$ ,  $C_{m\delta}$ , and  $C_{m\alpha}$  are also plotted against angle of attack in Figures 4, 5, 6, and 7, respectively. The corresponding phase angles are also shown in the four respective figures.

In Figure 4, the lift coefficient  $|C_{\ell\delta}|$  due to plunging increases gradually with increase in angle of attack whereas the corresponding phase angle  $\theta_1$  decreases with the increase in angle of attack. With the increase in reduced frequency,  $|C_{\ell\delta}|$  increases whereas the corresponding  $\theta_1$  decreases.

In Figure 5, the lift coefficient  $|C_{\ell\alpha}|$  due to pitching about the quarter chord axis and its corresponding phase angle  $\theta_2$  both increase with the increase in angle of attack. With the increase in reduced frequency,  $|C_{\ell\alpha}|$  decreases whereas  $|\theta_2|$  increases.

In Figure 6, the magnitude of the moment coefficient  $|C_{m\delta}|$  about the quarter chord axis due to plunging increases with the increase in angle of attack, whereas the corresponding phase angle  $\theta_3$  decreases with the increase in angle of attack. With the increase in reduced frequency,  $|C_{m\delta}|$  increases and  $\theta_3$  decreases.

In Figure 7, the magnitude of the moment coefficient  $|C_{m\alpha}|$  about the quarter chord axis due to pitching increases with the increase in angle of attack whereas the corresponding phase angle  $\theta_4$  decreases with increase in angle of attack. With the increase in reduced frequency,  $|C_{m\alpha}|$  increases and  $\theta_4$  decreases.

### c. Flutter Results

Based on the unsteady aerodynamic coefficients obtained in Table 1 for six angles of attack, flutter analysis was performed. The emphasis was to investigate the effect of angle of attack on flutter speed for various values of aeroelastic parameters.

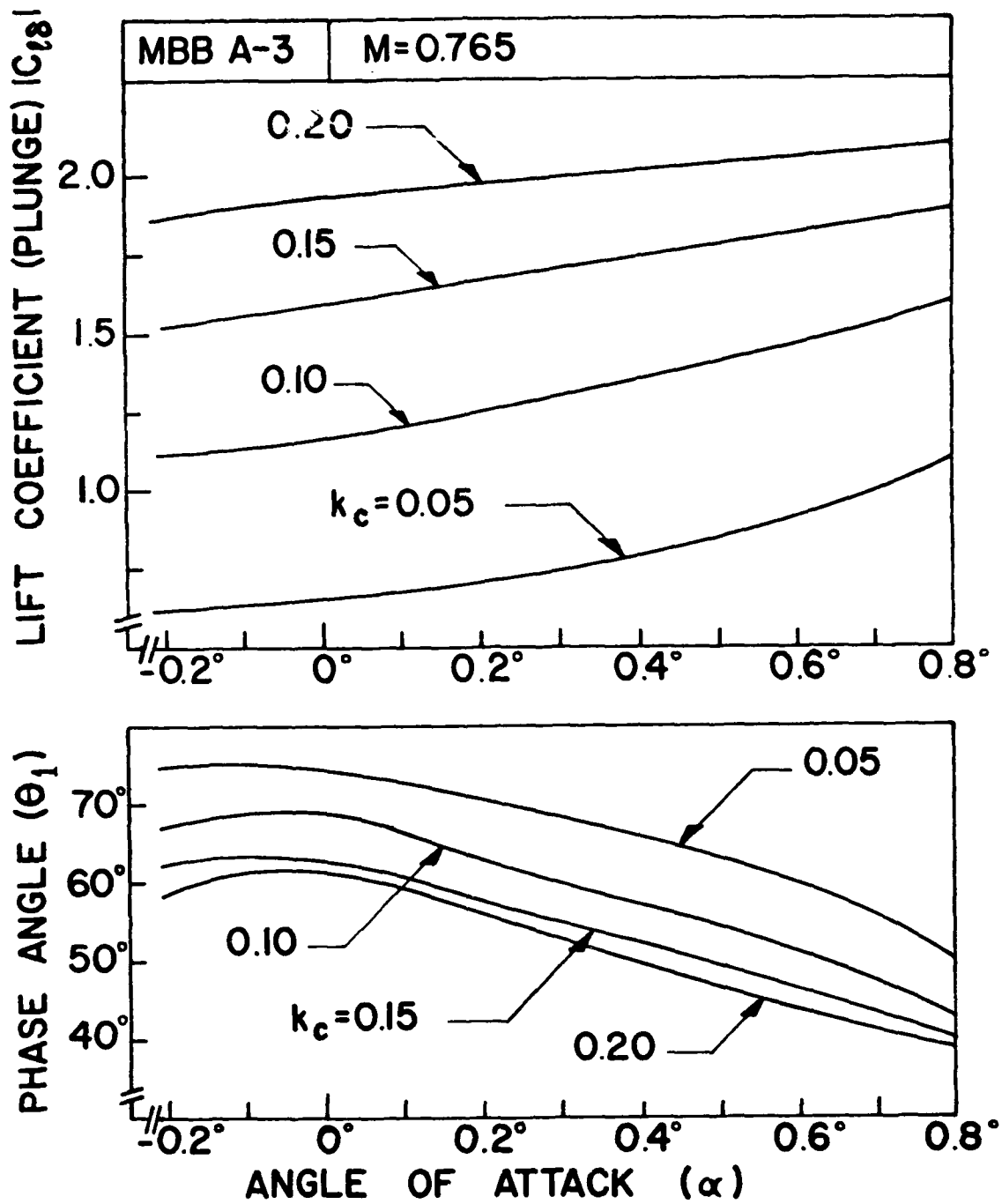


Figure 4. Effect of Angle of Attack on Lift Coefficient due to Plunging for MBB A-3 Airfoil by LTRAN2

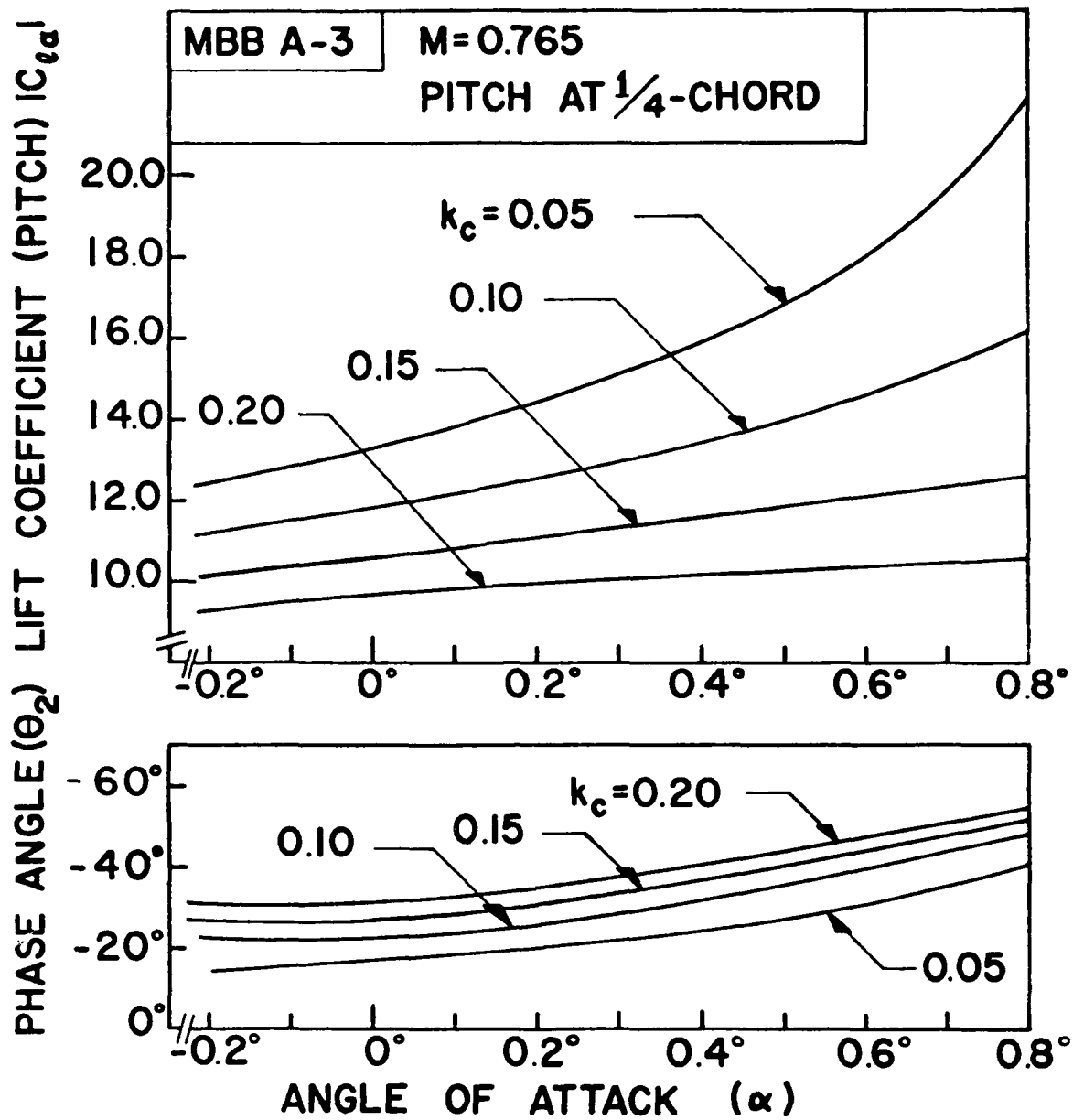


Figure 5. Effect of Angle of Attack on Lift Coefficient due to Pitching for MBB A-3 Airfoil by LTRAN2.

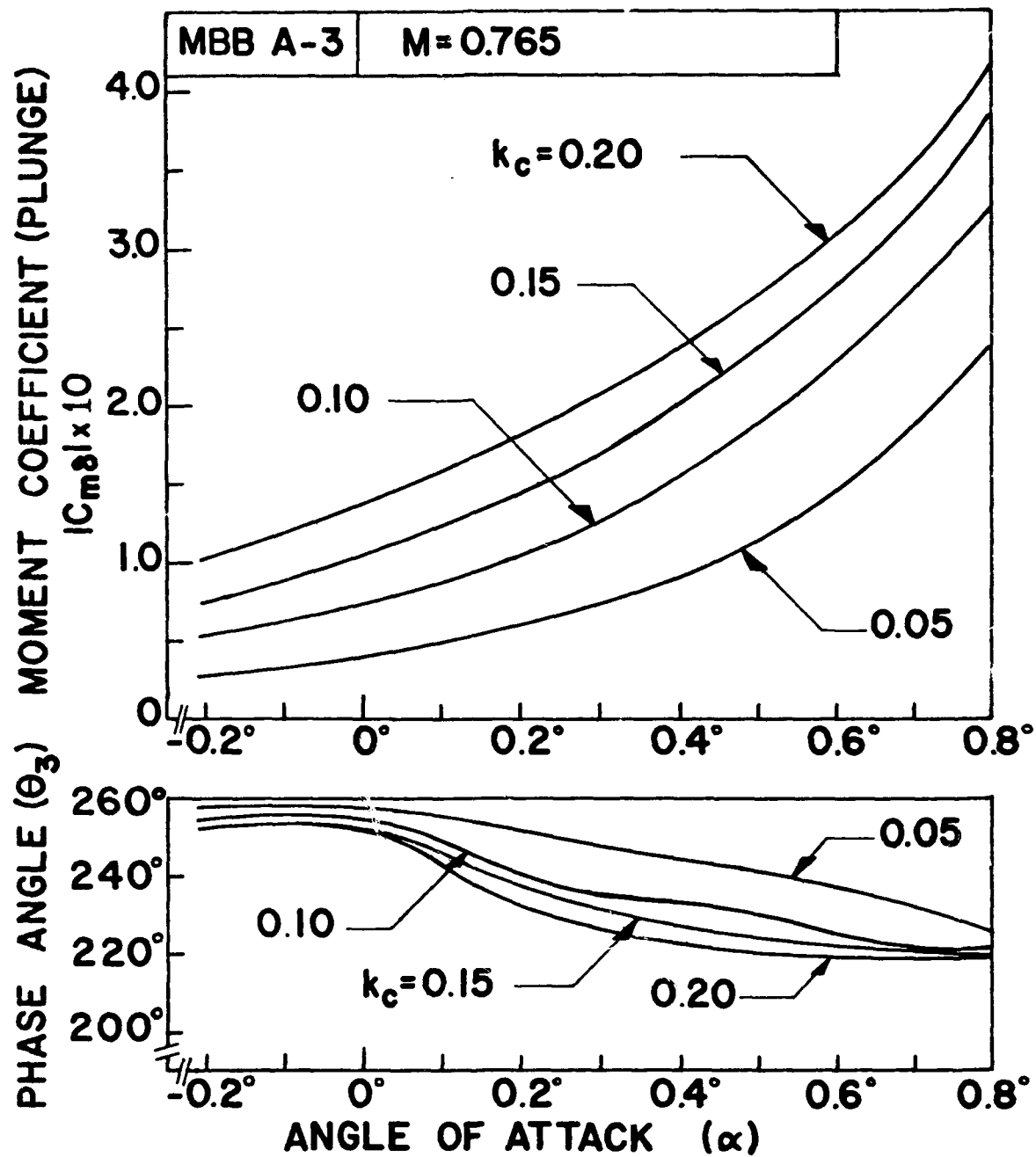


Figure 6. Effect of Angle of Attack on Moment Coefficient due to Plunging for MBB A-3 Airfoil by LTRAN2.

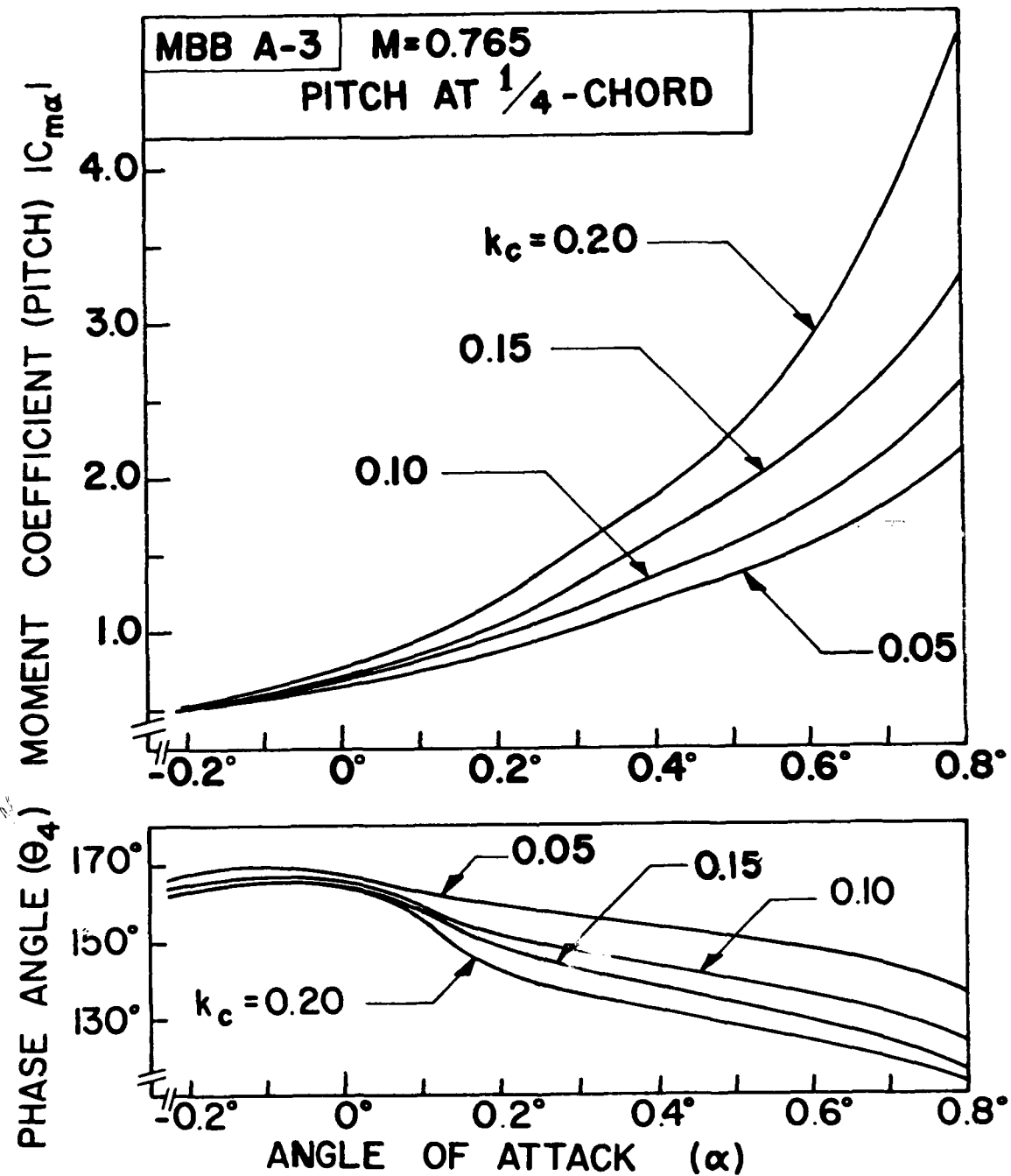


Figure 7. Effect of Angle of Attack on Moment Coefficient due to Pitching for MBB A-3 Airfoil by LTRAN2.



Figure 8 shows the curves for flutter speed and the corresponding reduced frequency versus the mean angle of attack for five different values of the position of mass center ( $x_\alpha = 0.25, 0.3, 0.4, 0.5, \text{ and } 0.6$ , respectively). The values for the airfoil-air mass density ratio  $\mu$ , plunge-to-pitch frequency ratio  $\omega_h/\omega_\alpha$ , and the position of the elastic axis  $a_h$ , were assumed as 100, 0.1, and -0.5, respectively.

It is seen in Figure 8 that the flutter speed increases as the mass center approaches the elastic axis or as  $x_\alpha$  becomes smaller. For smaller values of  $x_\alpha$  and higher values of  $\alpha$ , difficulty is encountered in obtaining a flutter solution. For a constant value of  $x_\alpha$ , the flutter speed increases with the increase in angle of attack. Such increasing trends are more rapid at higher angles of attack and at lower values of  $x_\alpha$ . These changes are the direct effect of changes in the unsteady coefficients shown in Table 1.

Figure 9 shows the curves for flutter speed and the corresponding reduced frequency versus angle of attack for three different values of airfoil-air mass density ratio ( $\mu = 100, 200, \text{ and } 300$ , respectively). The values for the other aeroelastic parameters  $x_\alpha$ ,  $a_h$ , and  $\omega_h/\omega_\alpha$  were assumed as 0.5, -0.5, and 0.1, respectively.

In Figure 9, the flutter speed increases with the increase in airfoil-air mass density ratio. Reduced frequency decreases with the increase in  $\mu$ . The flutter speed increases with the increase in angle of attack. The rate of increase is higher at higher angles of attack.

Figure 10 shows the curves for flutter speed and the corresponding reduced frequency versus angle of attack for two different values of plunge-to-pitch frequency ratio ( $\omega_h/\omega_\alpha = 0.1 \text{ and } 0.2$ , respectively). The values for the other aeroelastic parameters  $\mu$ ,  $x_\alpha$ , and  $a_h$  were assumed as 100, 0.5, and -0.5, respectively.

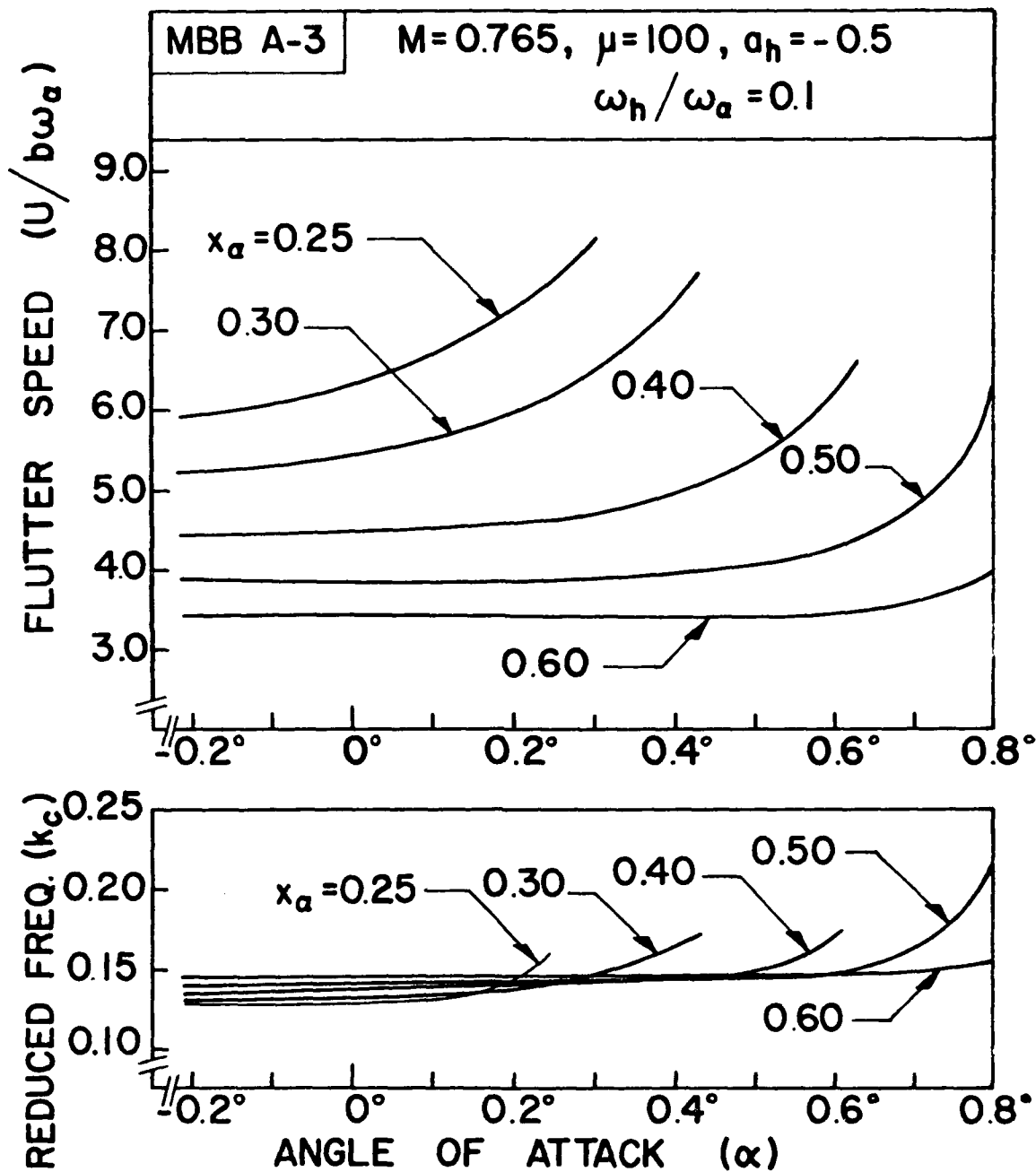


Figure 8. Effect of Angle of Attack on Flutter Speed for Five Positions of Mass Center for MBB A-3 Airfoil by LTRAN2.

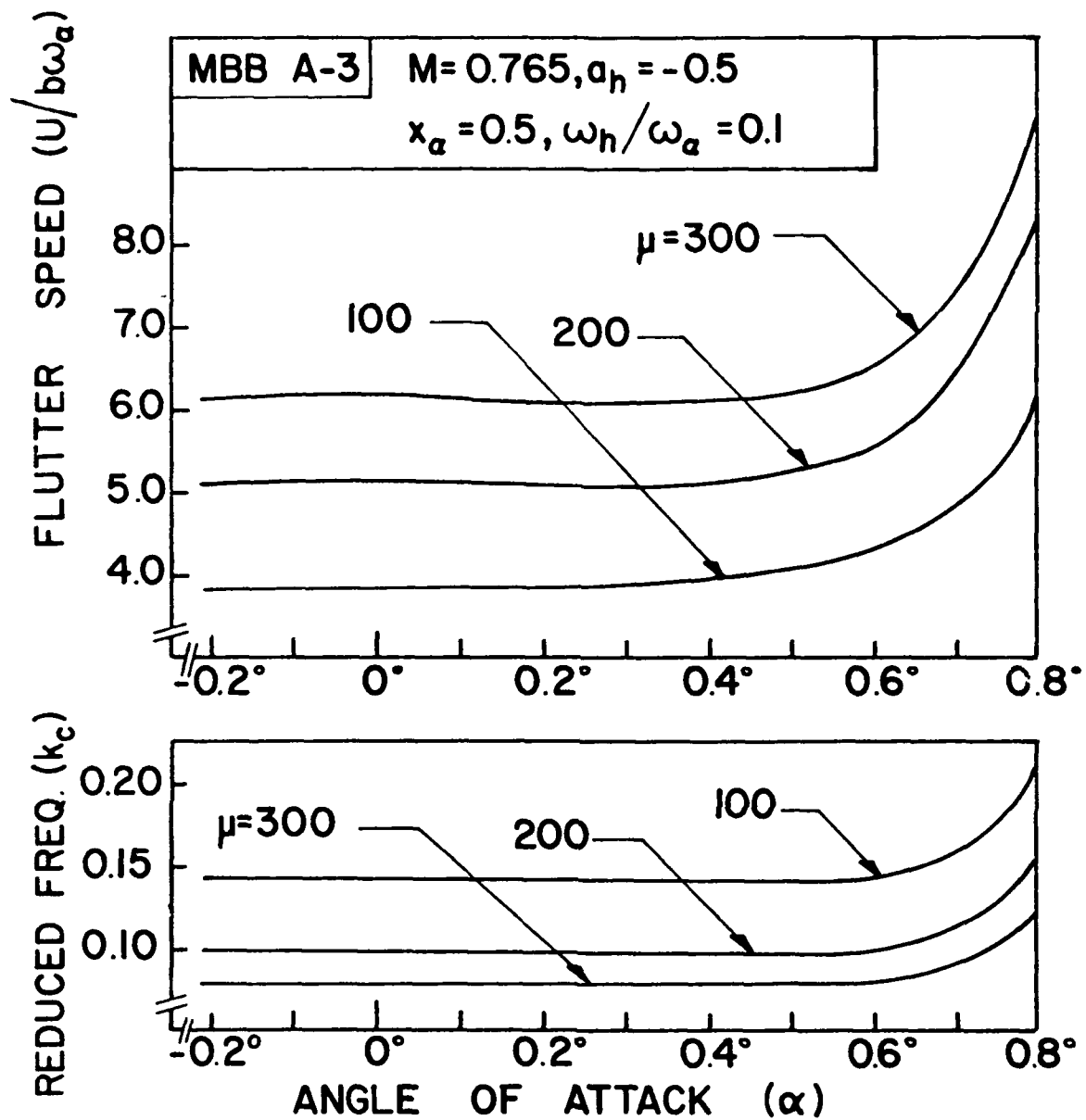


Figure 9. Effect of Angle of Attack on Flutter Speed for Three Values of Airfoil-Air Mass Density Ratio for MBB A-3 Airfoil by LTRAN2.

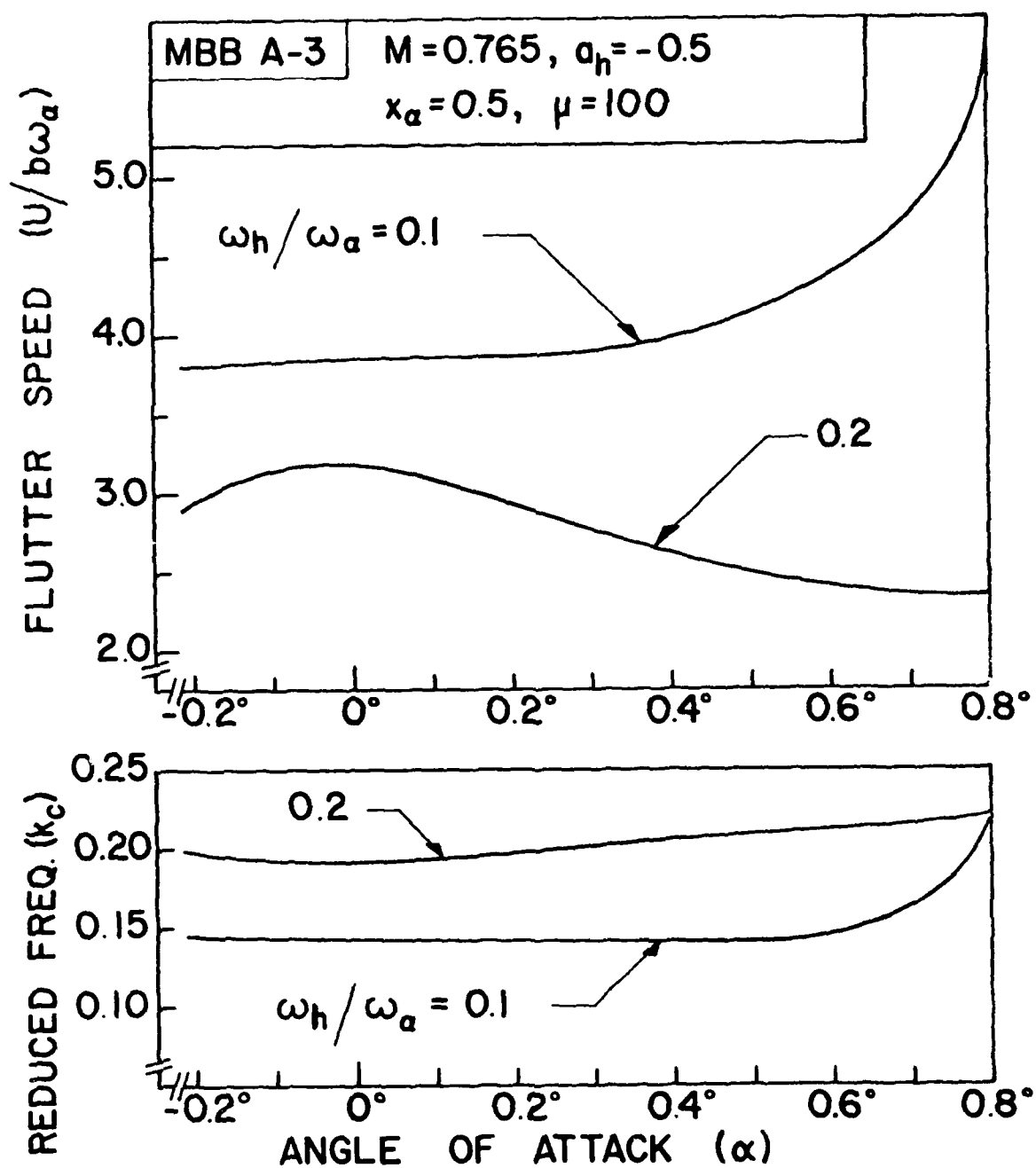


Figure 10. Effect of Angle of Attack on Flutter Speed for Two Values of Plunge-to-Pitch Frequency Ratio for MBB A-3 Airfoil by LTRAN2.

It is seen in Figure 10 that the flutter speed curve for the case  $\omega_h/\omega_\alpha = 0.1$  is higher than that for the case of  $\omega_h/\omega_\alpha = 0.2$ . The reduced frequency curve for the former case is lower than that for the latter.

The flutter speed curve for  $\omega_h/\omega_\alpha = 0.1$  increases with the increase in angle of attack. The increase is more rapid at higher angles of attack. On the other hand, the flutter speed curve for  $\omega_h/\omega_\alpha = 0.2$  first increases slightly with the increase of angle of attack ( $\alpha < 0.0^\circ$ ) and then decreases with the increase in angle of attack.

Figure 11 shows the curves for flutter speed and the corresponding reduced frequency versus the angle of attack for three different positions of elastic axis ( $a_h = -0.1, -0.3, \text{ and } -0.5$ , respectively). The mass center was fixed at mid-chord and values for  $\mu$  and  $\omega_h/\omega_\alpha$  were assumed as 100 and 0.1, respectively.

It is seen in Figure 11 that when the position of elastic axis is varied from  $a_h = -0.1$  to  $a_h = -0.5$ , there is not much change in flutter speed.

All the curves corresponding to  $\omega_h/\omega_\alpha = 0.1$  in Figures 8 to 11 show that flutter speed increases with the increase in angle of attack. Such increase becomes more rapid at higher angles of attack.

### 3. Results Based on STRANS2/UTRANS2

In this section, the aerodynamic data were obtained for the MBB A-3 supercritical airfoil by the harmonic analysis programs STRANS2/UTRANS2 at design Mach number  $M = 0.765$ . The values for angle of attack considered were  $-0.4^\circ, 0.0^\circ, 0.42^\circ, 0.75^\circ, 1.0^\circ, 1.2^\circ$ , and  $1.3^\circ$ , respectively. The value  $\alpha = 0.75^\circ$  corresponds to the equivalent design angle of attack that yields a design lift coefficient of 0.58 (Reference 3).

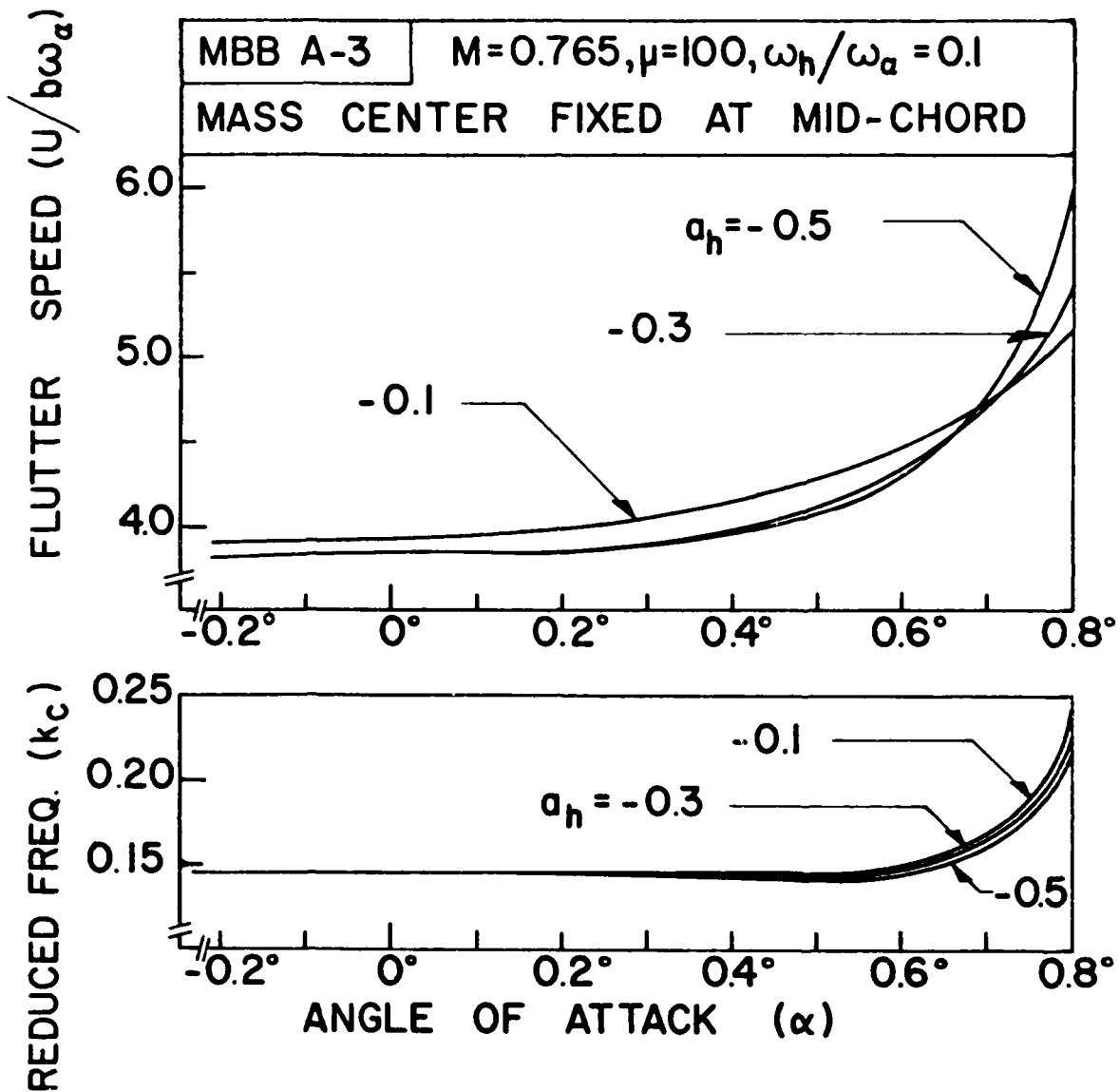


Figure 11. Effect of Angle of Attack on Flutter Speed for Three Positions of Elastic Axis for MBB A-3 Airfoil by LTRAN2.

#### a. Steady Pressure Curves

Figure 12 shows the upper and lower surface steady pressure curves for the MBB A-3 airfoil for eight mean angles of attack ranging from  $-1.2^\circ$  to  $1.3^\circ$  at  $M = 0.765$  obtained by STRANS2.

In Figure 12, the pressure curves for the upper surface move upward with the increase in angle of attack whereas the pressure curves for the lower surface move downward with the increase in angle of attack. A shock appears at an angle of attack of about  $0.0^\circ$  and grows stronger with the increase in angle of attack. Similar results were obtained by LTRAN2 in Figure 3. However, the shock in Figure 12 remains almost in the same position ( $x/c \approx 0.5$ ) for all angles of attack. On the other hand, the shock in Figure 3 moves towards the trailing edge with the increase in angle of attack. For the same flow conditions, the shock obtained by LTRAN2 is, in general, stronger than that obtained by STRANS2.

From the nature of the changes in the steady pressure curves shown in Figure 12, it can be expected that both lift and moment coefficients increase with increase in angle of attack.

#### b. Unsteady Aerodynamic Coefficients

Based on the steady state pressure curves shown in Figure 12, four unsteady aerodynamic coefficients,  $C_{l\delta}$ ,  $C_{l\alpha}$ ,  $C_{m\delta}$ , and  $C_{m\alpha}$ , were obtained by UTRANS2 for the MBB A-3 supercritical airfoil. The airfoil was assumed to pitch about the quarter chord at design Mach number  $M = 0.765$ . Seven angles of attack ( $-0.4^\circ$ ,  $0.0^\circ$ ,  $0.42^\circ$ ,  $0.75^\circ$ ,  $1.0^\circ$ ,  $1.2^\circ$ , and  $1.3^\circ$ ) were considered. Coefficients were computed at five reduced frequencies (0.0, 0.05, 0.10, 0.15, and 0.20).

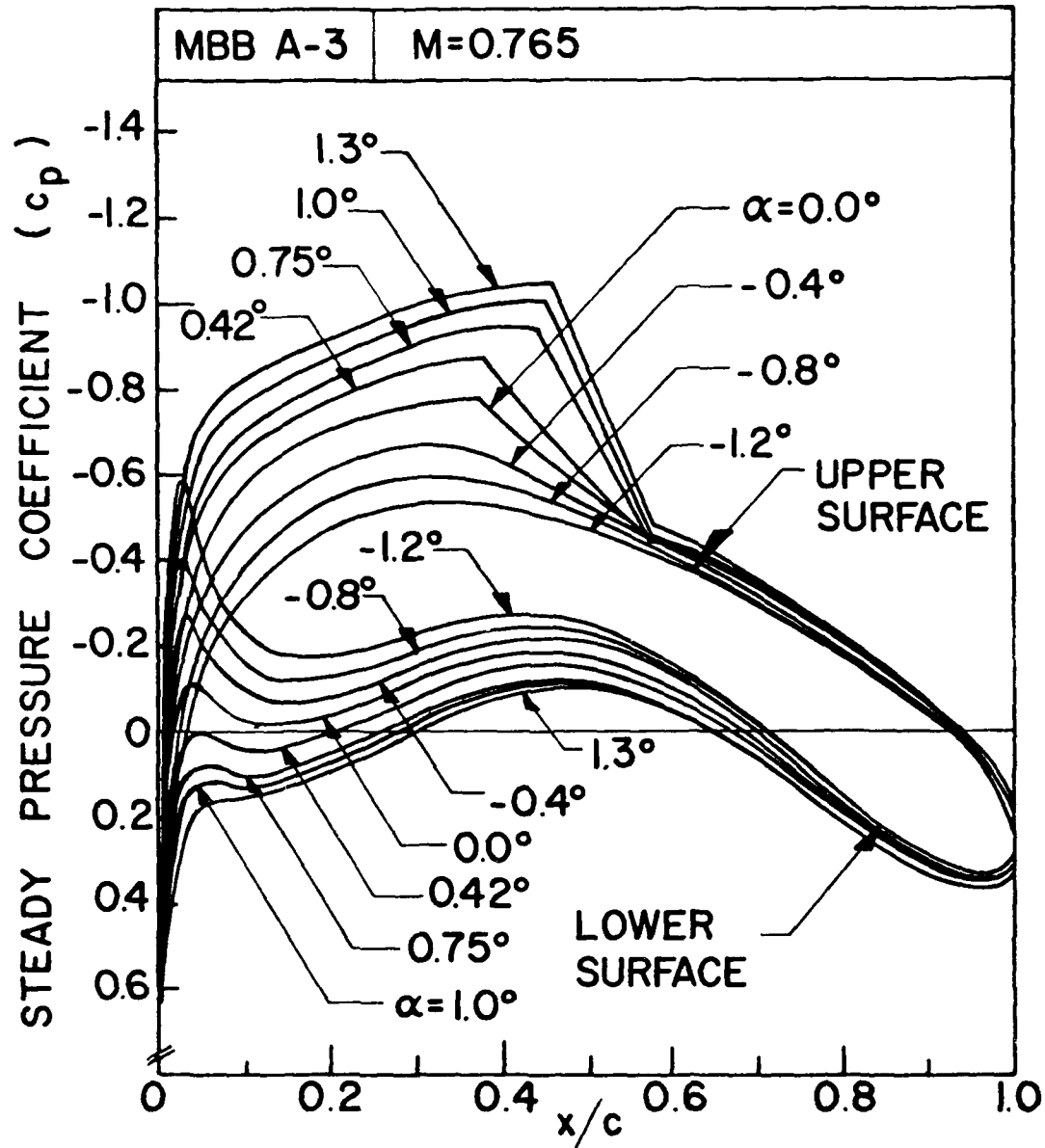


Figure 12. Effect of Angle of Attack on Steady Pressure Curves for MBB A-3 Airfoil by STRANS2.



Table 2 shows the real and imaginary parts of the four unsteady aerodynamic coefficients. The four coefficients  $C_{l\delta}$ ,  $C_{l\alpha}$ ,  $C_{m\delta}$ , and  $C_{m\alpha}$  and their corresponding phase angles  $\theta_1$ ,  $\theta_2$ ,  $\theta_3$ , and  $\theta_4$ , are plotted against the angle of attack in Figures 13, 14, 15, and 16, respectively.

In Figure 13, the magnitude of the lift coefficient due to plunge  $C_{l\delta}$ , does not appear to vary much with the change in angle of attack. Similar behavior is observed for the corresponding phase angle  $\theta_1$ . With the increase in reduced frequency,  $|C_{l\delta}|$  increases whereas  $\theta_1$  decreases.

In Figure 14, the magnitude of the lift coefficient due to pitch  $|C_{l\alpha}|$  about the quarter chord axis does not appear to vary much with the change in angle of attack. Similar behavior is observed for the corresponding phase angle  $\theta_2$ . With the increase in reduced frequency,  $|C_{l\alpha}|$  decreases whereas  $|\theta_2|$  increases.

In Figure 15, the magnitude of the moment coefficient about the quarter chord  $|C_{m\alpha}|$  due to plunge increases gradually with the increase in angle of attack. The corresponding phase angle  $\theta_3$  gradually decreases with the increase in angle of attack. The values of  $|C_{m\delta}|$  are higher for higher reduced frequencies, whereas, the curves for  $\theta_3$  do not show a definite trend.

In Figure 16, the magnitude of the moment coefficient about the quarter chord  $|C_{m\alpha}|$  due to pitch about the quarter chord increases with the increase in angle of attack  $\alpha$ . The corresponding phase angle  $\theta_4$  decreases with the increase in angle of attack. With the increase in reduced frequency,  $|C_{m\alpha}|$  increases for  $\alpha$  less than about  $0.5^\circ$  and decreases for  $\alpha$  greater than about  $0.5^\circ$ , whereas  $\theta_4$  increases for all  $\alpha$ -values considered.

The magnitudes of the moment coefficients seem to reach a local maximum at  $\alpha \approx 1.2^\circ$  whereas the corresponding phase angles seem to reach a local minimum at this angle of attack.

Table 2. Aerodynamic Coefficients for MBB A-3 Airfoil for Various Angles of Attack at  $M = 0.765$  by UTRANS2

Angle of Attack		Reduced Frequency ( $k_c$ )									
		0.0		0.05		0.10		0.15		0.20	
		Real	Imag.	Real	Imag.	Real	Imag.	Real	Imag.	Real	Imag.
$C_{z_\delta}$	1.3°	0.0	0.0	0.104	0.492	0.273	0.835	0.492	1.074	0.677	1.184
	1.2°	0.0	0.0	0.106	0.499	0.281	0.844	0.501	1.087	0.695	1.197
	1.0°	0.0	0.0	0.111	0.508	0.285	0.854	0.508	1.100	0.710	1.209
	.75°	0.0	0.0	0.119	0.557	0.279	0.906	0.539	1.172	0.772	1.277
	.42°	0.0	0.0	0.094	0.513	0.286	0.881	0.536	1.138	0.745	1.262
	0.0°	0.0	0.0	0.089	0.521	0.260	0.900	0.523	1.185	0.772	1.288
	-.4°	0.0	0.0	0.091	0.512	0.281	0.881	0.521	1.150	0.736	1.275
$C_{y_\alpha}$	1.3°	10.376	0.0	9.345	-1.724	8.254	-2.451	7.260	-2.718	6.362	-2.747
	1.2°	10.590	0.0	9.514	-1.768	8.389	-2.521	7.360	-2.808	6.435	-2.839
	1.0°	10.709	0.0	9.610	-1.803	8.463	-2.567	7.419	-2.853	6.483	-2.884
	.75°	11.388	0.0	10.171	-1.941	8.932	-2.818	7.757	-3.144	6.702	-3.180
	.42°	11.168	0.0	9.992	-1.915	8.757	-2.687	7.677	-2.948	6.744	-2.966
	0.0°	11.221	0.0	10.141	-1.949	8.843	-2.801	7.667	-3.060	6.710	-2.970
	-.4°	11.129	0.0	9.979	-1.878	8.780	-2.605	7.745	-2.857	6.845	-2.881
$C_{m_\delta}$	1.3°	0.0	0.0	-0.007	-0.044	-0.016	-0.077	-0.031	-0.106	-0.051	-0.125
	1.2°	0.0	0.0	-0.006	-0.043	-0.016	-0.076	-0.029	-0.106	-0.050	-0.126
	1.0°	0.0	0.0	-0.005	-0.040	-0.012	-0.071	-0.023	-0.100	-0.040	-0.121
	.75°	0.0	0.0	-0.003	-0.035	-0.003	-0.060	-0.009	-0.090	-0.020	-0.113
	.42°	0.0	0.0	0.0	-0.024	0.002	-0.047	0.002	-0.072	0.0	-0.096
	0.0°	0.0	0.0	0.003	-0.015	0.010	-0.031	0.017	-0.053	0.020	-0.076
	-.4°	0.0	0.0	0.003	-0.012	0.010	-0.026	0.018	-0.044	0.025	-0.065
$C_{m_\alpha}$	1.3°	-0.901	0.0	-0.829	0.073	-0.766	0.079	-0.715	0.066	-0.671	0.061
	1.2°	-0.899	0.0	-0.826	0.069	-0.764	0.073	-0.715	0.059	-0.673	0.052
	1.0°	-0.824	0.0	-0.759	0.048	-0.709	0.040	-0.672	0.019	-0.643	0.007
	.75°	-0.691	0.0	-0.640	0.006	-0.614	0.023	-0.597	0.056	-0.589	0.073
	.42°	-0.510	0.0	-0.482	-0.032	-0.472	-0.087	-0.476	-0.140	-0.489	-0.180
	0.0°	-0.311	0.0	-0.307	-0.074	-0.319	-0.148	-0.340	-0.212	-0.365	-0.265
	-.4°	-0.248	0.0	-0.246	-0.082	-0.262	-0.162	-0.285	-0.231	-0.314	-0.286

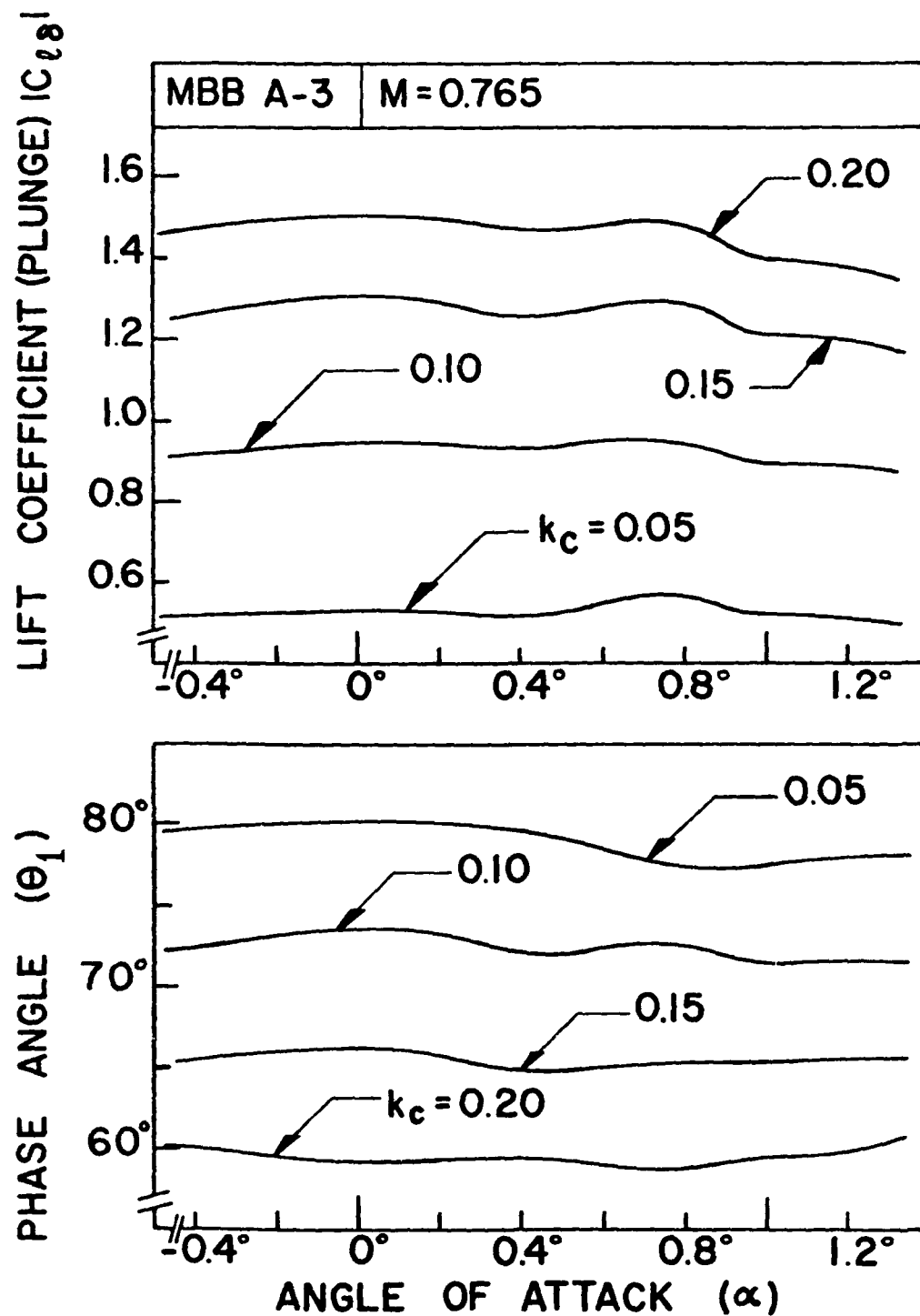


Figure 13. Effect of Angle of Attack on Lift Coefficient due to Plunging for MBB A-3 Airfoil by UTRANS2.

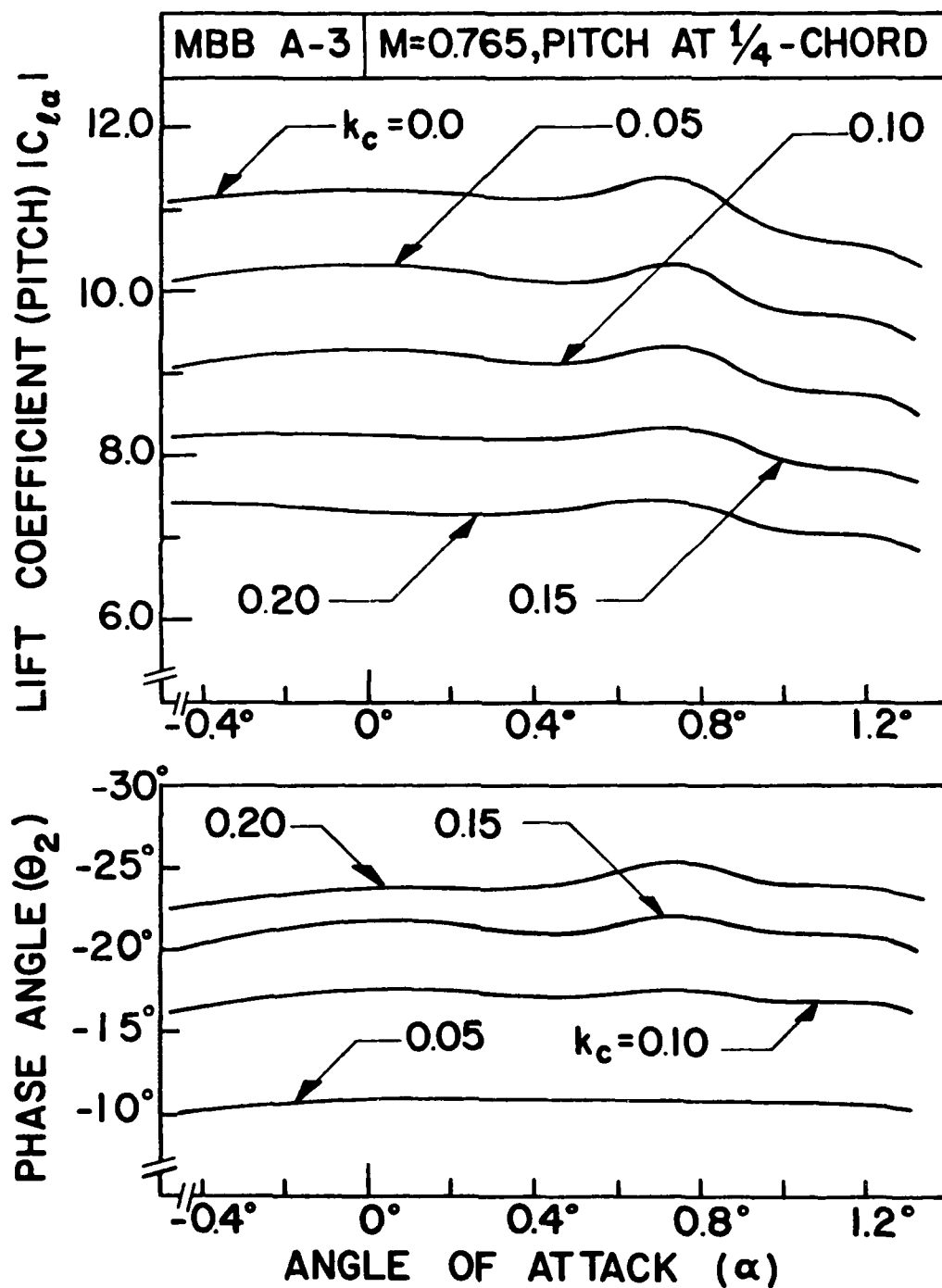


Figure 14. Effect of Angle of Attack on Lift Coefficient due to Pitching for MBB A-3 Airfoil by UTRANS2.

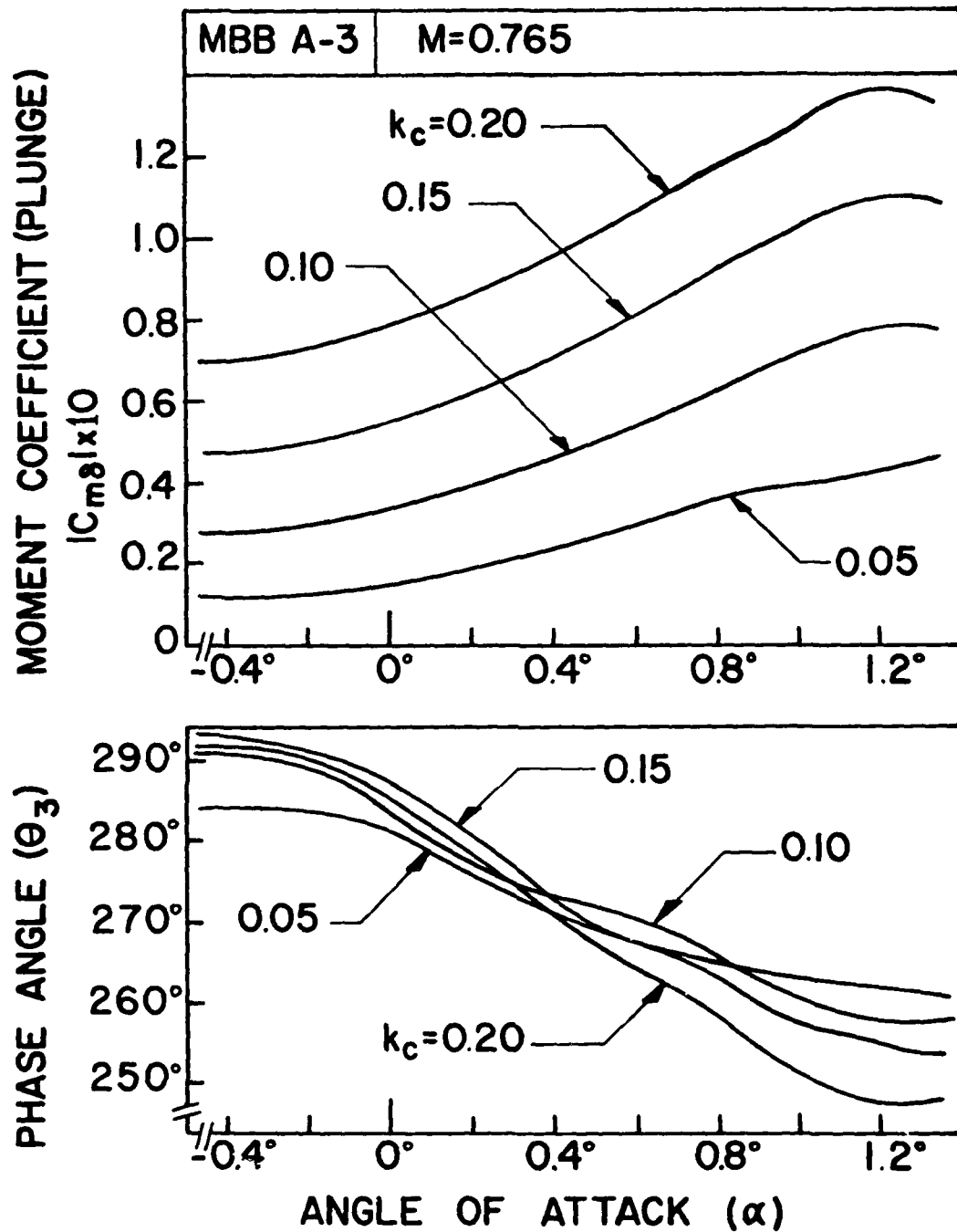


Figure 15. Effect of Angle of Attack on Moment Coefficient due to Plunging for MBB A-3 Airfoil by UTRANS2.

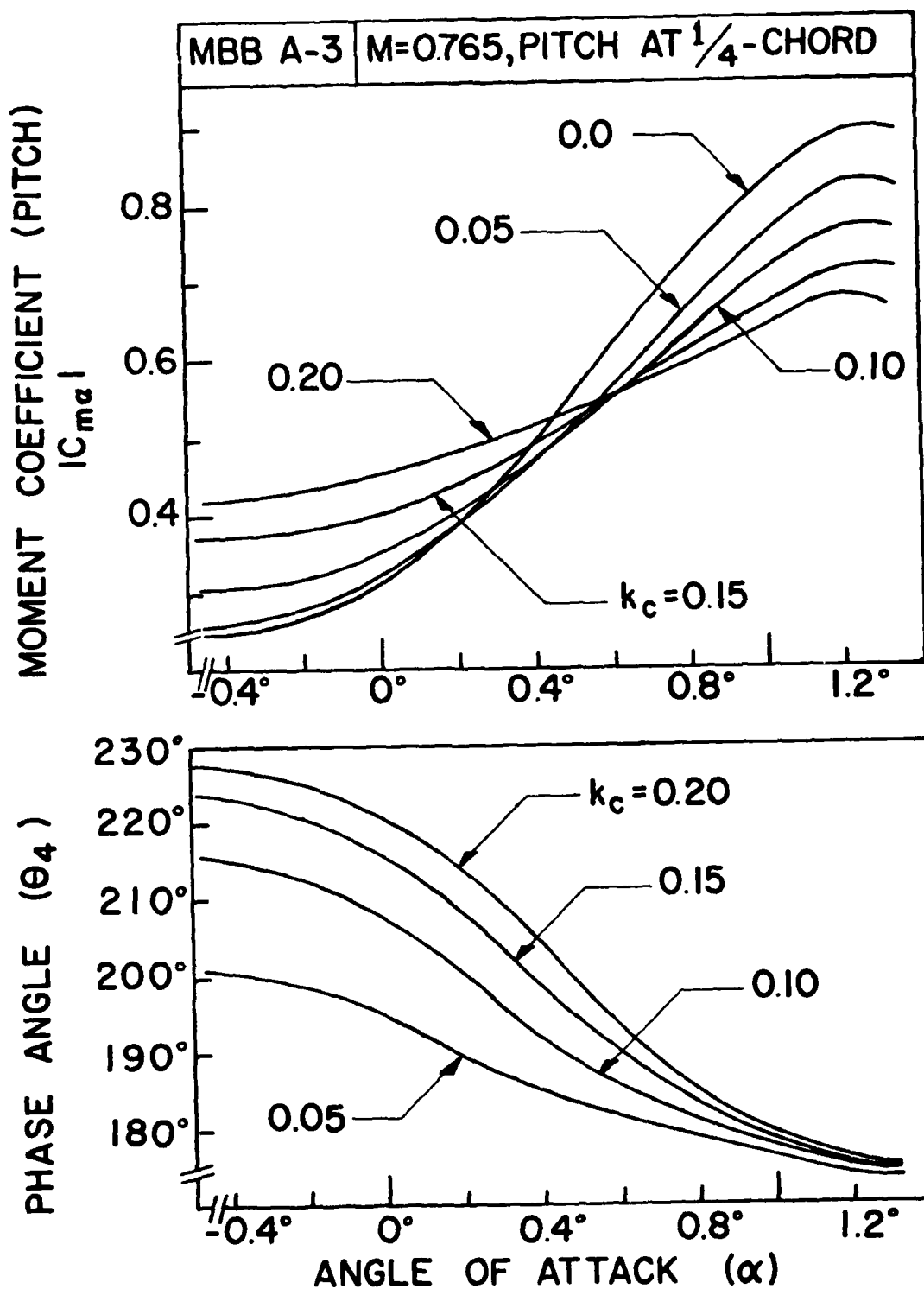


Figure 16. Effect of Angle of Attack on Moment Coefficient due to Pitching for MBB A-3 Airfoil by UTRANS2.

When comparing the results obtained by LTRAN2 in Figures 4 to 7 and those obtained by UTRANS2 in Figures 13 to 16, it is difficult to draw conclusions consistent among all figures. However, in both cases the moment coefficients,  $|C_{m\delta}|$  and  $|C_{m\alpha}|$ , increase with the increase in angle of attack. Also, all the coefficients in both cases vary with the reduced frequency in a similar way except for  $\alpha > 0.5^\circ$  in Figure 16.

### c. Flutter Results

Based on the unsteady aerodynamic coefficients shown in Table 2 for seven angles of attack, a flutter analysis of the MBB A-3 supercritical airfoil was performed. The emphasis was to investigate the effect of angle of attack on flutter speed for various values of aeroelastic parameters.

Figure 17 shows the curves for flutter speed and the corresponding reduced frequency versus angle of attack for six values of the position of mass center ( $x_\alpha = 0.1, 0.2, 0.3, 0.4, 0.5$ , and  $0.6$ , respectively). The values for the airfoil-air mass density ratio  $\mu$ , plunge-to-pitch frequency ratio  $\omega_h/\omega_\alpha$ , and the position of elastic axis  $a_h$ , were assumed as  $100, 0.1$ , and  $-0.5$ , respectively.

In Figure 17, the flutter speed increases rapidly as the mass center approaches the elastic axis or as  $x_\alpha$  becomes smaller. For  $x_\alpha = 0.1$ , difficulty is encountered in obtaining a flutter speed. The reduced frequency increases with the increase in  $x_\alpha$ . For a constant value of  $x_\alpha$ , the flutter speed increases with the increase in angle of attack. Such increasing rates are more rapid in the neighborhood of  $\alpha = 0.6^\circ$  to  $1.1^\circ$  and at lower values of  $x_\alpha$ .

Figure 18 shows curves for the flutter speed and the corresponding reduced frequency versus angle of attack for three different values of

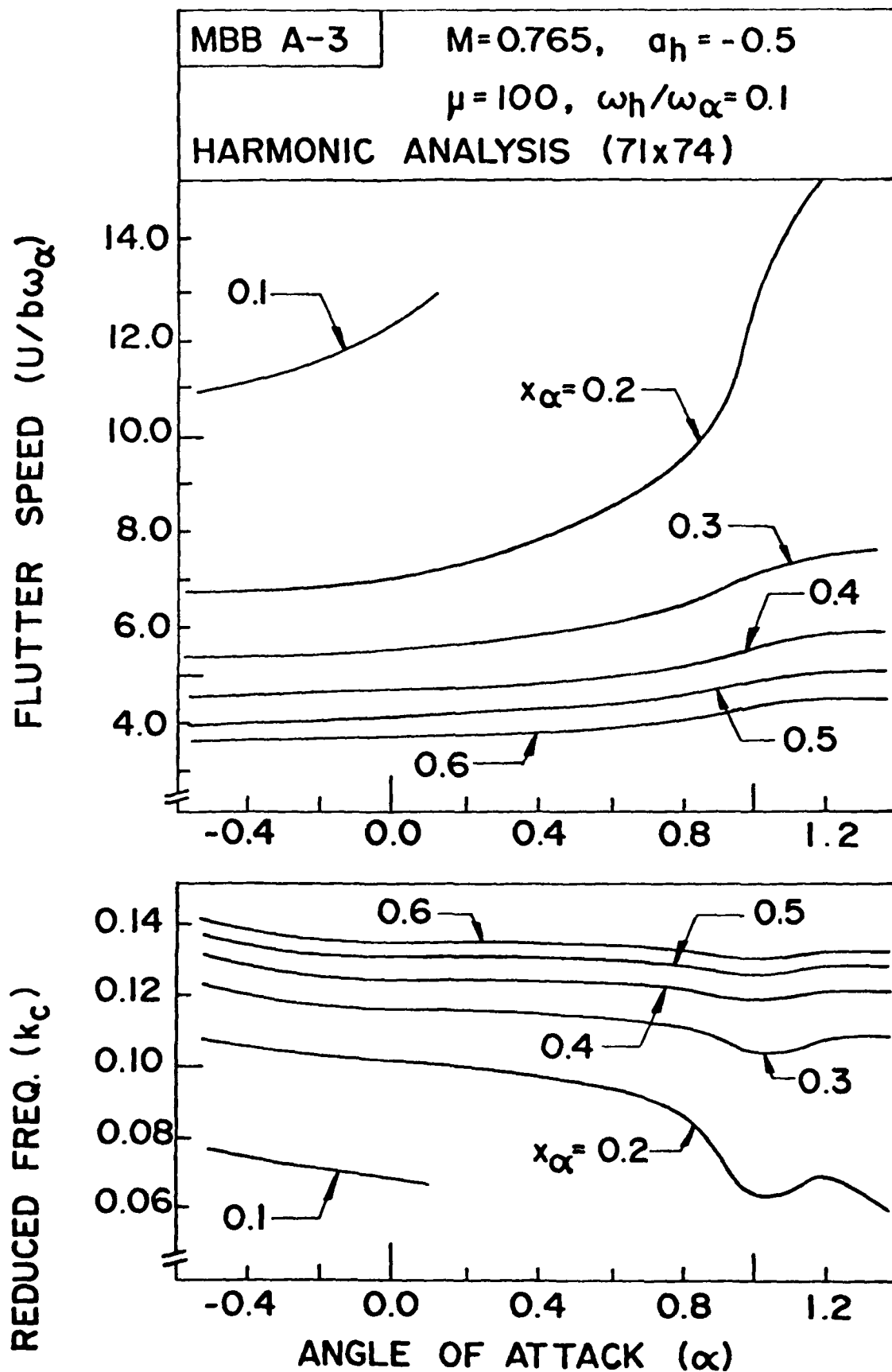


Figure 17. Effect of Angle of Attack on Flutter Speed for Six Positions of Mass Center for MBB A-3 Airfoil by STRANS2/UTRANS2.



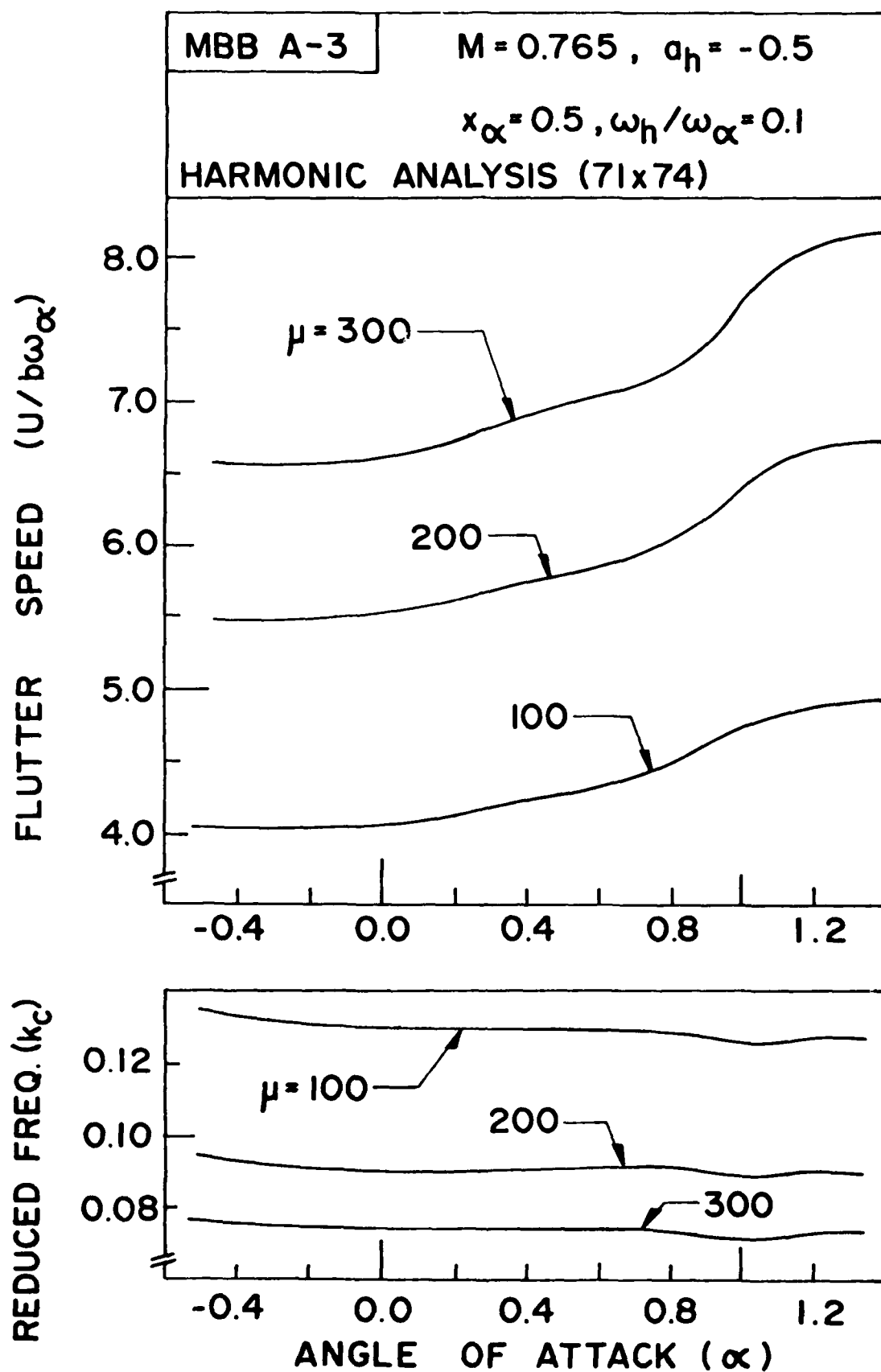


Figure 18. Effect of Angle of Attack on Flutter Speed for Three Values of Airfoil-Air Mass Density Ratio for MBB A-3 Airfoil by STRANS2/UTRANS2.

7

airfoil-air mass density ratio ( $\mu = 100, 200, \text{ and } 300$ ). The values for the other aeroelastic parameters  $x_\alpha$ ,  $a_h$ , and  $\omega_h/\omega_\alpha$  were assumed as 0.5, -0.5, and 0.1, respectively.

In Figure 18, the flutter speed increases with the increase in airfoil-air mass density ratio. The reduced frequency decreases with the increase in  $\mu$ . The flutter speed increases with the increase in angle of attack. The increase rate appears to be higher near higher angles of attack. This is due to the rapid changes in the moment coefficients at higher angles of attack (see Table 2). However, the flutter speed curves appear to peak near  $\alpha = 1.2^\circ$ .

Figure 19 shows the curves for flutter speed and the corresponding reduced frequency versus angle of attack for two different values of plunge-to-pitch frequency ratio ( $\omega_h/\omega_\alpha = 0.1 \text{ and } 0.2$ , respectively). The other aeroelastic parameters  $\mu$ ,  $x_\alpha$ , and  $a_h$  were assumed as 100, 0.5, and -0.5, respectively.

In Figure 19, the flutter speed curve for  $\omega_h/\omega_\alpha = 0.1$  is higher than that for  $\omega_h/\omega_\alpha = 0.2$ . The corresponding curves for reduced frequency show an opposite trend. Both flutter curves increase with the increase in angle of attack.

Figure 20 shows the curves for the flutter speed and the corresponding reduced frequency versus angle of attack for two different values of position of elastic axis ( $a_h = -0.1 \text{ and } -0.5$ , respectively). The mass center was fixed at mid-chord and the values for  $\mu$  and  $\omega_h/\omega_\alpha$  were assumed as 100 and 0.1, respectively.

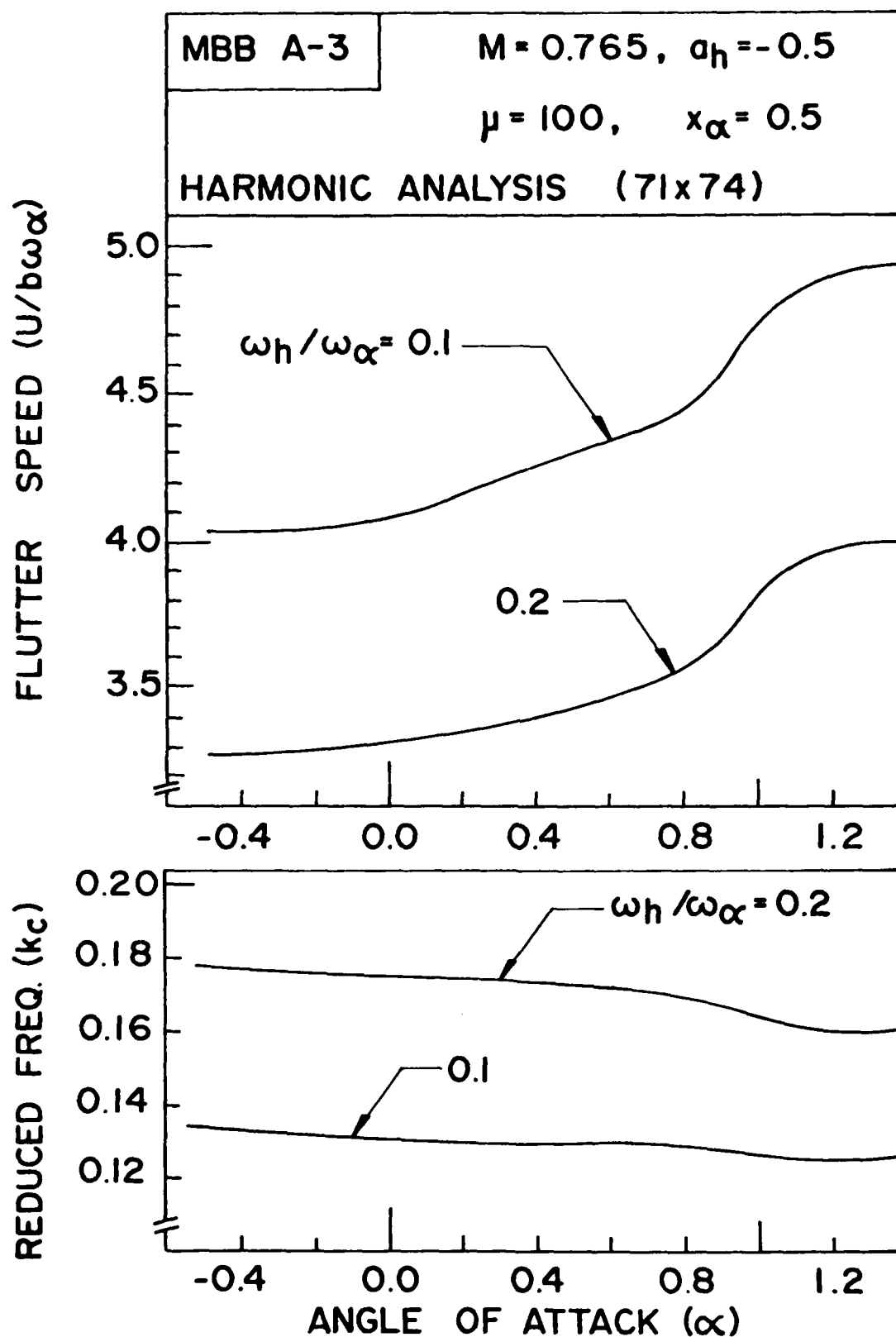


Figure 19. Effect of Angle of Attack on Flutter Speed for Two Values of Plunge-to-Pitch Frequency Ratio for MBB A-3 Airfoil by STRANS2/UTRANS2.

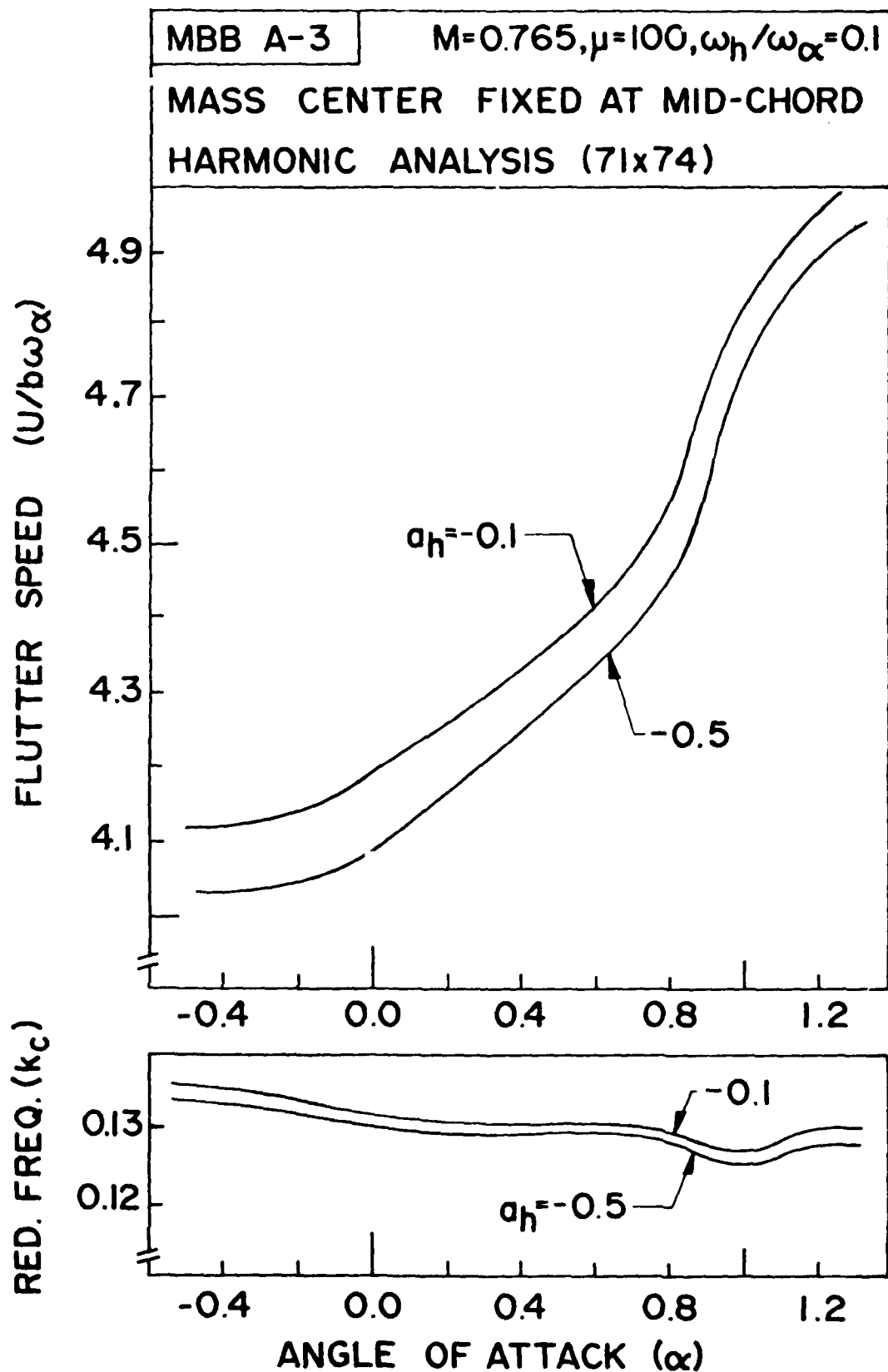


Figure 20. Effect of Angle of Attack on Flutter Speed for Two Positions of Elastic Axis for MBB A-3 Airfoil by STRANS2/UTRANS2.

In Figure 20, the flutter curve for  $a_h = -0.1$  is slightly higher than that for  $a_h = -0.5$ . The flutter speed increases with the increase in angle of attack. The rate of increase is higher at higher angles of attack. Such behavior may be due to the rapid changes in the moment coefficients at higher angles of attack.

Figures 17 to 20 show that the flutter speed increases with the increase in angle of attack. Comparing Figures 8 to 11 with Figures 17 to 20, it is seen that for the case of  $\omega_h/\omega_\alpha = 0.1$ , all the curves for flutter speed increase with the increase in angle of attack. However, for  $\omega_h/\omega_\alpha = 0.2$ , the flutter speed trend with angle of attack is different for the two sets of aerodynamics (LTRAN2 and UTRANS2).

## SECTION V

### FLUTTER ANALYSIS OF A CAST 7 SUPERCRITICAL AIRFOIL

The CAST 7 supercritical airfoil was designed by Dornier GmbH of the Federal Republic of Germany and is one of the AGARD standard airfoils suggested for aeroelastic applications of transonic unsteady aerodynamics (Reference 24). In this study, flutter characteristics of the airfoil in the transonic regime are investigated by using LTRAN2.

The airfoil was assumed to oscillate with two degrees of freedom, plunge and pitch, about the elastic axis. The aerodynamic data were obtained by pitching the airfoil about the quarter chord axis with zero mean angle of attack. Seven Mach numbers between 0.6 and 0.72 were considered.

Based on the aerodynamic data, a flutter analysis of the CAST 7 airfoil was conducted and the effect of Mach number on flutter speed for various values of aeroelastic parameters was studied.

Throughout this study, the values for the radius of gyration  $r_\alpha$  and the reference frequency  $\omega_r$  were assumed as 0.5 and 1.0, respectively.

#### 1. Airfoil Configuration

The configuration of the CAST 7 airfoil was obtained by Equation 9. The coefficients for one-segment fitting of the thickness (provided by Dr. J. J. Olsen) are:  $a_0 = 0.3315970$ ;  $a_1 = 0.0$ ;  $a_2 = -0.2393648$ ;  $a_3 = 0.3331678$ ;  $a_4 = -1.0215039$ ; and  $a_5 = 0.6030865$ . The coefficients for the camber function are:  $b_1 = 0.0$ ;  $b_2 = 0.1216041$ ;  $b_3 = -0.5012554$ ;  $b_4 = 0.8749108$ ; and  $b_5 = -0.4983959$ . A plot of the configuration is given in Figure 21.

CAST 7

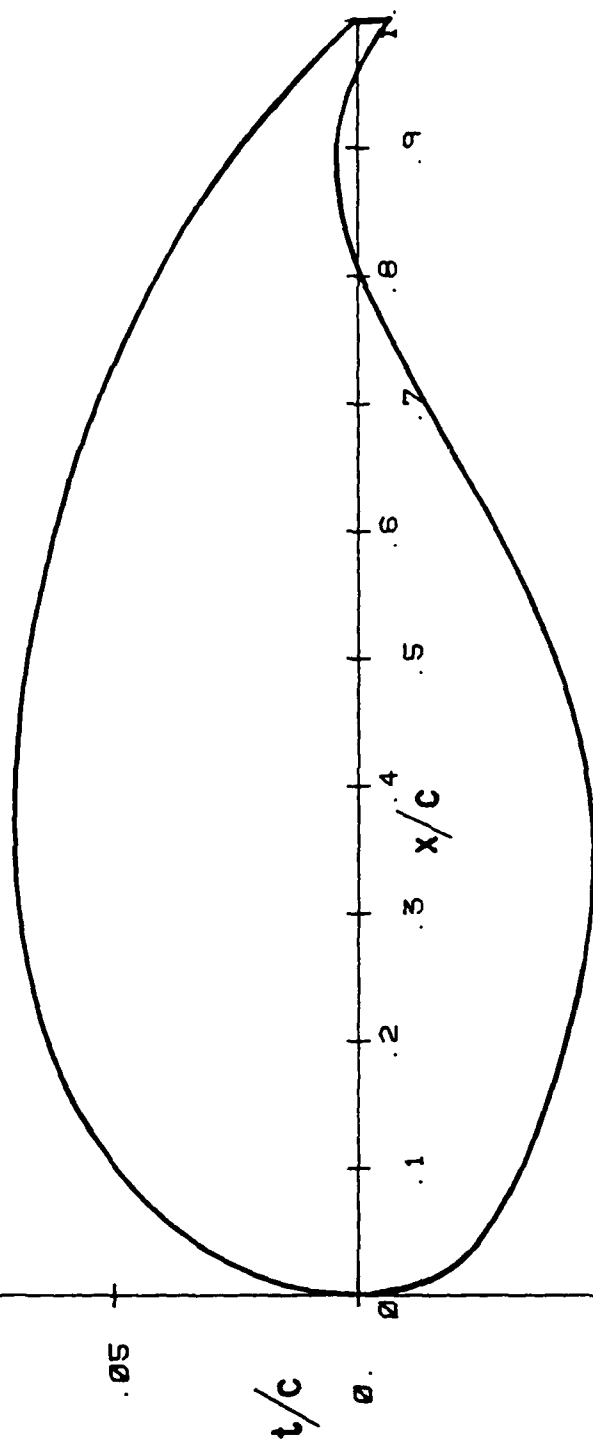


Figure 21. Airfoil Configuration for CAST 7.

It is seen in Figure 21 that the maximum thickness-to-chord ratio is 11.9%. The airfoil has a fairly blunt nose when compared to conventional airfoils.

## 2. Steady Pressure Curves

CAST 7 is a fairly thick supercritical airfoil (11.9%) when compared to other supercritical airfoils such as MBB A-3 (8.9%). LTRAN2 is based on inviscid and small disturbance transonic theory which is valid for thin airfoils (i.e.  $< 12\%$ ). Hence, it was of interest to compare present LTRAN2 steady pressure results with those obtained by experiment.

Figure 22 shows two sets of steady pressure curves, one obtained by LTRAN2 and the other by experiment in Reference 11. The values for Mach number and mean angle of attack were equal to  $0.602^\circ$  and  $0.5^\circ$ , respectively.

The two sets of curves appear to have similar overall shapes. LTRAN2 gives higher pressure coefficients, thus higher lift. The discrepancy appears to be larger on the lower surface near the trailing edge.

Reasons for the discrepancy between the two sets of curves may be attributed to: (1) viscous effects which are not considered in LTRAN2; (2) small disturbance theory used in LTRAN2; and (3) possible errors introduced due to both numerical and experimental difficulties.

Figure 23 shows the steady pressure curves for the upper and lower surfaces for eight different Mach numbers (0.60, 0.625, 0.65, 0.675, 0.70, 0.71, 0.72, and 0.73, respectively) obtained by LTRAN2. With increase in Mach number, the upper surface pressure curves change faster than the lower surface pressure curves. A shock develops at  $M \approx 0.7$ . When Mach number increases, the shock moves toward the trailing edge with increasing strength.



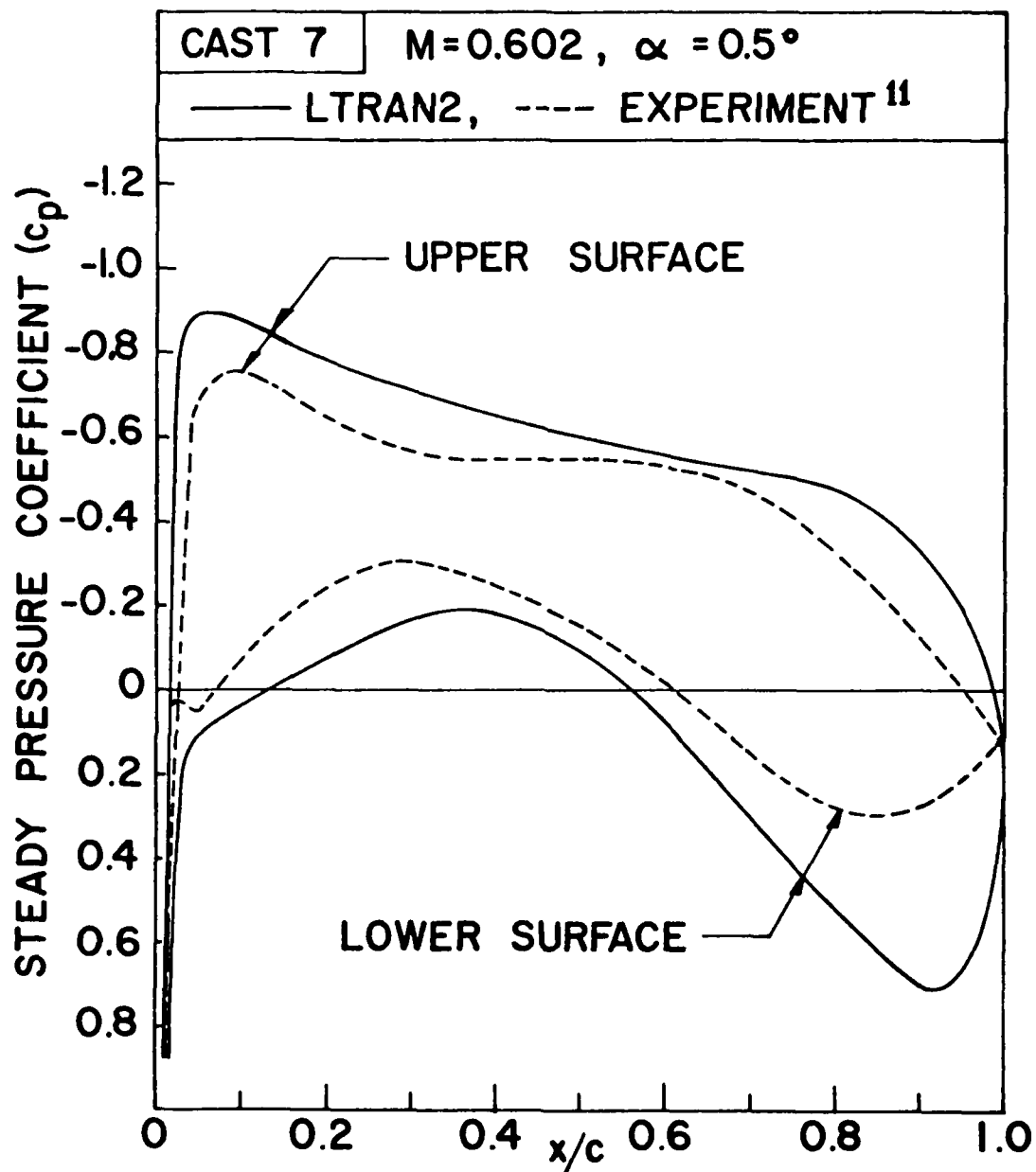


Figure 22. Comparison between Steady Pressure Curves by LTRAN2 and Experiment for CAST 7 Airfoil.

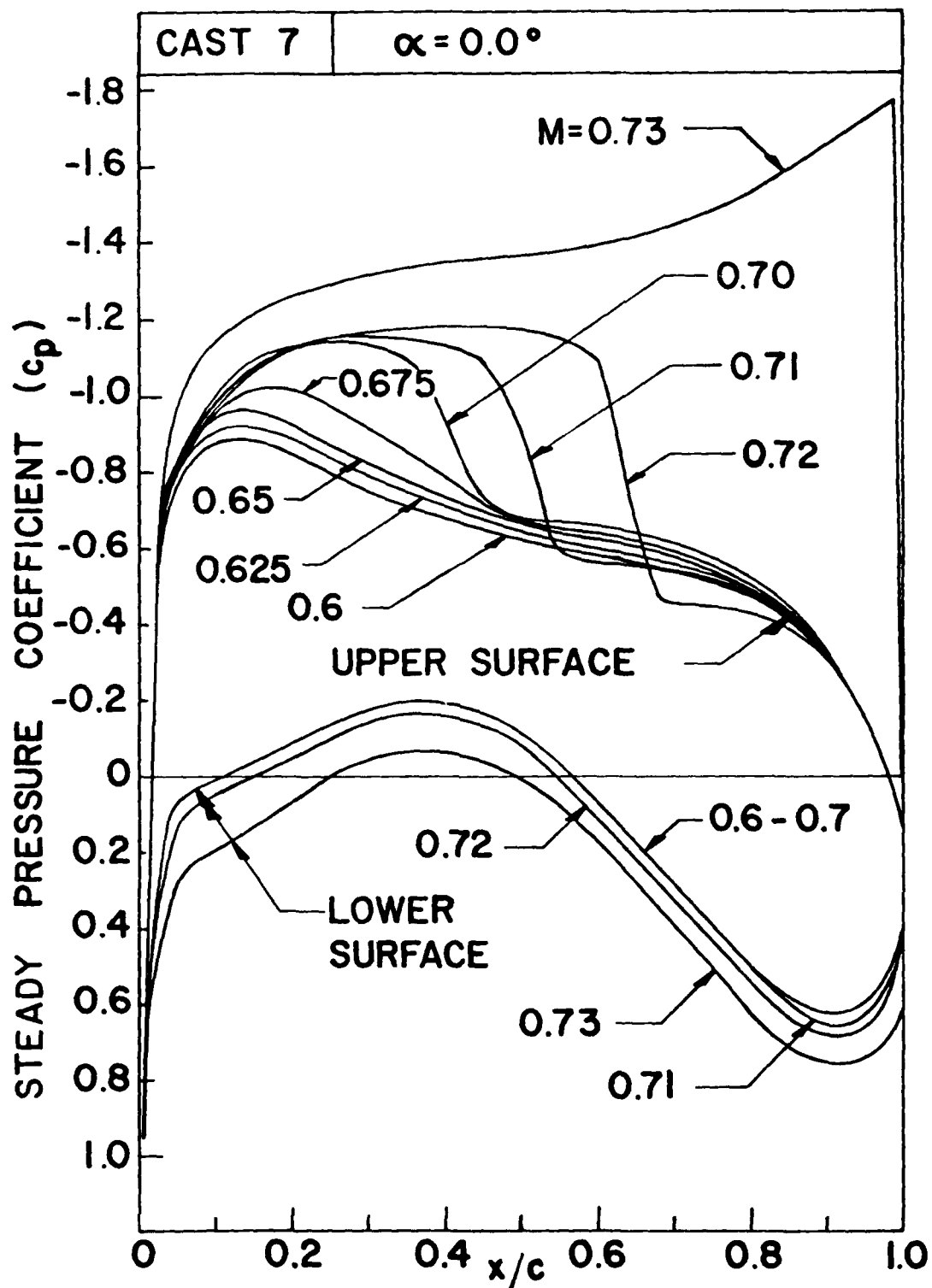


Figure 23. Effect of Mach Number on Steady Pressure Curves for CAST 7 Airfoil by LTRAN2.

As the Mach number approaches 0.73, the shock approaches the trailing edge. It appears that Mach number 0.72 is practically the highest Mach number that can be considered in the present analysis.

### 3. Unsteady Aerodynamic Coefficients

Four unsteady aerodynamic coefficients,  $C_{\ell\delta}$ ,  $C_{\ell\alpha}$ ,  $C_{m\delta}$ , and  $C_{m\alpha}$ , were obtained for the CAST 7 airfoil by pitching the airfoil about the quarter chord axis with zero mean angle of attack. Seven Mach numbers, 0.60, 0.625, 0.650, 0.675, 0.70, 0.71, and 0.72, were considered. Reduced frequencies assumed were 0.05, 0.10, 0.15, and 0.20, respectively. The coefficients are presented in Table 3 and plotted in Figures 24 to 27 against Mach number. Also plotted are the corresponding phase angles.

In Figure 24, the magnitude of the lift coefficient due to plunge  $|C_{\ell\delta}|$  gradually increases with increase in Mach number, whereas, the corresponding phase angle  $\theta_1$  decreases. With the increase in reduced frequency,  $|C_{\ell\delta}|$  increases and  $\theta_1$  decreases. The changes in both  $|C_{\ell\delta}|$  and  $\theta_1$  are more rapid above  $M = 0.70$ .

In Figure 25, both the magnitude of the lift coefficient  $|C_{\ell\delta}|$  due to pitch about the quarter chord axis and the corresponding phase angle  $|\theta_2|$  increase as Mach number increases. When the reduced frequency increases,  $|C_{\ell\delta}|$  decreases, whereas,  $|\theta_2|$  increases. All curves take a sharper increase as  $M$  becomes larger than approximately 0.7.

In Figure 26, the magnitude of the moment coefficient  $|C_{m\delta}|$  about the quarter chord axis due to plunge increases with increase in Mach number. The corresponding phase angle  $\theta_3$  first increases up to  $M < 0.68$  and then

Table 3. Aerodynamic Coefficients for CAST 7 Airfoil for Various Mach Numbers at  $\alpha = 0.0^\circ$  by LTRAN2

		Reduced Frequency ( $k_c$ )							
		0.05		0.10		0.15		0.20	
	Mach Number	Real	Imag.	Real	Imag.	Real	Imag.	Real	Imag.
$C_{\ell_\delta}$	0.600	0.033	0.413	0.116	0.798	0.229	1.153	0.355	1.480
	0.625	0.045	0.428	0.131	0.824	0.267	1.180	0.384	1.514
	0.650	0.047	0.449	0.159	0.855	0.293	1.221	0.458	1.544
	0.675	0.063	0.480	0.192	0.904	0.359	1.272	0.542	1.597
	0.700	0.088	0.553	0.285	1.051	0.532	1.387	0.759	1.705
	0.710	0.132	0.620	0.391	1.103	0.698	1.463	0.999	1.730
	0.720	0.258	0.759	0.653	1.241	1.047	1.523	1.372	1.695
$C_{\ell_\alpha}$	0.600	8.263	-0.650	7.976	-1.156	7.685	-1.529	7.402	-1.777
	0.625	8.566	-0.900	8.237	-1.305	7.864	-1.780	7.568	-1.922
	0.650	8.987	-0.945	8.549	-1.585	8.139	-1.954	7.722	-2.288
	0.675	9.593	-1.263	9.037	-1.921	8.483	-2.392	7.986	-2.711
	0.700	11.047	-1.750	10.513	-2.854	9.245	-3.549	8.527	-3.797
	0.710	12.400	-2.636	11.030	-3.906	9.753	-4.652	8.652	-4.995
	0.720	15.176	-5.152	12.407	-6.528	10.150	-6.977	8.473	-6.862
$C_{m_\delta}$	0.600	0.001	-0.001	0.003	-0.003	0.007	-0.005	0.011	-0.008
	0.625	0.001	-0.001	0.004	-0.003	0.008	-0.005	0.014	-0.009
	0.650	0.002	-0.001	0.006	-0.003	0.012	-0.005	0.018	-0.009
	0.675	0.004	0.004	0.009	0.002	0.018	-0.001	0.028	-0.007
	0.700	0.005	-0.001	0.016	-0.003	0.031	-0.013	0.047	-0.027
	0.710	0.006	-0.021	0.015	-0.040	0.026	-0.063	0.025	-0.091
	0.720	-0.011	-0.085	-0.040	-0.147	-0.078	-0.189	-0.119	-0.218
$C_{m_\alpha}$	0.600	-0.021	-0.020	-0.026	-0.034	-0.030	-0.046	-0.039	-0.057
	0.625	-0.023	-0.024	-0.027	-0.040	-0.036	-0.056	-0.047	-0.068
	0.650	-0.015	-0.032	-0.025	-0.059	-0.032	-0.077	-0.046	-0.091
	0.675	0.070	-0.074	0.022	-0.093	-0.003	-0.117	-0.034	-0.140
	0.700	-0.009	-0.089	-0.030	-0.162	-0.085	-0.205	-0.137	-0.237
	0.710	-0.414	-0.111	-0.399	-0.153	-0.417	-0.173	-0.457	-0.123
	0.720	-1.705	0.225	-1.472	0.395	-1.261	0.522	-1.092	0.593

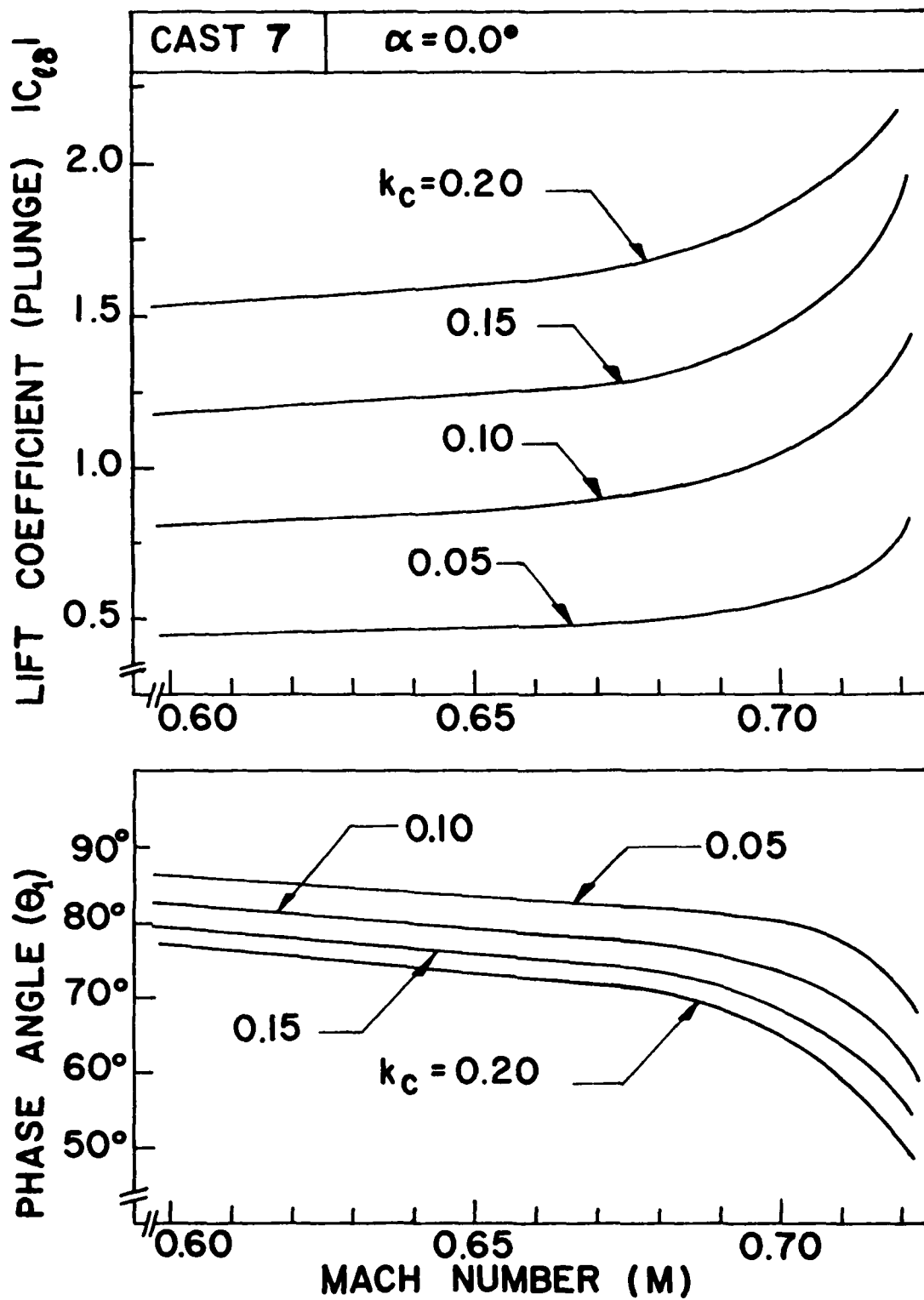


Figure 24. Effect of Mach number on Lift Coefficient due to Plunging for CAST 7 Airfoil by LTRAN2.

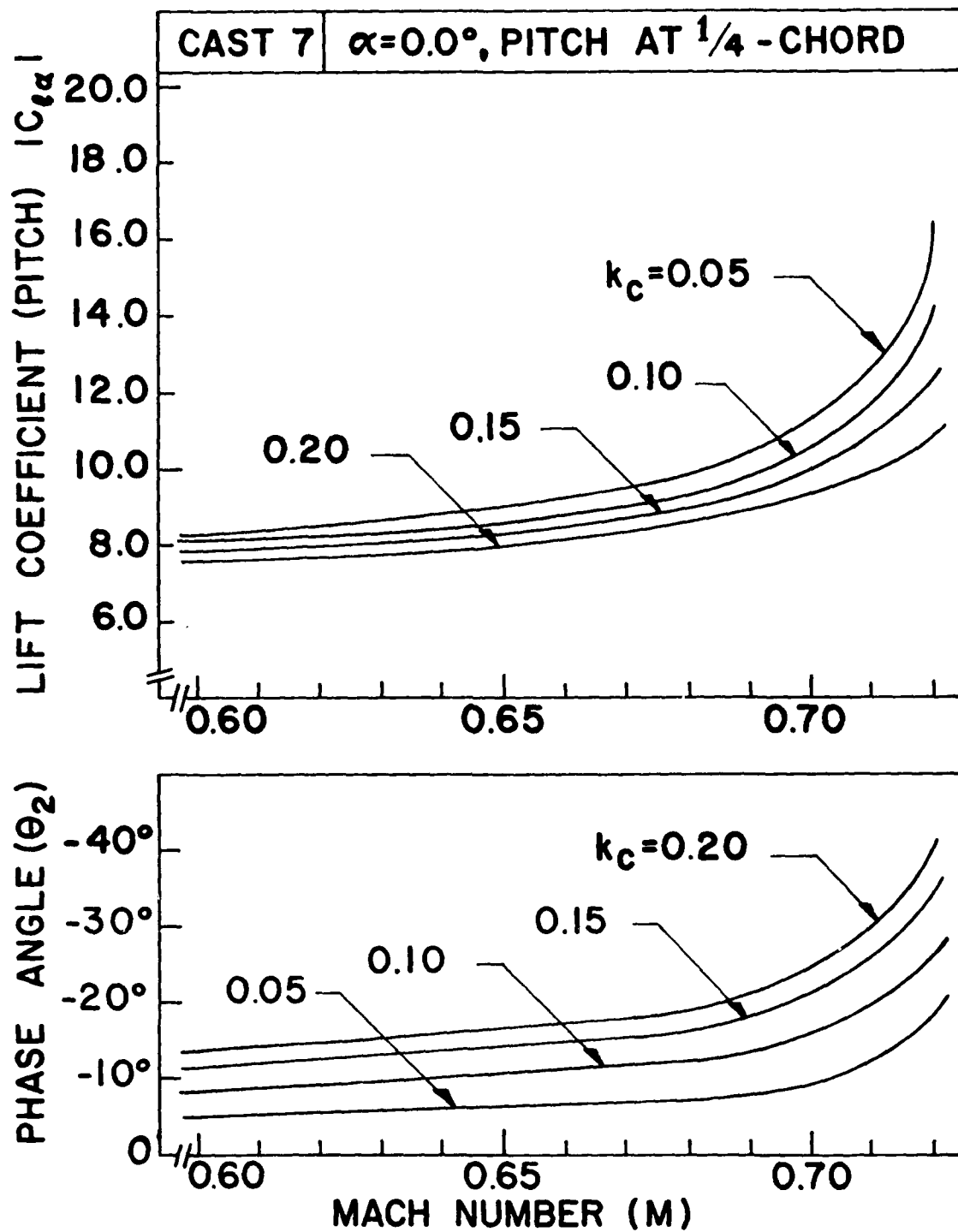


Figure 25. Effect of Mach Number on Lift Coefficient due to Pitching for CAST 7 Airfoil by LTRAN2.

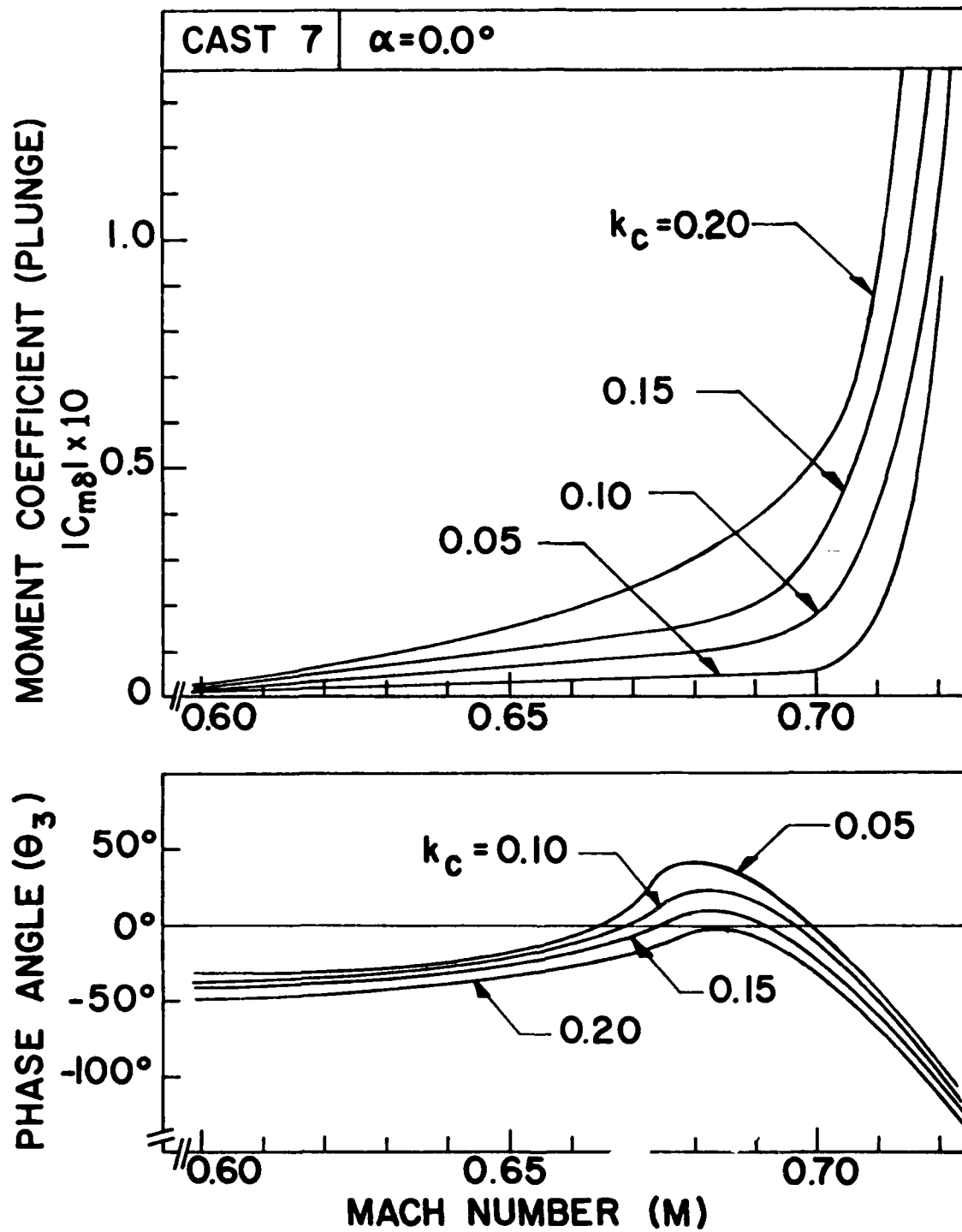


Figure 26. Effect of Mach Number on Moment Coefficient due to Plunging for CAST 7 Airfoil by LTRAN2.

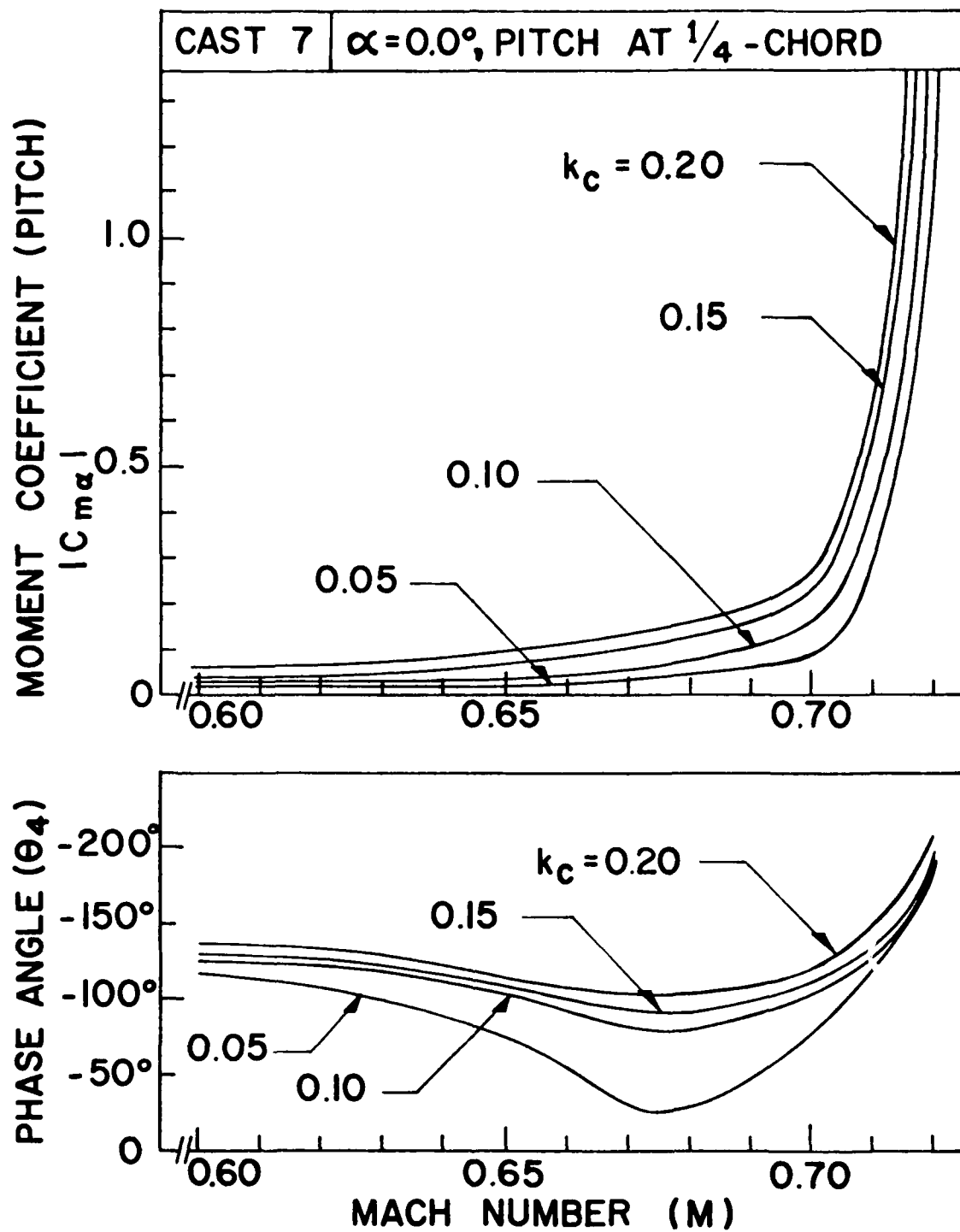


Figure 27. Effect of Mach Number on Moment Coefficient due to Pitching for CAST 7 Airfoil by LTRAN2.



decreases. With the increase in reduced frequency,  $|C_{m\delta}|$  increases whereas  $\theta_3$  decreases. The slopes of all the curves become much steeper when  $M$  is greater than approximately 0.7.

In Figure 27, the magnitude of the moment coefficient  $|C_{m\alpha}|$  about the quarter chord axis due to pitch about the same axis increases as  $M$  increases. The corresponding phase angle  $|\theta_4|$  first decreases and then increases with its minimum at  $M \approx 0.675$ . Both  $|C_{m\alpha}|$  and  $|\theta_4|$  increase when the reduced frequency increases. The slopes for all curves become much steeper when  $M > 0.7$ .

Figures 24 to 27 show that the magnitudes of all the four coefficients increase with the increase in Mach number. Such increase is more rapid in the higher Mach number region. The effect of such changes will reflect on the flutter behavior.

#### 4. Flutter Results

Based on the unsteady aerodynamic coefficients obtained in Table 3 for seven Mach numbers, flutter analysis was performed for the CAST 7 supercritical airfoil. The emphasis was to investigate the effect of Mach number on flutter speed for various values of aeroelastic parameters.

Figure 28 shows the curves for flutter speed and the corresponding reduced frequency versus Mach number for three different values of the position of mass center ( $x_\alpha = 0.1, 0.3, \text{ and } 0.5$ , respectively). The values for  $\mu$ ,  $\omega_h/\omega_\alpha$ , and  $a_h$  were assumed as 100, 0.1, and -0.5, respectively.

In this figure, the flutter speed increases as the mass center approaches the elastic axis or as  $x_\alpha$  becomes smaller. On the other hand, the reduced frequency decreases as  $x_\alpha$  becomes smaller.

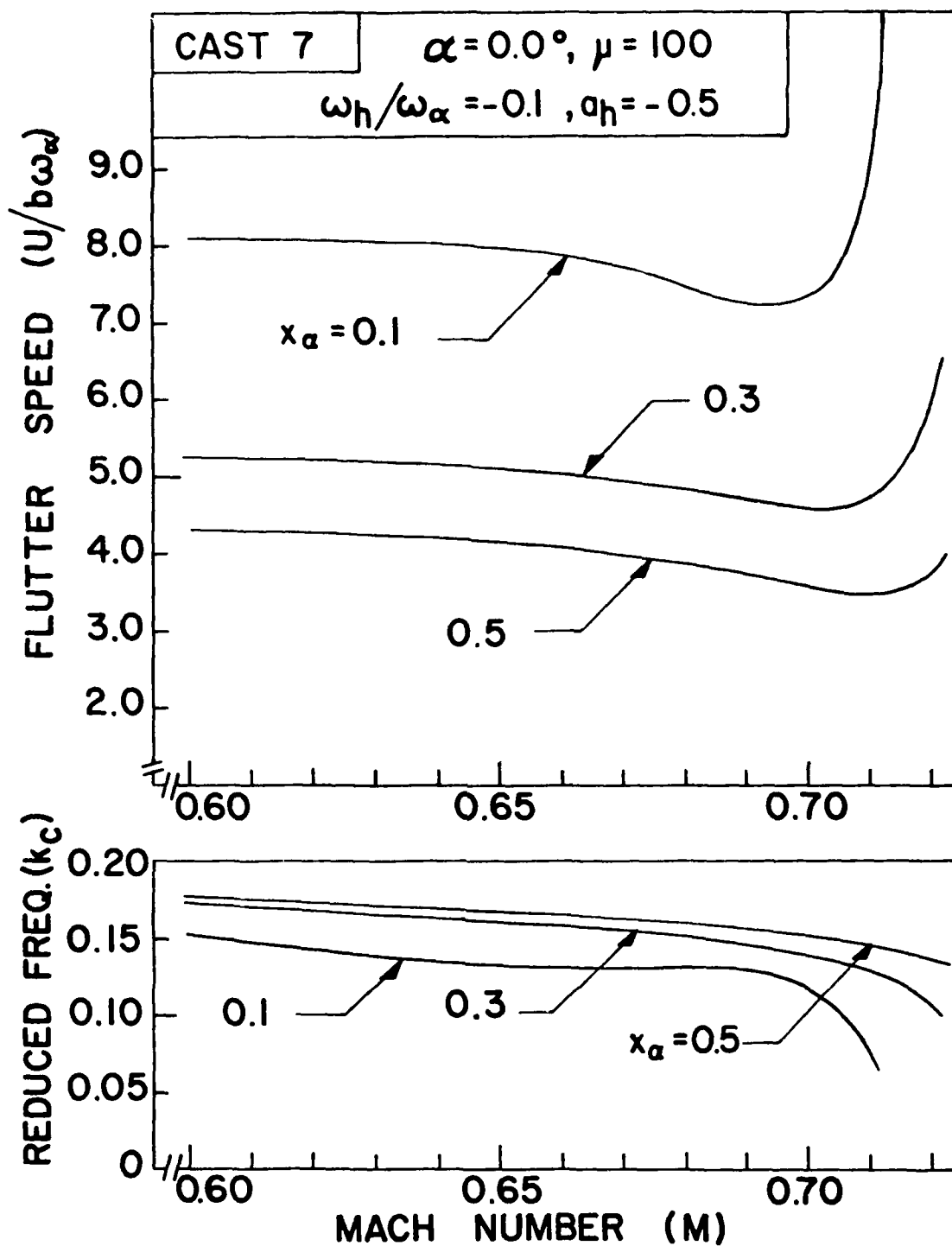


Figure 28. Effect of Mach Number on Flutter Speed for Three Positions of Mass Center for CAST 7 Airfoil by LTRAN2.

All the flutter speed curves present a dip phenomenon. The dip appears to be more pronounced and occurs at relatively lower Mach numbers as the mass center approaches the elastic axis.

Figure 29 shows the curves of flutter speed and the corresponding reduced frequency versus Mach number for three values of airfoil-air mass density ratio ( $\mu = 100, 200, \text{ and } 300$ , respectively). The values for the other aeroelastic parameters  $x_\alpha$ ,  $a_h$ , and  $\omega_h/\omega_\alpha$  were assumed as  $0.5, -0.5$ , and  $0.1$ , respectively.

In this figure, flutter speeds are higher for higher  $\mu$ -values whereas the corresponding reduced frequencies are lower for higher  $\mu$ -values. For low values of  $\mu$ , the  $k_c$ -values corresponding to flutter solution exceed  $0.2$  and are beyond the limitation of LTRAN2. All the three flutter curves present a dip phenomenon with their minimum values occurring near a Mach number of  $0.71$ .

Figure 30 shows the curves of flutter speed and the corresponding reduced frequency versus Mach number for two values of plunge-to-pitch frequency ratio ( $\omega_h/\omega_\alpha = 0.1 \text{ and } 0.2$ , respectively). The values for the other aeroelastic parameters  $\mu$ ,  $x_\alpha$ , and  $a_h$  were assumed as  $100, 0.5$ , and  $-0.5$ , respectively.

In this figure, the flutter speed curve for  $\omega_h/\omega_\alpha = 0.1$  is higher than that for  $\omega_h/\omega_\alpha = 0.2$  whereas the reduced frequency curve for the former case is lower than that for the latter case. Flutter speeds for  $\omega_h/\omega_\alpha > 0.2$  are not obtainable because the corresponding reduced frequencies  $k_c$  exceed  $0.2$ .

Both flutter curves present a clear transonic dip phenomenon with the lowest flutter speed occurring at  $M \approx 0.71$ .

Figure 31 shows the curves of flutter speed and the corresponding reduced frequency versus Mach number for two different positions of elastic

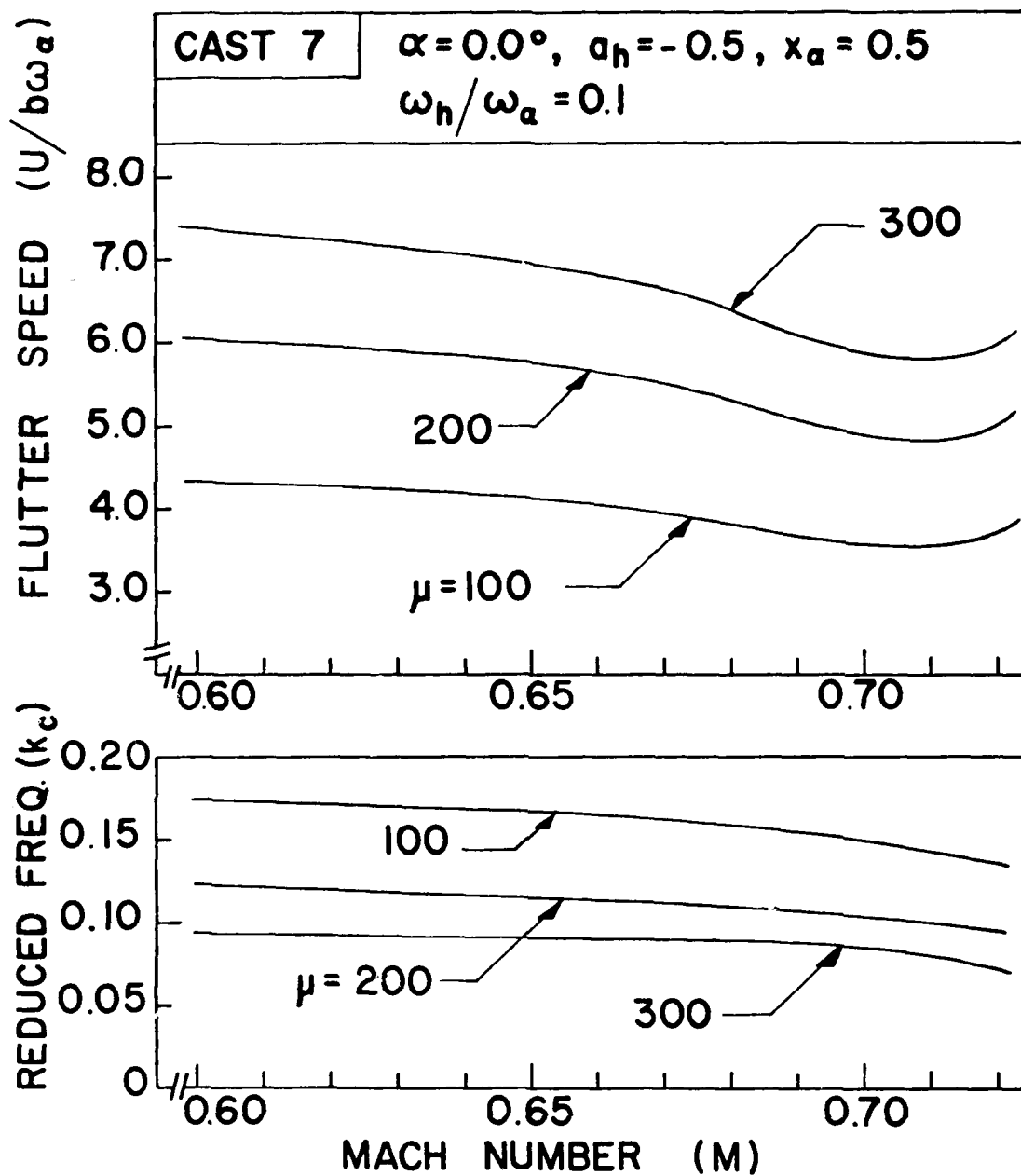


Figure 29. Effect of Mach Number on Flutter Speed for Three Values of Airfoil-Air Mass Density Ratio for CAST 7 Airfoil by LTRAN2.

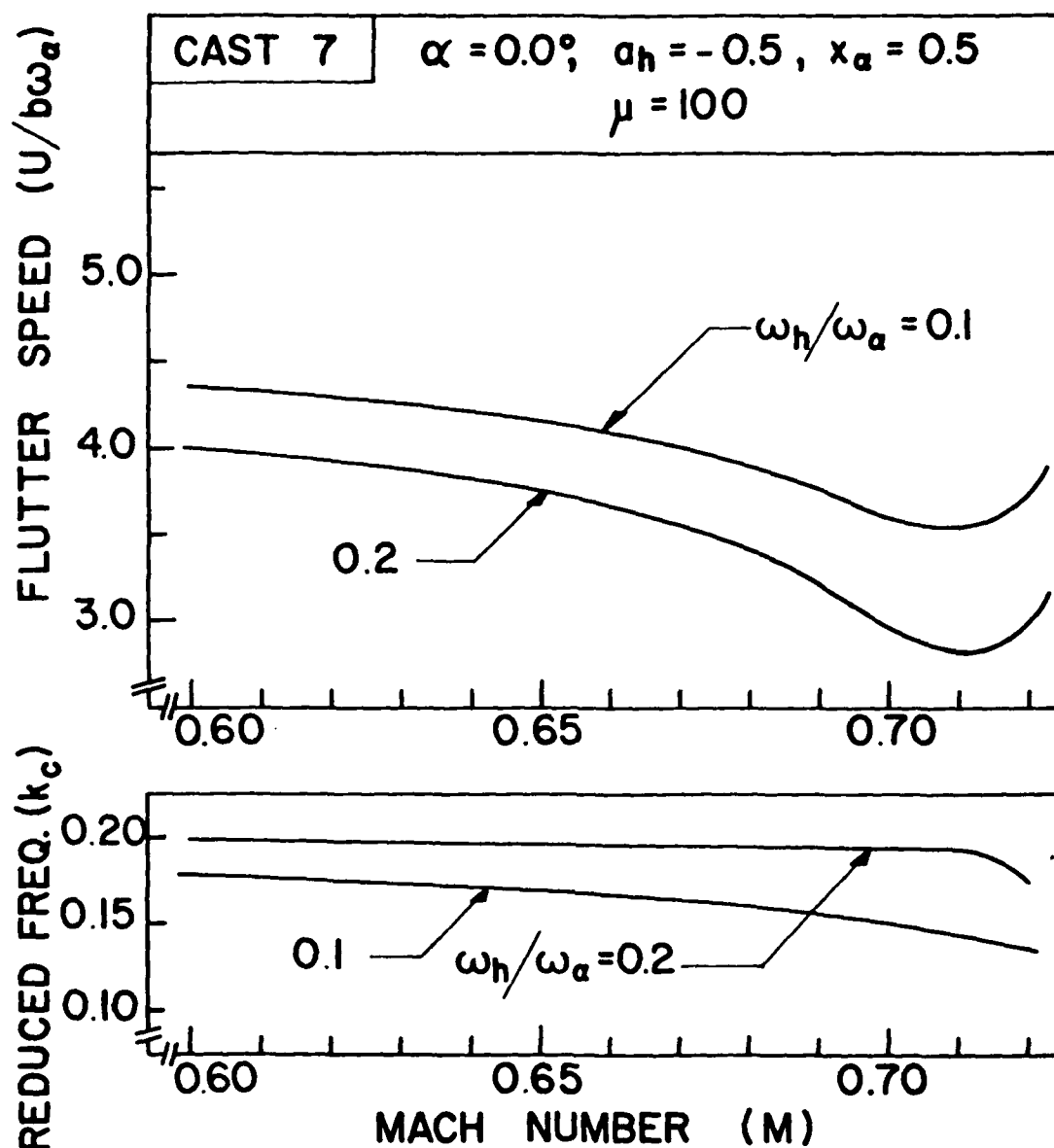


Figure 30. Effect of Mach Number on Flutter Speed for Two Values of Plunge-to-Pitch Frequency Ratio for CAST 7 Airfoil by LTRAN2.

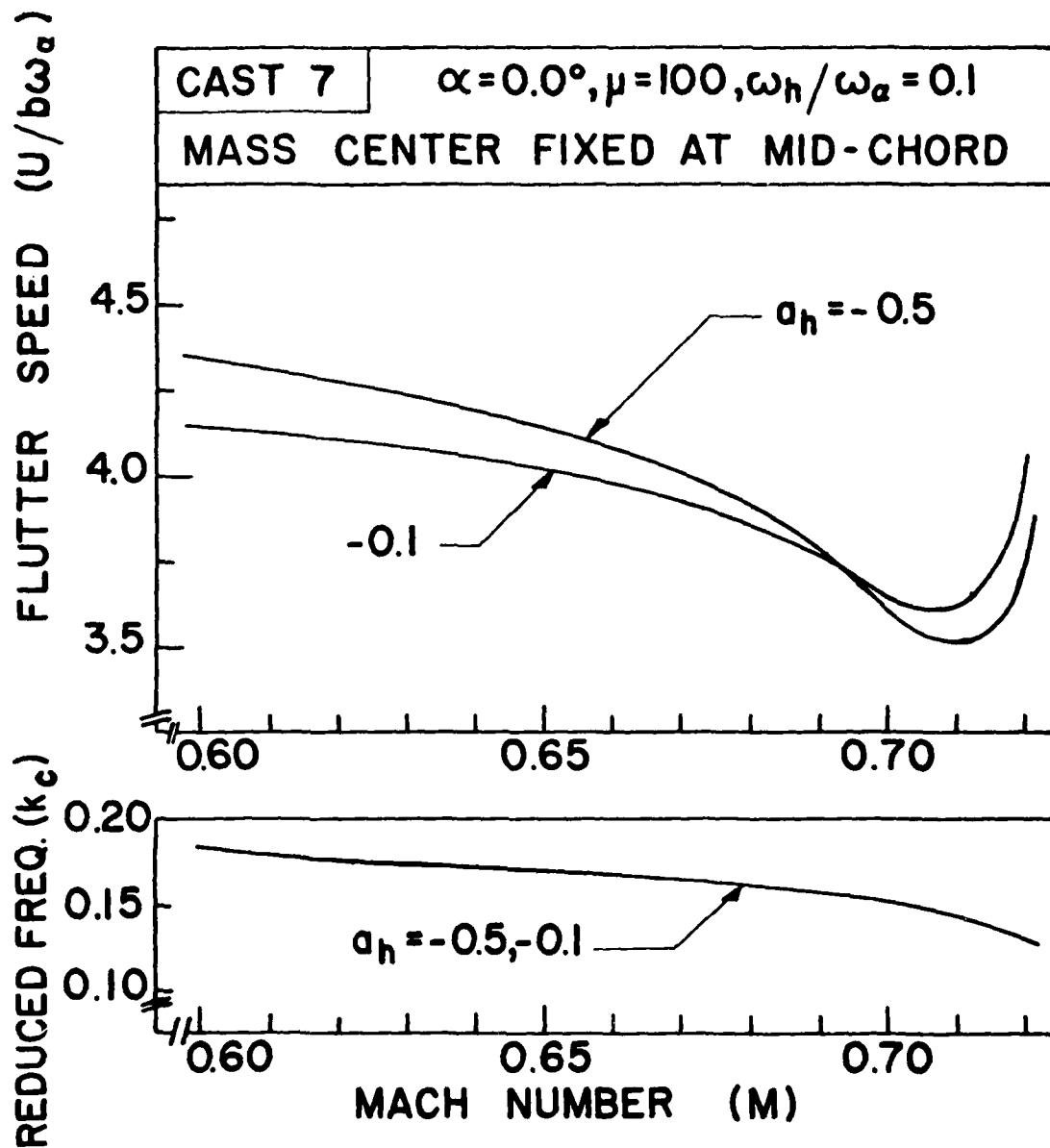


Figure 31. Effect of Mach Number on Flutter Speed for Two Positions of Elastic Axis for CAST 7 Airfoil by LTRAN2.

axis ( $a_h = -0.1$  and  $-0.5$ , respectively). The mass center was fixed at mid-chord. The other aeroelastic parameters,  $\mu$  and  $\omega_h/\omega_\alpha$ , were assumed as 100 and 0.1, respectively.

In this figure, it appears that the change in flutter speed due to variation of  $a_h$  is considerably less than the changes due to variation of the other three aeroelastic parameters as shown in Figures 28, 29, and 30, respectively. The two curves of corresponding reduced frequencies for  $a_h = -0.5$  and  $-0.1$  practically coincide. Again, both flutter curves show a dip in the neighborhood of  $M \approx 0.71$ .

As explained in Reference 29, the transonic dip is caused by the compensating effects of the lift coefficient  $|C_{l\alpha}|$  due to pitch and the position of the center of pressure  $e$  (measured from the leading edge with  $e$  being a fraction of chord and  $c$  being the full chord length). For the CAST 7 airfoil, plots are presented in Figure 32 to show such compensating effects.

In this figure, it is first seen that  $|C_{l\alpha}|$  increases quite rapidly as  $M$  becomes greater than approximately 0.68. Such increase has an effect of reducing the flutter speed. It is then seen that  $e$  remains as 0.25 (center of pressure remains at 1/4-chord) until  $M \approx 0.7$ . When  $M > 0.7$ ,  $e$  increases rapidly, i.e., the center of pressure moves aft. Such movement has an effect of increasing the flutter speed. The net effects of both  $|C_{l\alpha}|$  and  $e$  are shown in the flutter curve with the transonic dip.

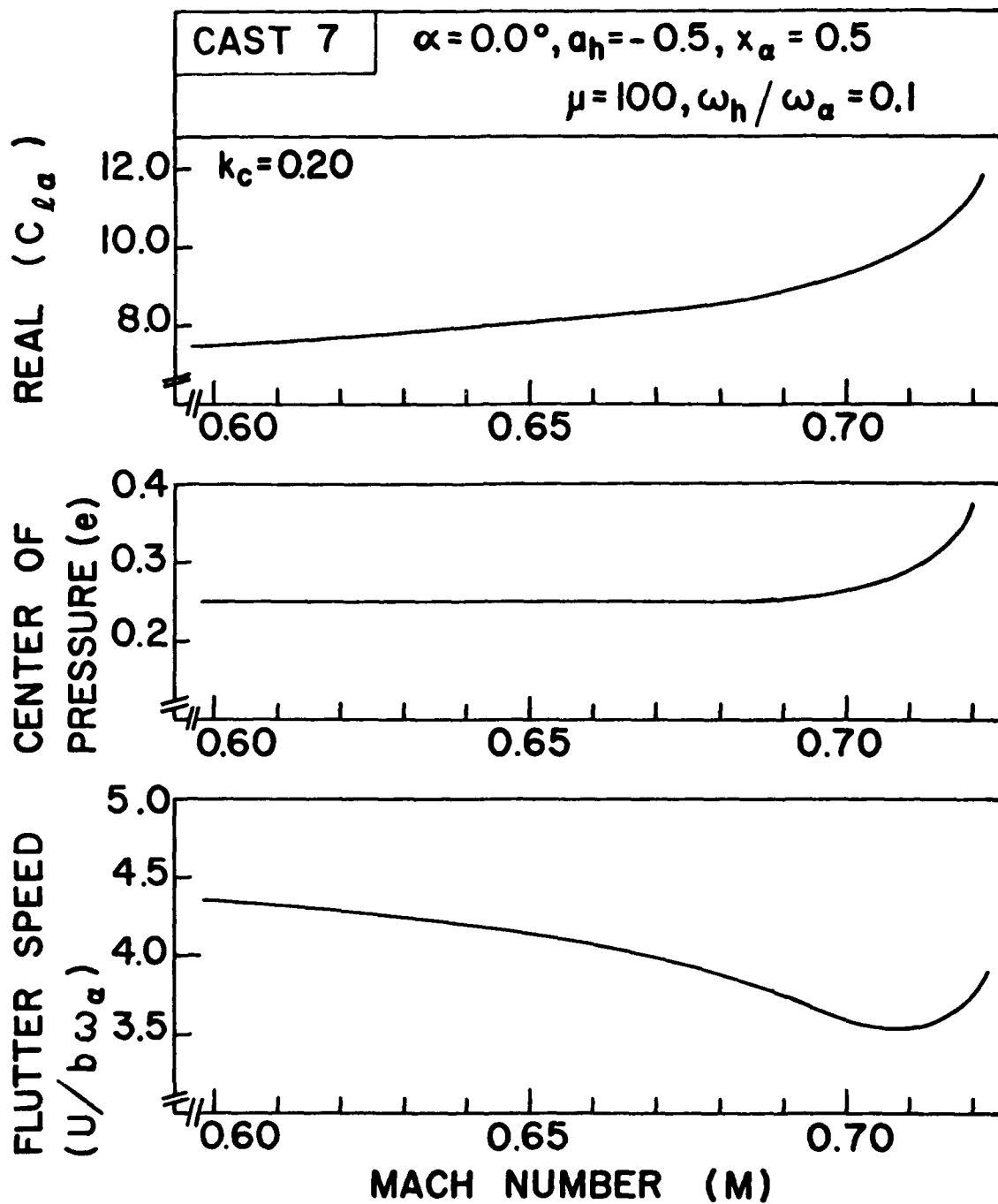


Figure 32. Compensating Effects of  $\text{Re } (C_{l\alpha})$  and the Position of Center of Pressure on Flutter Speed for CAST 7 Airfoil by LTRAN2.



## SECTION VI

### FLUTTER ANALYSIS OF A TF-8A WING SECTION

The TF-8A supercritical wing was developed by NASA and it has been subjected to various aerodynamic and aeroelastic studies (References 12, 20, 21, and 22). In this study, flutter analysis of the typical TF-8A wing section at the 65.3% semispan station was carried out by using STRANS2 and UTRANS2. Flutter results for the same wing section were obtained by Ashley in Reference 22 by using steady wind tunnel data.

It was noticed during flight tests of the TF-8A wing that because of twist of the wing, when corresponding to a zero mean angle of attack of the zero-twist station at the 1-g design condition, the angle of attack at the 65.3% semispan station was  $-3.0^\circ$  (Figure 4 of Reference 26). Based on the wind tunnel test data from Reference 26, a transonic dip was found for the TF-8A wing section in Reference 22. Therefore, the flutter analysis for the present wing section was performed at  $\alpha = -3.0^\circ$  as well as  $\alpha = 0.0^\circ$ .

In this flutter analysis, two degrees of freedom were assumed, plunge and pitch about the 1/4-chord axis. Seven Mach numbers between 0.7 and 0.8 were considered. Emphasis was placed upon the effect of Mach number on the flutter speed.

#### 1. Airfoil Configuration

The data for the configuration of the TF-8A wing section at the 65.3% semispan station were taken from Table 2 of Reference 26. Based on these

measured data, the coefficients in Equation 9 for one-segment fitting of the thickness and camber were provided by Dr. Olsen of Flight Dynamics Laboratory.

The coefficients for the thickness function are:  $a_0 = 0.3725526$ ;  $a_1 = 0.0$ ;  $a_2 = -0.5942223$ ;  $a_3 = 0.9453364$ ;  $a_4 = -1.3072624$ ; and  $a_5 = 0.5916402$ . The coefficients for the camber function are:  $b_1 = 0.0$ ;  $b_2 = 0.0272615$ ;  $b_3 = -0.2440222$ ;  $b_4 = 0.6069286$ ; and  $b_5 = -0.3901679$ . A plot of the configuration is given in Figure 33. The maximum thickness-to-chord ratio is 7.9%. The nose is relatively blunt.

## 2. Steady Pressure Curves

The present TF-8A wing section has a blunter nose than other supercritical airfoils such as MBB A-3 and CAST 7. It is desirable to evaluate the applicability of STRANS2 and UTRANS2 for this section.

Figure 34 shows two sets of steady pressure curves, one obtained by STRANS2 and the other by experiment in Reference 26. The values for Mach number and mean angle of attack were 0.5 and  $-0.75^\circ$ , respectively.

In this figure, the two sets of curves agree fairly well in overall shape. The discrepancy appears to be comparatively larger on the lower surface near the trailing edge. Similar discrepancy was found between LTRAN2 and experimental steady pressure curves obtained for the CAST 7 airfoil (Figure 22).

Reasons for the discrepancy between the two sets of curves can be attributed to: (1) viscous effects which are not considered in STRANS2; (2) small disturbance theory used in STRANS2; and (3) possible losses of accuracy during both the computational and experimental process.

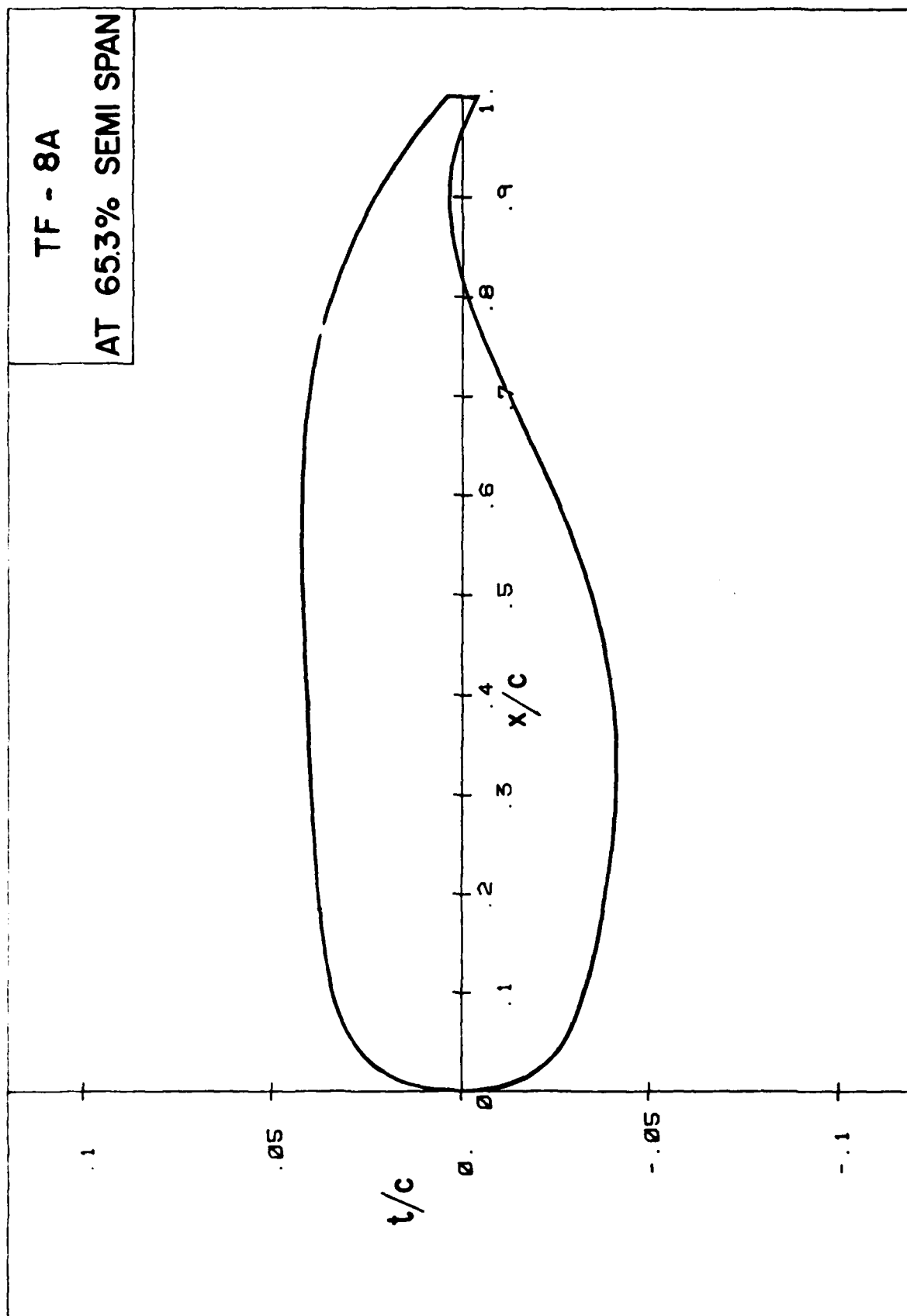


Figure 33. Airfoil Configuration for TF-8A Wing Section at 65.3% Semispan Station.

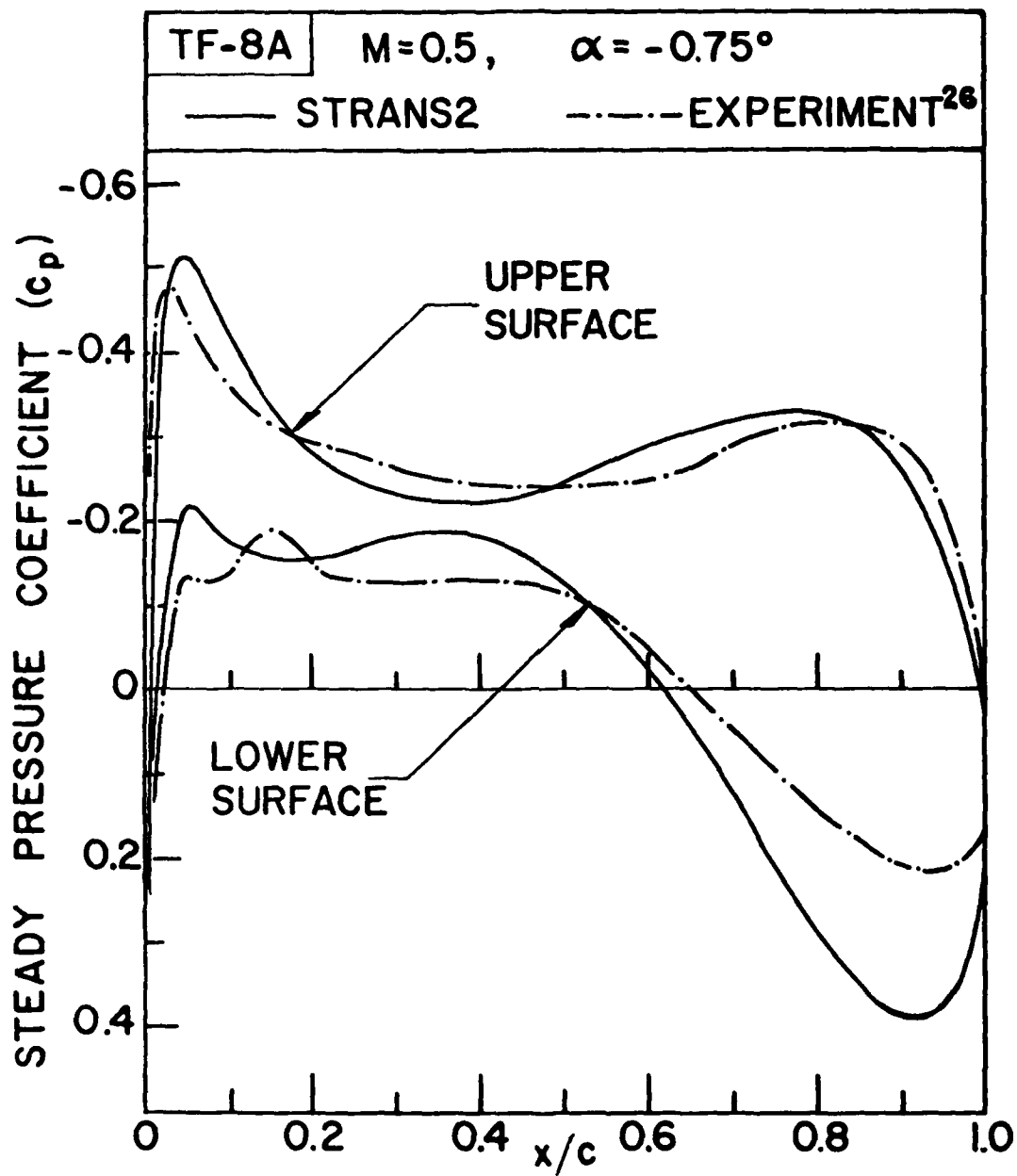


Figure 34. Comparison between Steady Pressure Curves by STRANS2 and Experiment for TF-8A Airfoil.

Figure 35 shows the upper and lower surface steady pressure curves obtained for the TF-8A wing section for seven Mach numbers (0.70, 0.74, 0.76, 0.77, 0.78, 0.79, and 0.80, respectively) at  $\alpha = -3.0^\circ$  by STRANS2. The steady pressure curves on the upper surface gradually increase with the increase in Mach number. The lower surface steady pressure curves have shocks near the leading edge. With the increase in Mach number, the shock moves toward the trailing edge with decreasing strength.

Figure 36 shows the upper and lower surface steady pressure curves obtained for the TF-8A wing section for seven Mach numbers (0.70, 0.72, 0.74, 0.76, 0.78, 0.80, and 0.82, respectively) at  $\alpha = 0.0^\circ$  by STRANS2. With the increase in Mach number, the upper surface pressure curves change much more pronounced than the lower surface pressure curves. For  $M > 0.76$ , each curve appears to have two shocks on the upper surface, one near the leading edge and the other near the trailing edge. The shock near the leading edge decreases in strength and moves toward the trailing edge as Mach number increases. The shock near the trailing edge increases in strength and moves toward the trailing edge as the Mach number increases.

The shocks at the leading edge were encountered at all Mach numbers considered here and for both angles of attack (on the lower surface at  $\alpha = -3.0^\circ$  and on the upper surface at  $\alpha = 0^\circ$ ). They seem to be due to the effect of the blunt nose of the airfoil.

### 3. Unsteady Aerodynamic Coefficients

Four unsteady aerodynamic coefficients,  $C_{l\delta}$ ,  $C_{l\alpha}$ ,  $C_{m\delta}$ , and  $C_{m\alpha}$ , were obtained for the TF-8A wing section by UTRANS2. The airfoil was pitched about

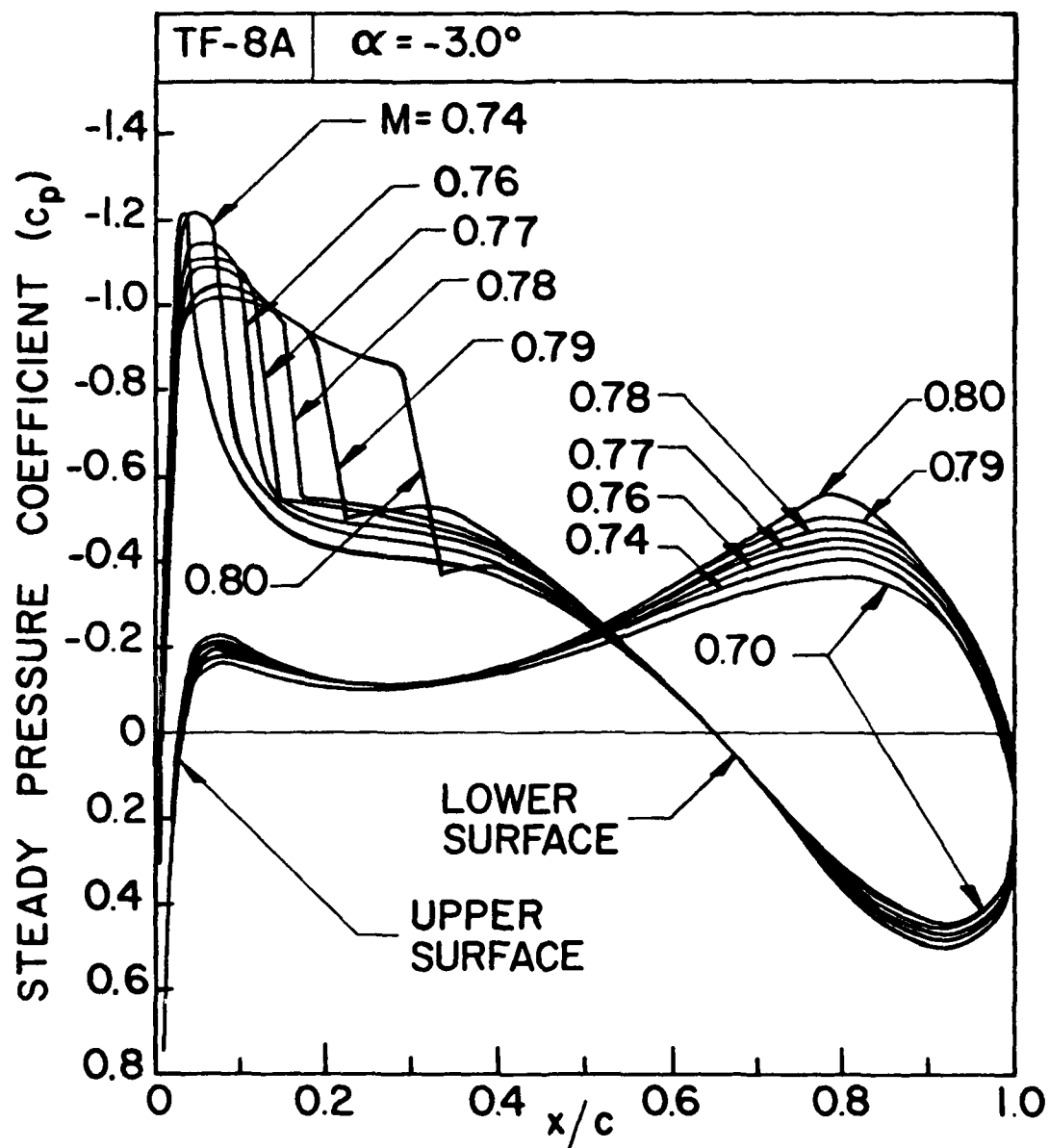


Figure 35. Effect of Mach Number on Steady Pressure Curves for TF-8A Airfoil at  $\alpha = -3.0^\circ$  by STRANS2.

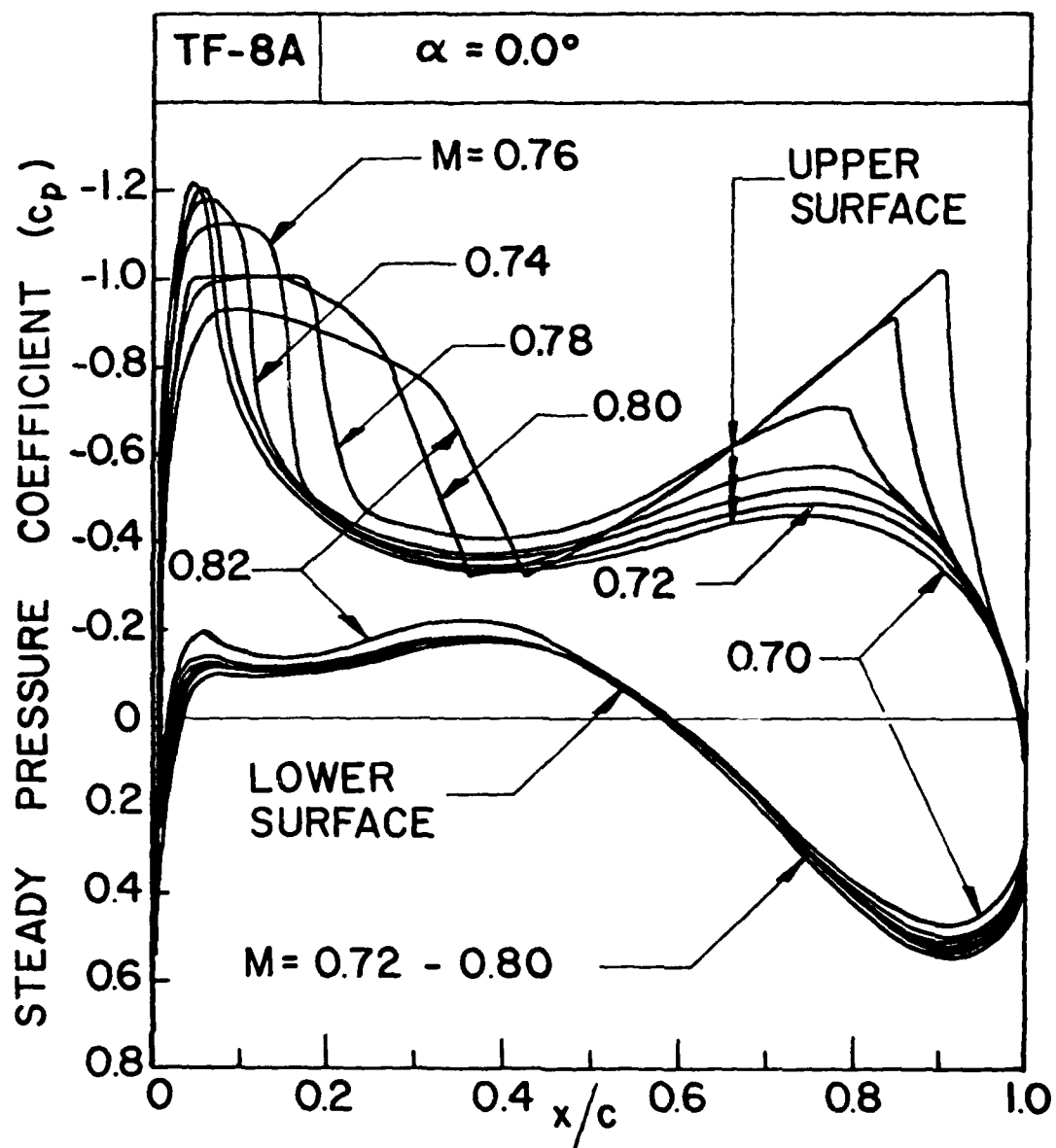


Figure 36. Effect of Mach Number on Steady Pressure Curves for TF-8A Airfoil at  $\alpha = 0.0^\circ$  by STRANS2.

the quarter chord at various Mach numbers for two angles of attack ( $\alpha = -3.0^\circ$  and  $\alpha = 0^\circ$ ).

Mach numbers considered were 0.7, 0.74, 0.76, 0.77, 0.78, 0.79, and 0.80 for  $\alpha = -3.0^\circ$  and 0.7, 0.72, 0.74, 0.76, and 0.78 for  $\alpha = 0.0^\circ$ . The reduced frequencies assumed for both cases were 0.0, 0.05, 0.10, 0.15, and 0.20. Table 4 and Table 5 give the four unsteady coefficients obtained at  $\alpha = -3.0^\circ$  and  $\alpha = 0.0^\circ$ , respectively. These four coefficients and their corresponding phase angles are also plotted against Mach number in Figures 37, 38, 39, and 40, respectively.

In Figure 37, the magnitude of the lift coefficient due to plunge  $|C_{\delta}|$  for  $\alpha = -3.0^\circ$  increases very slightly as the Mach number increases. The curve shows a bump in the neighborhood of  $M = 0.78$ . The corresponding phase angle  $\theta_1$  decreases slightly as  $M$  increases. As the reduced frequency increases,  $|C_{\delta}|$  increases whereas  $\theta_1$  decreases. Also shown in the same figure are those curves for  $\alpha = 0.0^\circ$ . In this case, slightly flatter bumps in the  $|C_{\delta}|$  curves appear in the neighborhood of  $M = 0.76$ .

In Figure 38, the magnitude of the lift coefficient  $|C_{\delta\alpha}|$  due to pitch about the quarter chord axis for  $\alpha = -3.0^\circ$  increases as  $M$  increases. Again, bumps are present in the neighborhood of  $M = 0.78$ . The corresponding phase angle  $|\theta_2|$  increases as  $M$  increases. As the reduced frequency increases,  $|C_{\delta\alpha}|$  decreases whereas  $|\theta_2|$  increases. Also shown in the same figure are those curves for  $\alpha = 0.0^\circ$ . The bumps are much milder and appear at lower  $M$  than those for  $\alpha = -3.0^\circ$ .

In Figure 39, the magnitude of the moment coefficient  $|C_{m\delta}|$  about the quarter chord axis due to plunge for  $\alpha = -3.0^\circ$  increases as  $M$  increases. The corresponding phase angle  $\theta_3$  decreases as  $M$  increases. As the reduced frequency increases,  $|C_{m\delta}|$  increases whereas  $\theta_3$  does not show any clear



Table 4. Aerodynamic Coefficients for TF-8A Airfoil for Various Mach Numbers at  $\alpha = -3.0^\circ$  by UTRANS2

	Mach Number	Reduced Frequency ( $k_c$ )									
		0.0		0.05		0.10		0.15		0.20	
		Real	Imag.	Real	Imag.	Real	Imag.	Real	Imag.	Real	Imag.
$C_{x_\alpha}$	.70	0.0	0.0	0.057	0.471	0.218	0.828	0.395	1.094	0.549	1.312
	.74	0.0	0.0	0.081	0.485	0.251	0.844	0.453	1.104	0.619	1.290
	.76	0.0	0.0	0.088	0.496	0.279	0.864	0.494	1.113	0.668	1.268
	.77	0.0	0.0	0.095	0.513	0.299	0.889	0.531	1.138	0.722	1.276
	.78	0.0	0.0	0.108	0.535	0.335	0.909	0.574	1.132	0.752	1.283
	.79	0.0	0.0	0.105	0.510	0.323	0.858	0.543	1.067	0.697	1.201
	.80	0.0	0.0	0.113	0.516	0.340	0.854	0.555	1.057	0.706	1.186
$C_{y_\alpha}$	.70	9.444	0.0	9.430	-1.634	8.219	-1.674	7.568	-1.941	6.971	-2.043
	.74	10.174	0.0	9.358	-1.462	8.455	-2.095	7.629	-2.368	6.886	-2.438
	.76	10.631	0.0	9.649	-1.689	8.581	-2.376	7.634	-2.631	6.796	-2.661
	.77	11.161	0.0	10.034	-1.876	8.840	-2.640	7.776	-2.893	6.851	-2.891
	.78	11.768	0.0	10.440	-2.141	9.068	-2.917	7.904	-3.156	6.889	-3.130
	.79	11.236	0.0	9.904	-2.056	8.560	-2.761	7.436	-2.934	6.486	-2.861
	.80	11.366	0.0	9.939	-2.124	8.552	-2.843	7.394	-3.013	6.424	-2.932
$C_{m_\xi}$	.70	0.0	0.0	0.004	-0.001	0.011	-0.004	0.022	-0.012	0.035	-0.021
	.74	0.0	0.0	0.003	-0.007	0.010	-0.015	0.019	-0.026	0.029	-0.039
	.76	0.0	0.0	0.002	-0.012	0.007	-0.026	0.014	-0.040	0.021	-0.056
	.77	0.0	0.0	0.002	-0.015	0.006	-0.029	0.012	-0.046	0.018	-0.063
	.78	0.0	0.0	0.001	-0.016	0.006	-0.032	0.011	-0.049	0.018	-0.066
	.79	0.0	0.0	-0.002	-0.030	-0.005	-0.054	-0.008	-0.075	-0.007	-0.094
	.80	0.0	0.0	-0.006	-0.042	-0.018	-0.073	-0.028	-0.096	-0.033	-0.116
$C_{m_{\eta}}$	.70	-0.013	0.0	-0.019	-0.096	-0.042	-0.170	-0.066	-0.240	-0.090	-0.301
	.74	-0.115	0.0	-0.122	-0.086	-0.139	-0.165	-0.161	-0.234	-0.184	-0.293
	.76	-0.238	0.0	-0.235	-0.070	-0.243	-0.143	-0.256	-0.209	-0.273	-0.266
	.77	-0.285	0.0	-0.277	-0.065	-0.283	-0.136	-0.293	-0.203	-0.307	-0.262
	.78	-0.311	0.0	-0.301	-0.066	-0.305	-0.141	-0.316	-0.209	-0.331	-0.270
	.79	-0.611	0.0	-0.560	-0.003	-0.522	-0.042	-0.499	-0.099	-0.484	-0.163
	.80	-0.890	0.0	-0.797	0.073	-0.718	0.057	-0.658	0.011	-0.615	-0.059

AD-A100 334

PURDUE UNIV LAFAYETTE IND SCHOOL OF AERONAUTICS AND --ETC F/8 20/4  
FLUTTER ANALYSIS OF TWO-DIMENSIONAL AND TWO-DEGREE-OF-FREEDOM M--ETC(U)  
MAR 81 T Y YANG, A G STRIZ, P GURUSWAMY AFOSR-78-3523

UNCLASSIFIED

AFWAL-TR-81-3004

NL

2 OF 2

AD A  
100334



END

DATE

FILED

7-81

DTIC

Table 5. Aerodynamic Coefficients for TF-8A Airfoil for  
Various Mach Numbers at  $\alpha = 0.0^\circ$  by UTRANS2

Mach Number		Reduced Frequency ( $k_c$ )									
		0.0		0.05		0.10		0.15		0.20	
		Real	Imag.	Real	Imag.	Real	Imag.	Real	Imag.	Real	Imag.
$C_{z_\delta}$	.70	0.0	0.0	0.064	0.479	0.217	0.830	0.403	1.086	0.551	1.304
	.72	0.0	0.0	0.075	0.478	0.229	0.850	0.436	1.112	0.605	1.301
	.74	0.0	0.0	0.086	0.493	0.263	0.862	0.483	1.108	0.661	1.261
	.76	0.0	0.0	0.098	0.522	0.298	0.902	0.543	1.156	0.759	1.282
	.78	0.0	0.0	0.106	0.516	0.328	0.877	0.581	1.087	0.765	1.162
$C_{z_\alpha}$	.70	9.376	0.0	9.329	-0.620	8.122	-1.656	7.483	-1.934	6.888	-2.041
	.72	9.857	0.0	9.136	-1.294	8.345	-1.903	7.595	-2.194	6.904	-2.286
	.74	10.354	0.0	9.451	-1.540	8.493	-2.196	7.633	-2.476	6.860	-2.558
	.76	11.202	0.0	10.129	-1.890	8.916	-2.699	7.830	-2.995	6.880	-3.042
	.78	11.503	0.0	10.100	-2.160	8.672	-2.985	7.450	-3.210	6.369	-3.187
$C_{m_\delta}$	.70	0.0	0.0	0.003	-0.004	0.010	-0.011	0.019	-0.019	0.031	-0.031
	.72	0.0	0.0	0.003	-0.006	0.010	-0.014	0.019	-0.024	0.029	-0.037
	.74	0.0	0.0	0.001	-0.016	0.004	-0.031	0.008	-0.047	0.011	-0.064
	.76	0.0	0.0	-0.001	-0.026	-0.002	-0.049	-0.003	-0.072	-0.008	-0.093
	.78	0.0	0.0	-0.005	-0.042	-0.015	-0.077	-0.031	-0.107	-0.054	-0.131
$C_{m_\alpha}$	.70	-0.072	0.0	-0.078	-0.091	-0.095	-0.157	-0.115	-0.225	-0.136	-0.284
	.72	-0.110	0.0	-0.115	-0.082	-0.131	-0.159	-0.152	-0.226	-0.175	-0.285
	.74	-0.316	0.0	-0.304	-0.050	-0.303	-0.111	-0.310	-0.168	-0.322	-0.216
	.76	-0.545	0.0	-0.513	-0.009	-0.490	-0.049	-0.478	-0.093	-0.476	-0.128
	.78	-0.926	0.0	-0.838	0.076	-0.769	0.075	-0.723	0.056	-0.697	0.064

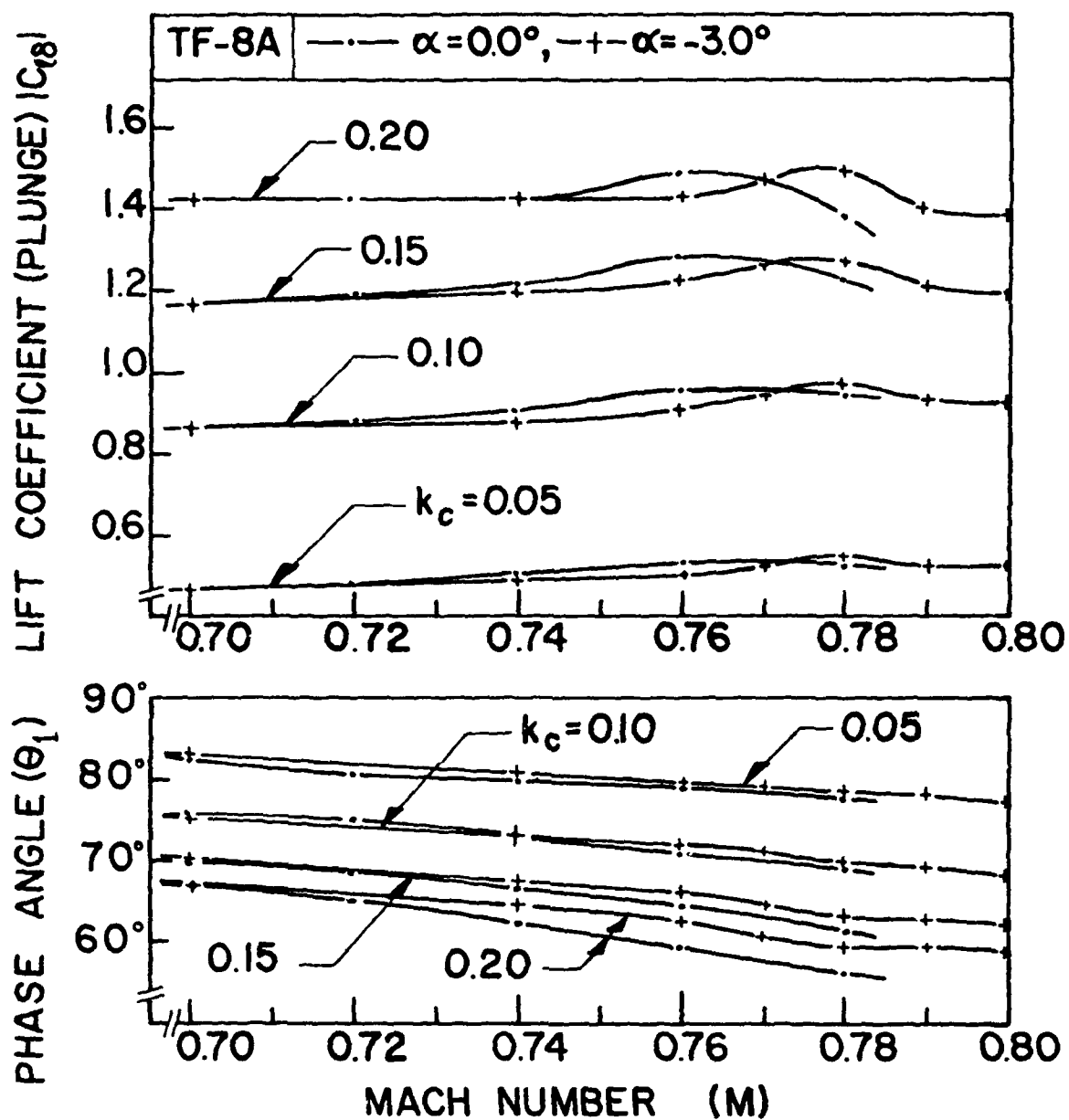


Figure 37. Effect of Mach Number on Lift Coefficient due to Plunging for TF-8A Airfoil by UTRANS2.

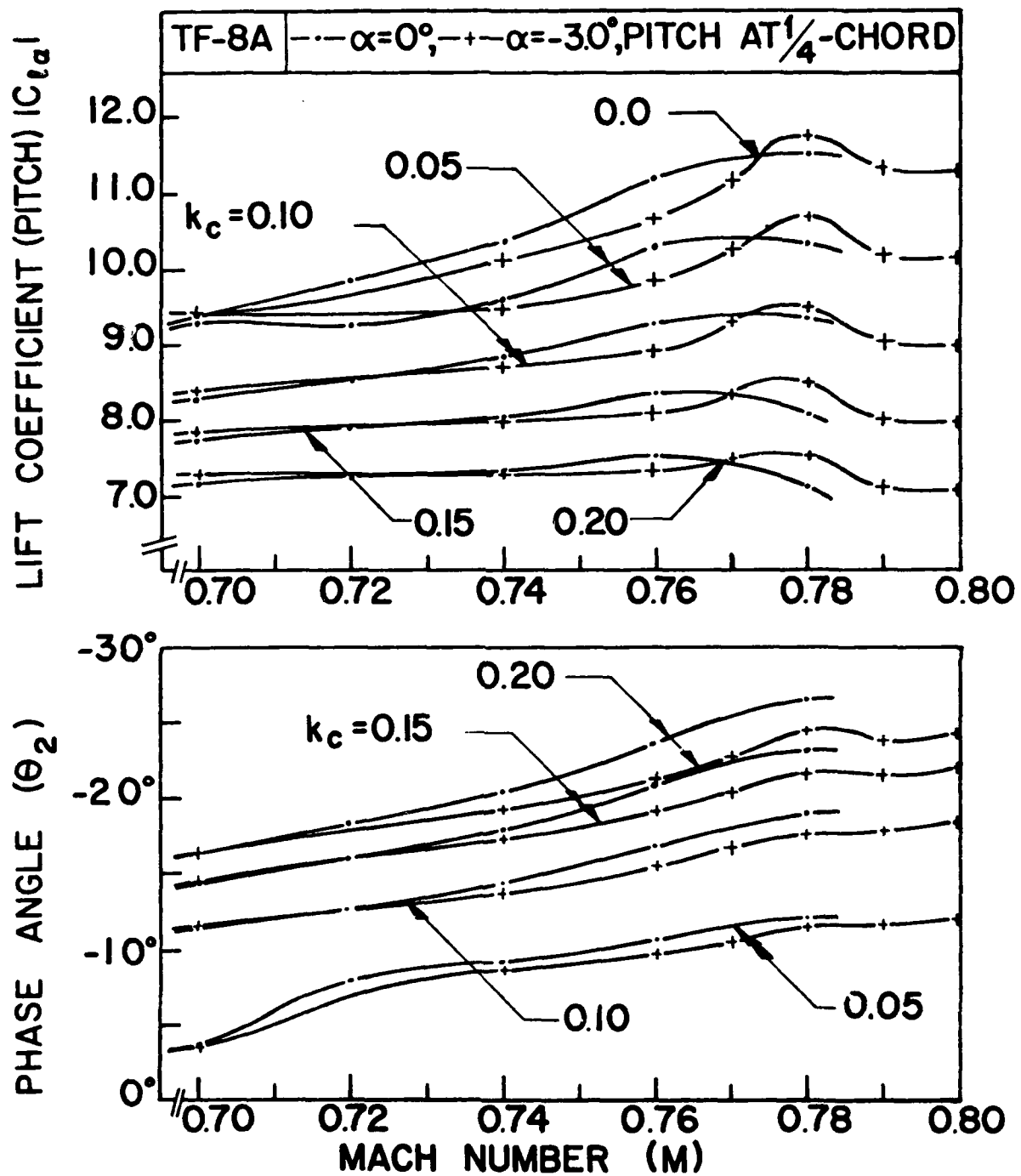


Figure 38. Effect of Mach Number on Lift Coefficient due to Pitching for TF-8A Airfoil by UTRANS2.

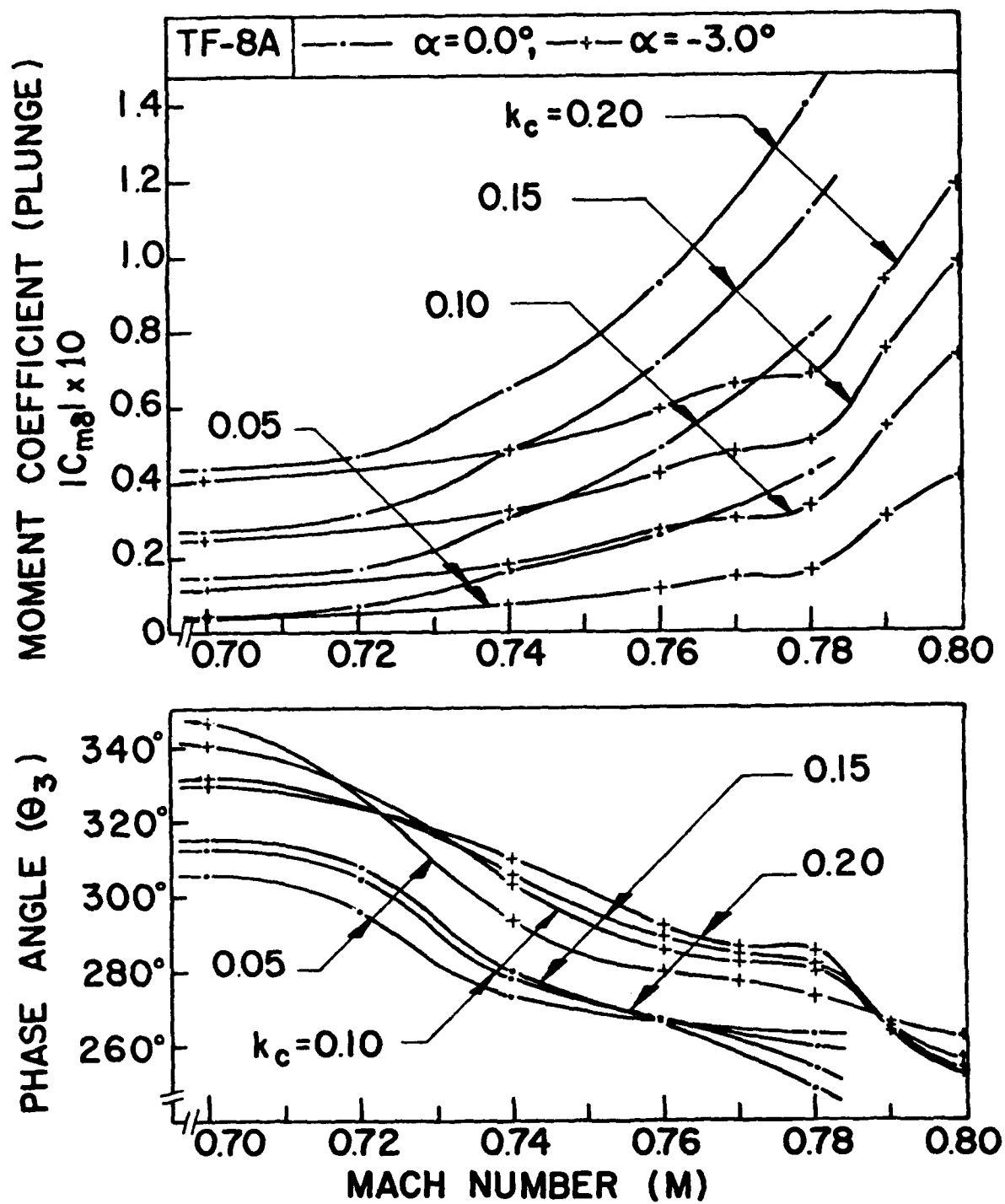


Figure 39. Effect of Mach Number on Moment Coefficient due to Plunging for TF-8A Airfoil by UTRANS2.

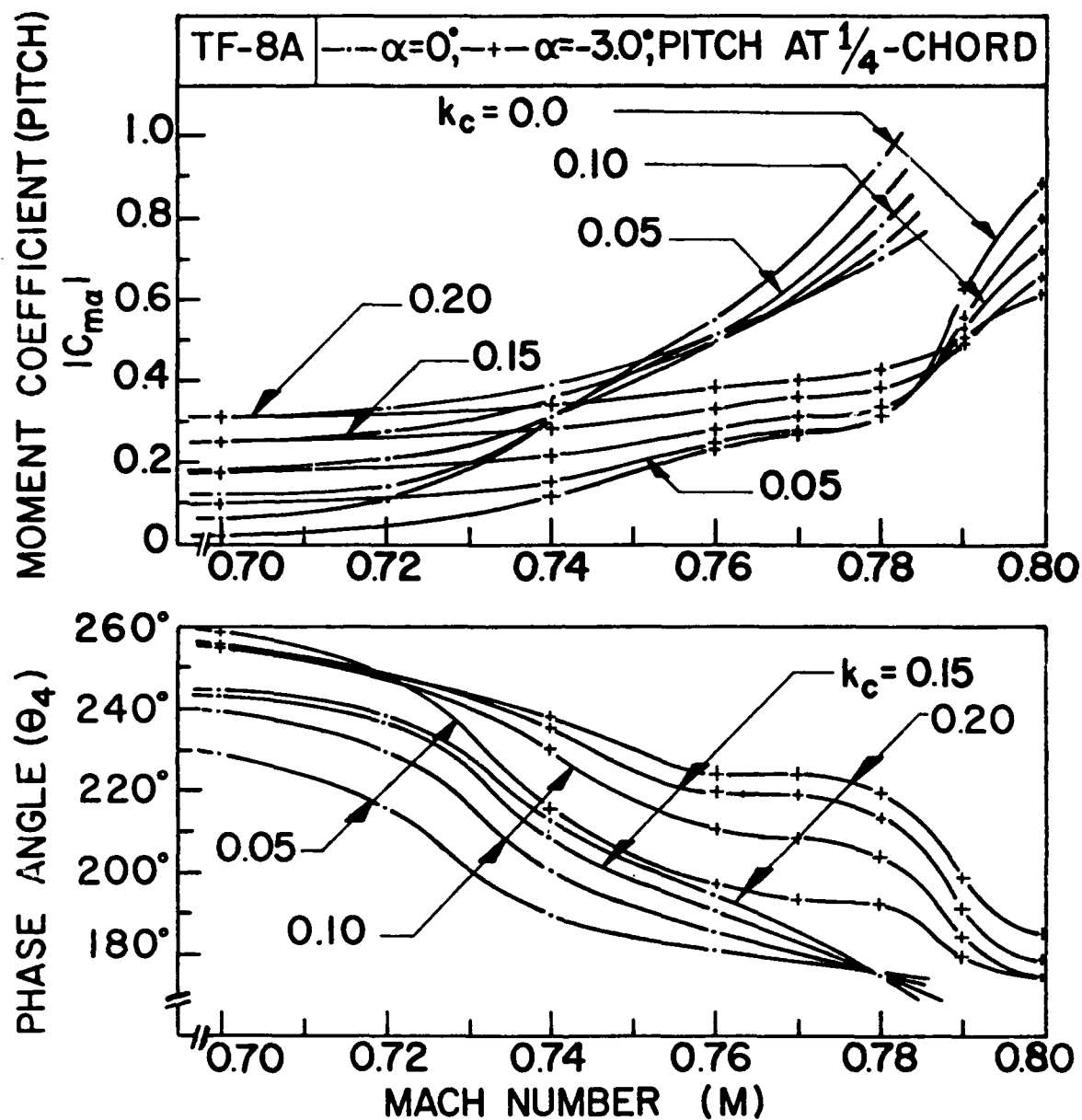


Figure 40. Effect of Mach Number on Moment Coefficient due to Pitching for TF-8A Airfoil by UTRANS2.

trend. Also shown in the same figure are those curves for  $\alpha = 0.0^\circ$ .

These curves show a similar trend as those for  $\alpha = -3.0^\circ$  but are smoother.

In Figure 40, the magnitude of the moment coefficient  $|C_{m\alpha}|$  about the quarter chord axis due to pitch about the same axis for  $\alpha = -3.0^\circ$  increases as  $M$  increases. The corresponding phase angle  $\theta_4$  decreases as  $M$  increases. As  $k_c$  increases,  $|C_{m\alpha}|$  increases when  $M < 0.785$  approximately and decreases when  $M > 0.785$  approximately. As  $k_c$  increases,  $\theta_4$  increases when  $M > 0.72$ . Also shown in the same figure are those curves for  $\alpha = 0.0^\circ$ . Both sets of curves show a similar trend. However, the crossover of the  $|C_{m\alpha}|$ -curves for  $\alpha = 0.0^\circ$  takes place at  $M \approx 0.75$  and the crossover of the  $\theta_4$ -curves takes place at  $M \approx 0.78$ .

#### 4. Flutter Results

Based on the unsteady aerodynamic coefficients obtained for various Mach numbers in Tables 4 and 5 for  $\alpha = -3.0^\circ$  and  $0.0^\circ$ , respectively, flutter analysis was carried out for the TF-8A wing section. The emphasis was to investigate the effect of Mach number on flutter speed for various values of aeroelastic parameters.

Figure 41 shows curves of flutter speed and corresponding reduced frequency versus Mach number at  $\alpha = -3.0^\circ$  for four values of the position of mass center ( $x_\alpha = 0.3, 0.4, 0.5$ , and  $0.6$ ). The values for  $\mu$ ,  $\omega_h/\omega_\alpha$ , and  $a_h$  were assumed as 100, 0.1, and -0.5, respectively.

In this figure, the flutter speed curves shift to higher levels as the mass center moves toward the elastic axis or as  $x_\alpha$  decreases. The corresponding reduced frequency curves show a reversed trend.



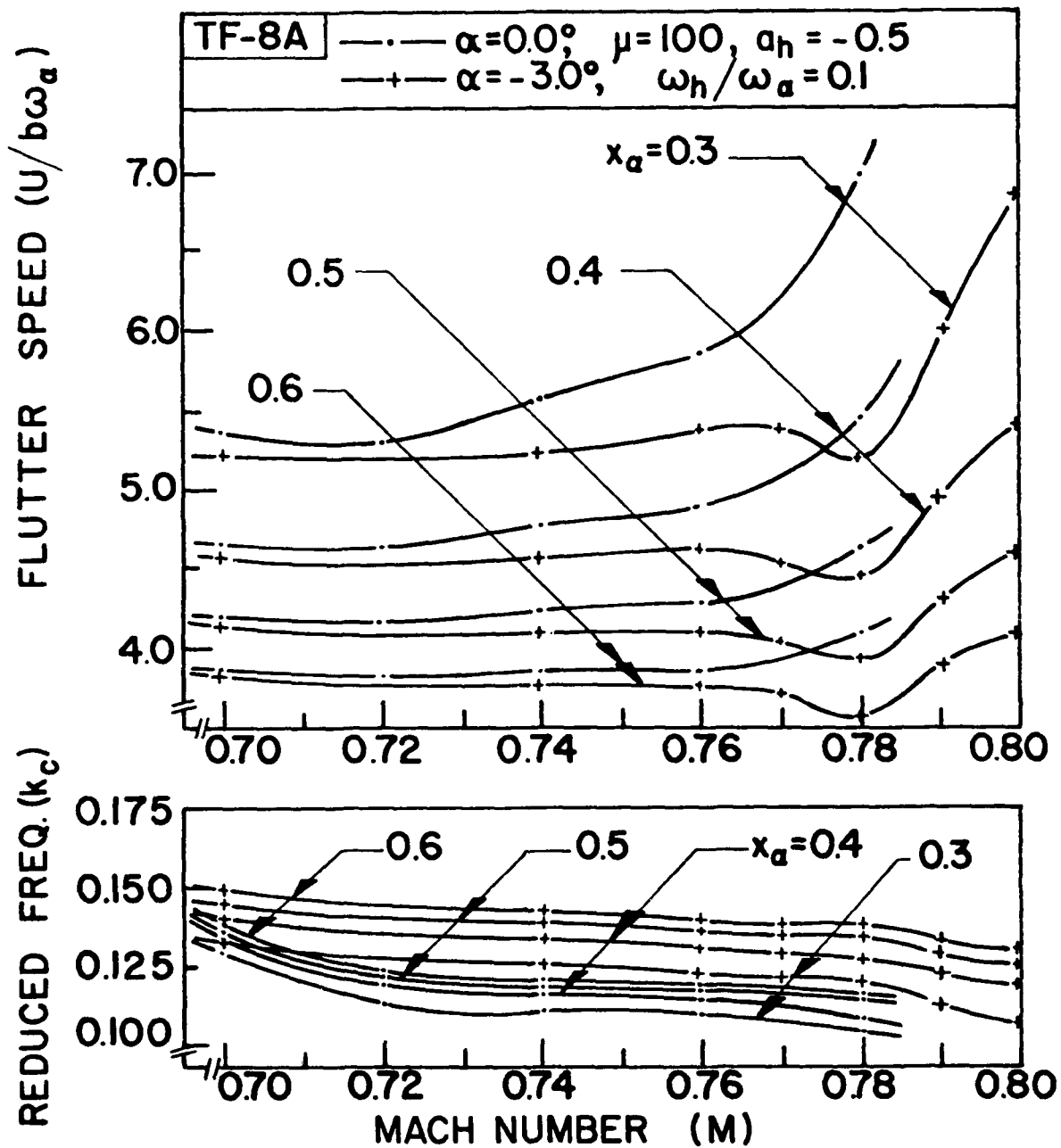


Figure 41. Effect of Mach Number on Flutter Speed for Four Positions of Mass Center for TF-8A Airfoil by STRANS2/UTRANS2.

For  $\alpha = -3.0^\circ$ , all the flutter curves show a dip in the neighborhood of  $M = 0.78$ . The dip appears to be more pronounced when the mass center is closer to the elastic axis.

Also shown in Figure 41 are the flutter results for  $\alpha = 0.0^\circ$  for comparison. No obvious dips are present in these flutter curves. However, it appears that the flutter speeds are lowest in the neighborhood of  $M = 0.72$ .

Figure 42 shows the flutter results for both cases:  $\alpha = -3.0^\circ$  and  $\alpha = 0.0^\circ$ . Three  $\mu$ -values of 100, 200, and 300, respectively, were considered. The values selected for  $x_\alpha$ ,  $a_h$ , and  $\omega_h/\omega_\alpha$  were 0.5, -0.5, and 0.1, respectively.

In this figure, the flutter speed curves are higher at higher altitude or at higher  $\mu$ -values. The corresponding reduced frequency curves show a reversed trend.

All three flutter curves for  $\alpha = -3.0^\circ$  present a dip in the neighborhood of  $M = 0.78^\circ$ . The three curves for  $\alpha = 0.0^\circ$  do not show obvious dips. These three curves are wavy and each has two lower points in the neighborhood of  $M = 0.72$  and  $0.76$ , respectively. However, the curves obviously show increasing trend when the Mach number goes beyond  $M = 0.76$ .

Figure 43 shows the flutter results for both  $\alpha = -3.0^\circ$  and  $0.0^\circ$  and for  $\omega_h/\omega_\alpha = 0.1$  and  $0.2$ , respectively. The values selected for  $x_\alpha$ ,  $a_h$ , and  $\mu$  were 0.5, -0.5, and 100, respectively.

In this figure, the flutter speed curves for  $\omega_h/\omega_\alpha = 0.1$  are higher than those for  $\omega_h/\omega_\alpha = 0.2$ . The corresponding reduced frequency curves have an opposite relationship with the two frequency ratios.

Again, the two flutter curves for  $\alpha = -3.0^\circ$  present a dip in the neighborhood of  $M = 0.78$ . The two flutter curves for  $\alpha = 0.0^\circ$  do not show obvious

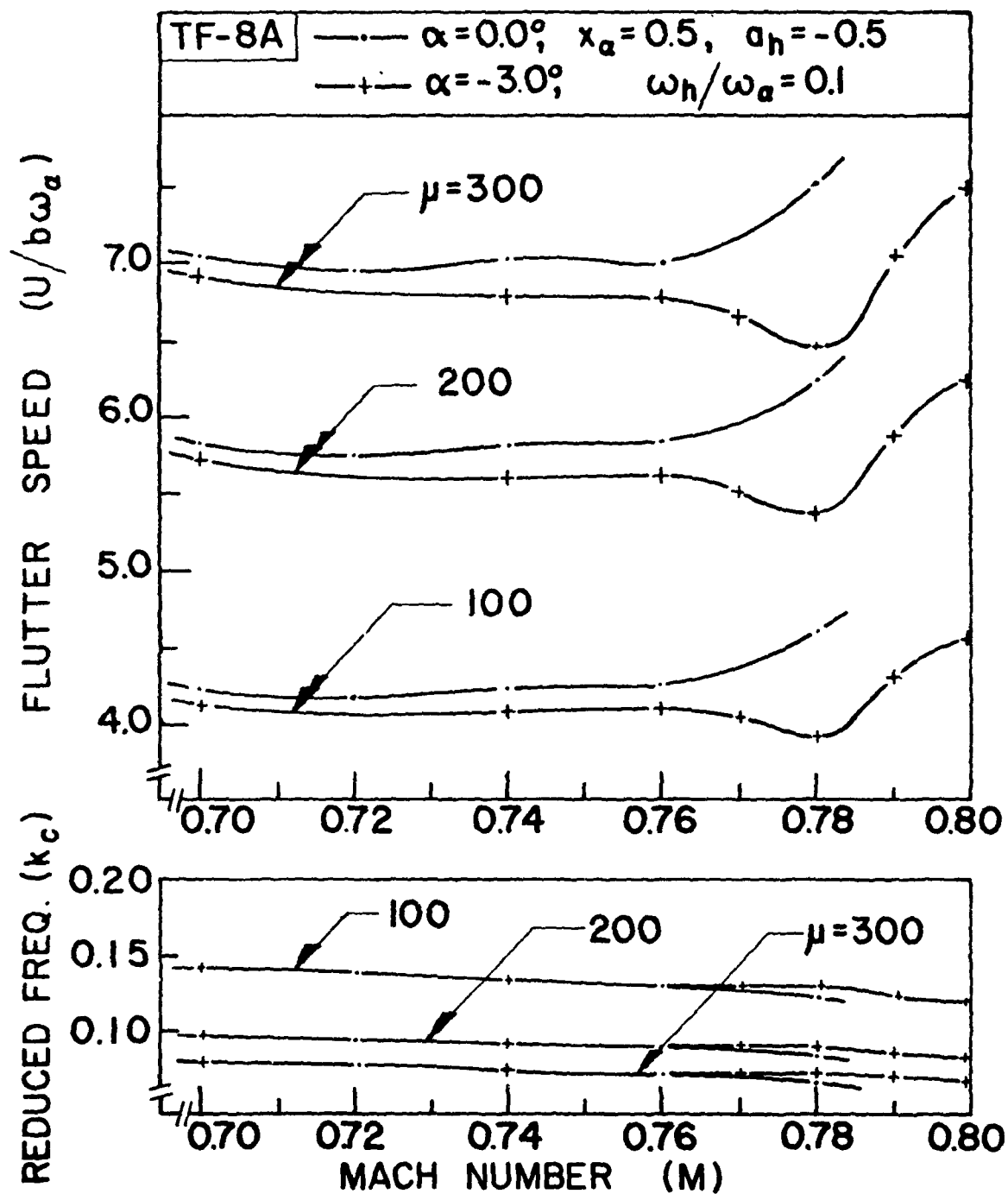


Figure 42. Effect of Mach Number on Flutter Speed for Three Values of Airfoil-Air Mass Density Ratio for TF-8A Airfoil by STRANS2/UTRANS2.

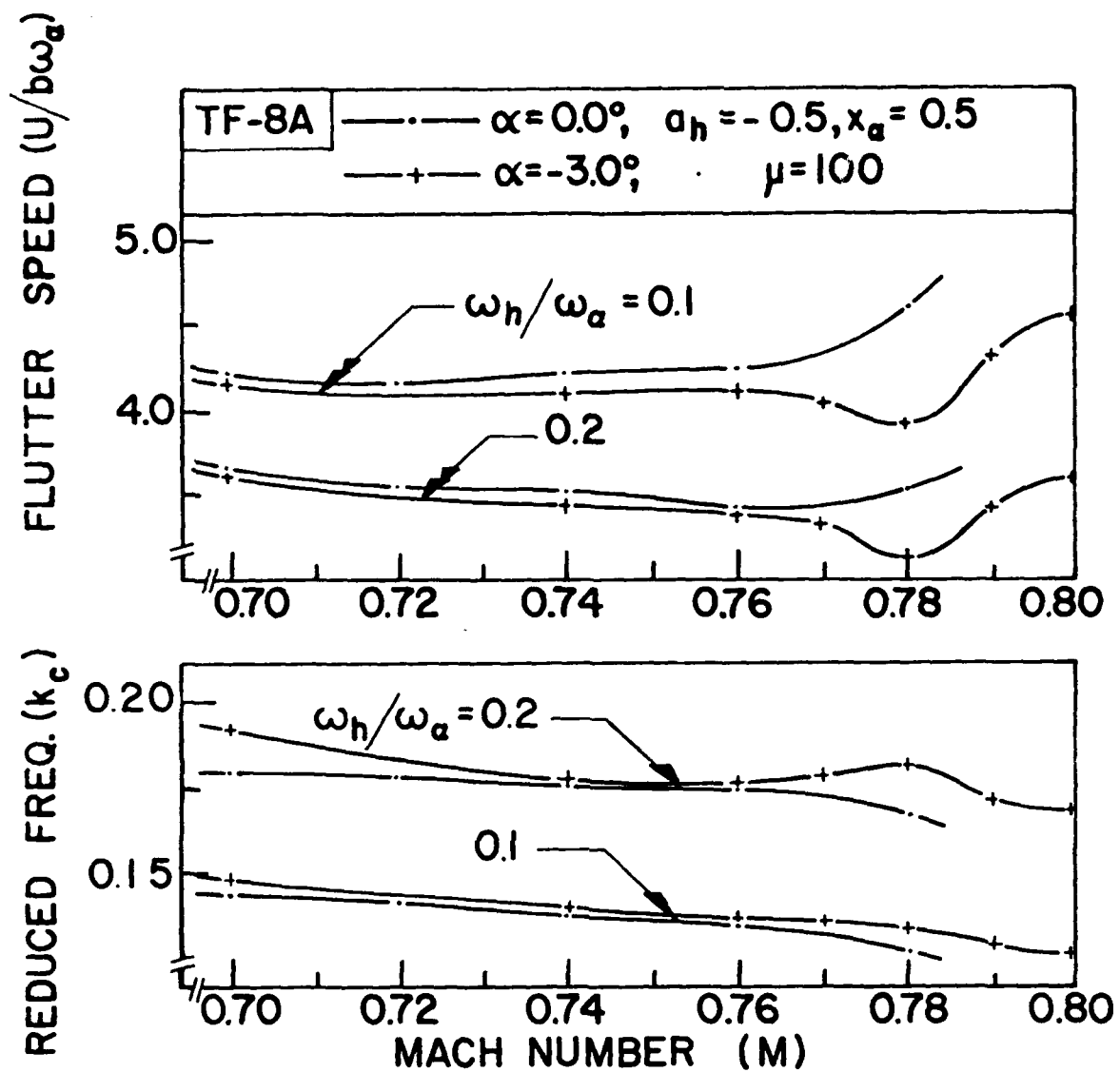


Figure 43. Effect of Mach Number on Flutter Speed for Two Values of Plunge-to-Pitch Frequency Ratio for TF-8A Airfoil by STRANS2/UTRANS2.

dips except two very mild lower waves, one near  $M = 0.72$  and the other near  $M = 0.76$ . However, the flutter speeds do tend to rise obviously when the Mach number goes beyond  $M = 0.76$ .

Figure 44 shows the flutter results for both  $\alpha = -3.0^\circ$  and  $0.0^\circ$  and for  $a_h = -0.1$  and  $-0.5$ , respectively. The mass center was fixed at mid-chord as the elastic axis moved. The values for  $\mu$  and  $\omega_h/\omega_\alpha$  were assumed as 100 and 0.1, respectively.

For either case ( $\alpha = -3.0^\circ$  or  $0.0^\circ$ ), the flutter speed curves for  $a_h = -0.1$  and  $a_h = -0.5$  are not much different. Such differences are even less obvious between the curves for the corresponding reduced frequencies.

As also shown in the previous two figures, the two flutter speed curves for  $\alpha = -3.0^\circ$  exhibit a transonic dip in the neighborhood of  $M = 0.78$ . The two flutter speed curves for  $\alpha = 0.0^\circ$  do not exhibit obvious dips. However, the two curves do show obvious rising tendency when  $M$  becomes greater than 0.76.

As discussed in Reference 29, the transonic dip phenomenon may be physically explained by looking at the compensating effects of the increase in magnitude of the lift coefficient  $|C_{l\alpha}|$  due to pitch which tends to decrease the flutter speed and the aft-movement of the center of pressure which tends to increase the flutter speed. When the airfoil goes supersonic, the center of pressure moves to the mid-chord on the airfoil and flutter speed becomes much higher.

The real part of lift coefficient ( $C_{l\alpha}$ ), the position of center of pressure  $e$ , and the flutter speed are plotted against Mach number in Figure 45 for the TF-8A section. The position of the center of pressure is defined as at a distance  $e$  times  $c$  aft of the leading edge.

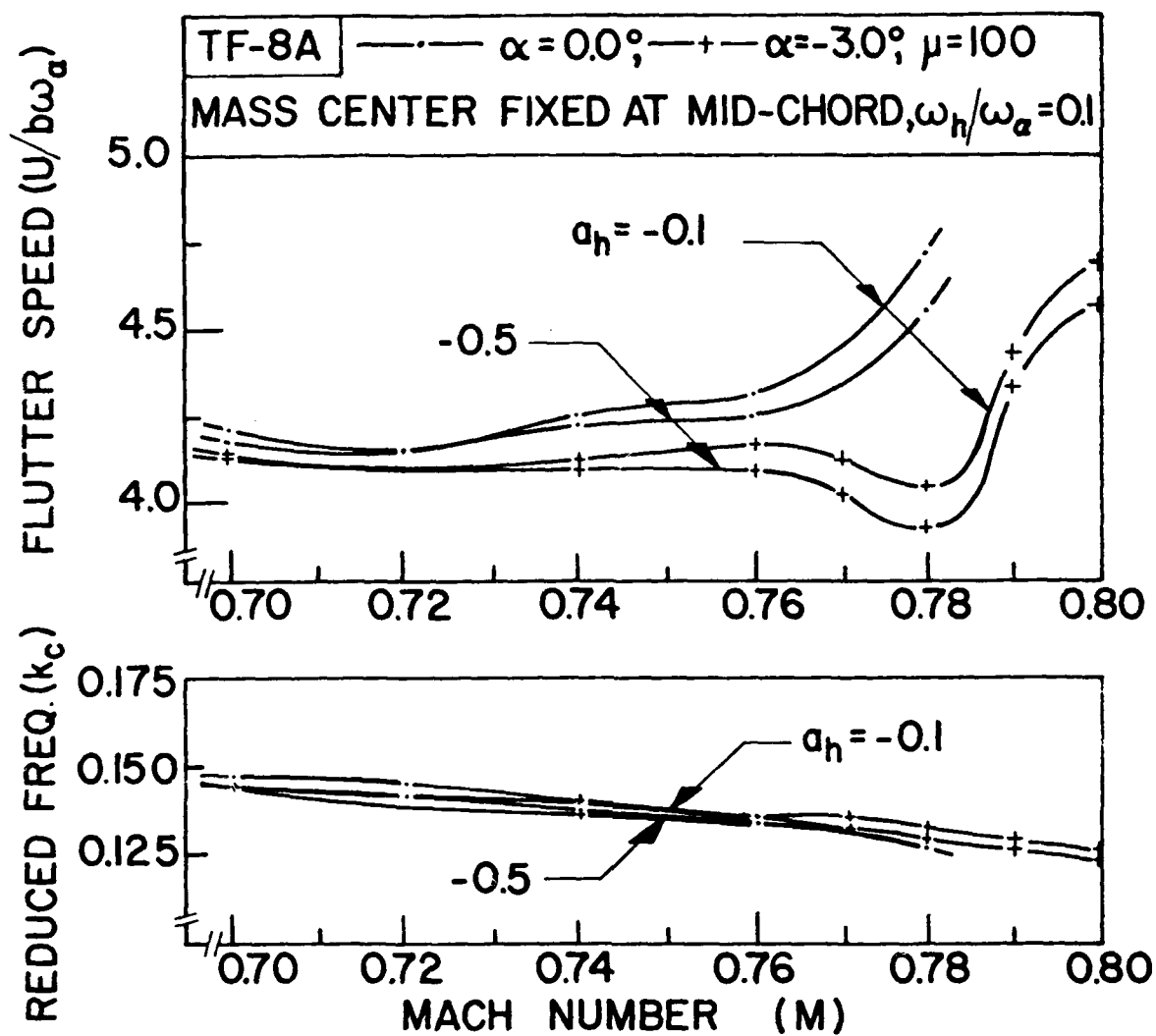


Figure 44. Effect of Mach Number on Flutter Speed for Two Positions of Elastic Axis for TF-8A Airfoil by STRANS2/UTRANS2.

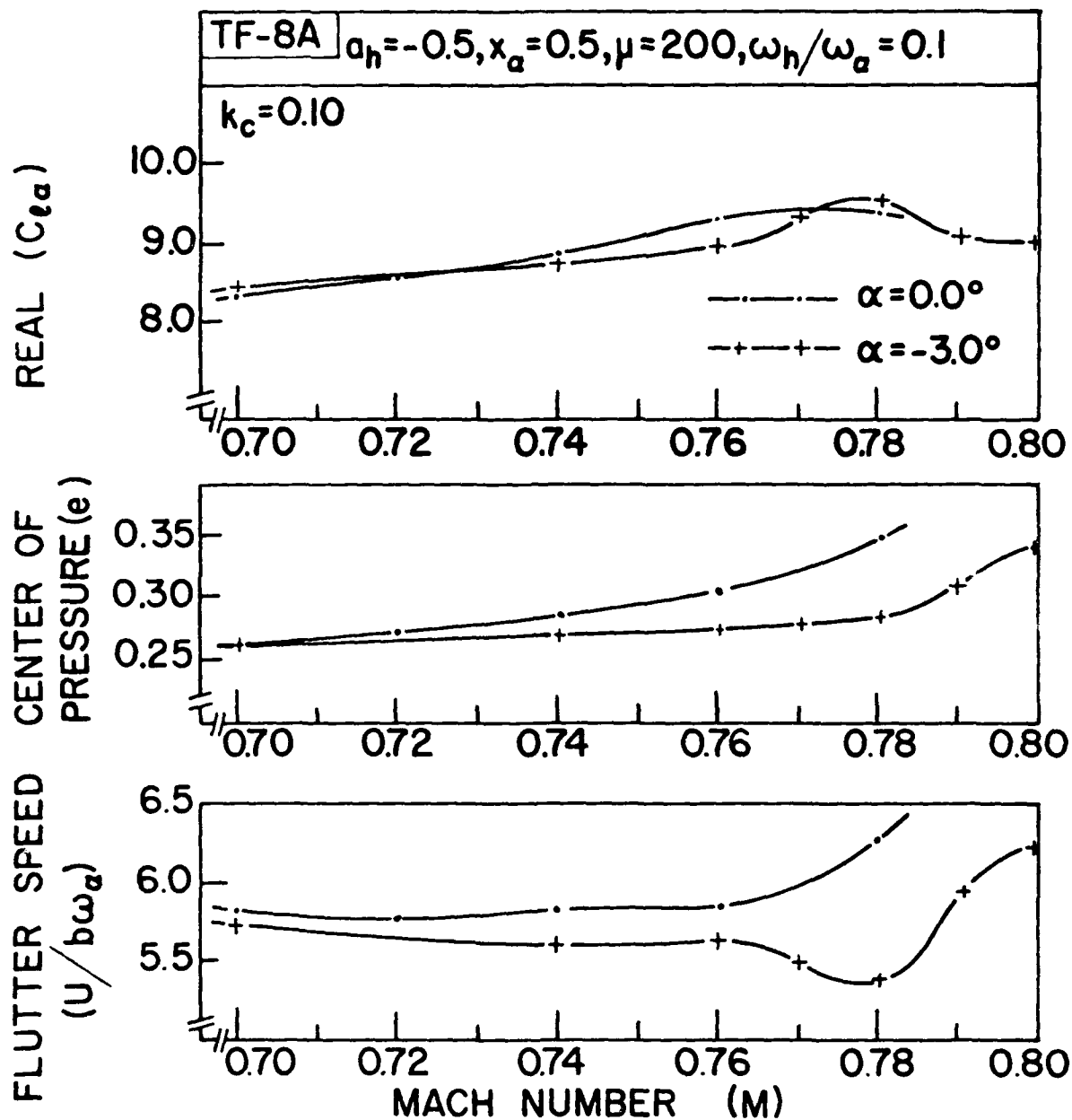


Figure 45. Compensating Effects of  $\text{Re}(C_{l\alpha})$  and the Position of Center of Pressure on Flutter Speed for TF-8A Airfoil by STRANS2/UTRANS2.

For the case  $\alpha = -3.0^\circ$ , the lift coefficient curve shows an obvious peak at  $M = 0.78$  which strongly suggests a dip in flutter speed. The center of pressure plot shows a gradual and steady aft-shift from 1/4-chord axis when  $M$  becomes higher than 0.76. Such movement suggests a comparable increase in flutter speed. The flutter speed curve is a result of these two effects.

For  $\alpha = 0.0^\circ$ , the lift coefficient curve suggests decrease in flutter speed with no obvious dip whereas the e-curve suggests an increase in flutter speed earlier and sharper than that for  $\alpha = -3.0^\circ$ .



## SECTION VII

### CONCLUDING REMARKS

The purpose of this research was to study the flutter behavior of three supercritical airfoils: MBB A-3, CAST 7, and TF-8A, through the use of LTRAN2 and STRANS2/UTRANS2 so that some indications or conclusions may be drawn in the aspects such as: (1) applicability and limitation of the two codes; (2) trends and flutter behavior of the subject airfoils for the parameters considered; and (3) correlation and interpretation of the results for various cases. In the interest of simplicity, the airfoil geometries were represented by the simplest possible one-segment fits with a minimum of constraints. More elaborate descriptions may be necessary for highly cambered airfoils.

For the MBB A-3 airfoil, both codes were used to investigate the effect of small mean angles of attack on its flutter behavior at the design Mach number of 0.765.

For the CAST 7 airfoil, LTRAN2 was used to investigate the effect of Mach number on its flutter behavior at zero mean angle of attack.

For the TF-8A wing section at the 65.3% semispan station, STRANS2/UTRANS2 were used to investigate the effect of Mach number on its flutter behavior at  $\alpha = 0.0^\circ$  and  $-3.0^\circ$  (In Reference 26, when the TF-8A wing was tested in the 1-g design cruise condition with zero angle of attack at the zero-twist station, the 65.3%-section had an  $\alpha$ -value of  $-3.0^\circ$ ).

As a result of this study, the following concluding remarks are made.

a. In general, flutter results obtained by both codes for the MBB A-3 airfoil at  $M = 0.765$  appear to show a similar trend. For the parameters assumed ( $\mu = 100, 200, 300$ ;  $x_\alpha = 0.1, 0.3, 0.5$ ;  $a_h = -0.1, -0.5$ ; and  $\omega_h/\omega_\alpha = 0.1$ ), most of the flutter speed plots show a trend that increases with angle of attack. This is, however, not the case for those obtained by LTRAN2 at  $\omega_h/\omega_\alpha = 0.2$ .

b. For the same flow conditions, LTRAN2 gives stronger shocks than STRANS2.

c. Because of the limitations in both LTRAN2 and STRANS2/UTRANS2,  $0.8^\circ$  and  $1.3^\circ$  are approximately the highest  $\alpha$  the two respective programs can treat for the MBB A-3 cases considered.

d. For the CAST 7 airfoil, the steady pressure curves obtained by LTRAN2 at  $M = 0.602$  and  $\alpha = 0.5^\circ$  compare fairly well with those obtained from wind tunnel test (Reference 11) in overall shape. However, the LTRAN2 coefficients are higher than those from test.

e. For all the parameters assumed for the CAST 7 airfoil, the various plots of the flutter speed curves show a dip in the neighborhood of  $M = 0.705$ .

f. For the TF-8A wing section, the steady pressure curves obtained by STRANS2 at  $M = 0.5$  and  $\alpha = 0.75^\circ$  compare fairly well with experimental data (Reference 26).

g. For all the parameters assumed for the TF-8A section, the various plots of the flutter speed curves show a dip in the neighborhood of  $M = 0.78$  when  $\alpha = -3.0^\circ$ . The plots for the case  $\alpha = 0.0^\circ$  do not, however, show obvious dips other than a drop in flutter speed over the range  $0.71 \leq M \leq 0.76$ .

h. The reasons for the discrepancies between the steady pressure curves obtained by computations and experiments in Figures 22 and 34 may be attributed to the reasons that (a) viscous effects have not been included in both computer codes, (b) small disturbance theory is used in both codes, and (c) inaccuracies may have been introduced in both the numerical and experimental procedures.

i. Numerical convergence problems are encountered when the shock grows with Mach number. For the cases studied, upper limits of Mach number have been found by both codes.

j. Due to the low-frequency approximation used in LTRAN2, the reduced frequencies  $k_c$  are limited to be not higher than 0.2. Although the low-frequency approximation is not used in UTRANS2, convergence difficulty is usually encountered when  $k_c > 0.2$ .

k. For a more complete understanding of the transonic flutter behavior of supercritical airfoils, the present computer codes have to be improved to be applicable to a wider range of flow and aeroelastic parameters. The limitations on Mach number, angle of attack, inviscid flow, small disturbances, and reduced frequency, etc., must be relaxed. Such developments have been under way (References 18 and 19).

l. More developments in 3-D transonic codes and their applications to flutter analysis of full wings are needed. Some preliminary 3-D flutter analysis using TDSTRN and TDUTRN was given in Reference 30.

m. The present results may be of use to those who are interested in the transonic codes and flutter behavior of supercritical airfoils. They may also serve as a comparative basis for experimental results. On the other hand, more experimental unsteady pressure and flutter data are needed.

## REFERENCES

1. Whitcomb, R.T. and Clark, L.R., "An Airfoil Shape for Efficient Flight at Supercritical Mach Numbers", NASA TM X-1109, July 1965.
2. Pearcey, H.H., "The Aerodynamic Design of Section Shapes for Swept Wings", Advances in Aeronautical Sciences, Vol. 3, 1962, pp. 277-322.
3. Yang, T.Y., Guruswamy, P., and Striz, A.G., "Flutter Analysis of a Two-Dimensional and Two-Degree-of-Freedom Supercritical Airfoil in Small Disturbance Unsteady Transonic Flow", AFWAL-TR-80-3010, March 1980.
4. Whitcomb, R.T., "The NASA Supercritical Airfoil and its Application to Swept Wings", NASA SP-301, February 1972, pp. 1-12.
5. Whitcomb, R.T., "Comments on Wind-Tunnel-Flight Correlations for the F-8 Supercritical Wing Configuration", NASA SP-301, February 1972, pp. 111-120.
6. Yu, N.J., "Efficient Transonic Shock-Free Wing Redesign Procedure Using a Fictitious Gas Method", AIAA Journal, Vol. 18, No. 2, February 1980, pp. 143-148.
7. Bauer, F., Garabedian, P., and Korn, D., "Supercritical Wing Sections I", Lecture Notes in Economics and Mathematical Systems, Vol. 66, Springer-Verlag, New York, 1972.
8. Bauer, F., Garabedian, P., Korn, D., and Jameson, A., "Supercritical Wing Sections II", Lecture Notes in Economics and Mathematical Systems, Vol. 108, Springer-Verlag, New York, 1975.
9. Bauer, F., Garabedian, P., and Korn, D., "Supercritical Wing Sections III", Lecture Notes in Economics and Mathematical Systems, Vol. 150, Springer-Verlag, New York, 1977.
10. Bucciattini, G., Oggiano, M.S., and Onorato, M., "Supercritical Airfoil MBB A-3. Surface Pressure Distributions, Wake and Boundary Condition Measurements", Paper No. 8, AGARD Advisory Report No. 138, May 1979.
11. Stanewsky, E., Puffert, W., Müller, R. and Bateman, T.E.B., "Supercritical Airfoil CAST 7 Surface Pressure, Wake and Boundary Layer Measurements", Paper No. 3, AGARD Advisory Report No. 138, May 1979.

12. Harris, C.D. and Bartlett, D.W., "Tabulated Pressure Measurements on an NASA Supercritical-Wing Research Airplane Model With and Without Fuselage Area-Rule Additions at Mach 0.25 to 1.00", NASA TM X-2634, December 1972.
13. Davis, S.S. and Malcolm, G.N., "Unsteady Aerodynamics of Conventional and Supercritical Airfoils", AIAA Paper 80-0734, May 1980.
14. Borland, C.J., "A Bibliography of Recent Developments in Unsteady Transonic Flow, Volume I", AFFDL-TR-78-189, February 1979.
15. Yang, T.Y., Striz, A.G., and Guruswamy, P., "Flutter Analysis of Two-Dimensional and Two-Degree-of-Freedom Airfoils in Small-Disturbance Unsteady Transonic Flow", AFFDL-TR-78-202, December 1978.
16. Traci, R.M., Albano, E.D., and Farr, J.L. Jr., "Perturbation Method for Transonic Flows About Oscillating Airfoils", AIAA Journal, Vol. 14, No. 9, September 1976, pp. 1258-1265.
17. Ballhaus, W.F. and Goorjian, P.M., "Implicit Finite-Difference Computations of Unsteady Transonic Flows About Airfoils, Including the Treatment of Irregular Shock-Wave Motions", AIAA Paper 77-205, January 1977.
18. Houwink, R. and Van der Vooren, J., "Results of an Improved Version of LTRAN2 for Computing Unsteady Airloads on Airfoils Oscillating in Transonic Flow", AIAA Paper 79-1553, July 1979.
19. Rizzetta, D.P. and Yoshihara, H., "Computations of the Pitching Oscillation of a NACA 64A010 Airfoil in the Small Disturbance Limit", AIAA Paper No. 80-0128, January 1980.
20. Farmer, M.G. and Hanson, P.W., "Comparison of Supercritical and Conventional Wing Flutter Characteristics", Proceedings AIAA/ASME/SAE 17th Structures, Structural Dynamics, and Materials Conference, King of Prussia, Pa., April 1976, pp. 608-611.
21. McGrew, J.A., Giesing, J.P., Pearson, R.M., Zuhuruddin, K., Schmidt, M., and Kalman, T.P., "Supercritical Wing Flutter", AFFDL-TR-78-37, March 1978.
22. Ashley, H., "On the Role of Shocks in the 'Sub-Transonic' Flutter Phenomenon", AIAA Paper 79-0765, AIAA/ASME/ASCE/AHS 20th Structures, Structural Dynamics, and Materials Conference, St. Louis, Mo., April 4-6, 1979.
23. Yang, T.Y., Striz, A.G., and Guruswamy, P., "Flutter Analysis of a Two-Degree-of-Freedom MBB A-3 Supercritical Airfoil in Two-Dimensional Transonic Flow", AIAA Paper No. 80-0736, May 1980.

24. Olsen, J.J., "AGARD Standard Configurations for Aeroelastic Applications of Transonic Unsteady Aerodynamics, PART IV, Airfoil Potential Analytical Descriptions", AFFDL-TM-78-6-FBR, 1978.
25. Yang, T.Y., Guruswamy, P., Striz, A.G., and Olsen, J.J., "Flutter Analysis of a NACA 64A006 Airfoil in Small Disturbance Transonic Flow", Journal of Aircraft, Vol. 17, No. 4, April 1980, pp. 225-232.
26. Montoya, L.C. and Banner, R.D., "F-8 Supercritical Wing Flight Pressure, Boundary Layer, and Wake Measurements and Comparisons with Wind Tunnel Data", NASA TM X-3544, June 1977.
27. Yang, T.Y., Guruswamy, P., and Striz, A.G., "Aeroelastic Response Analysis of Two Dimensional, Single and Two Degree of Freedom Airfoils in Low-Frequency, Small-Disturbance, Unsteady Transonic Flow", AFFDL-TR-79-3077, June 1979.
28. Davis, S.S. and Malcolm, G.N., "Experiments in Unsteady Transonic Flow", AIAA Paper 79-0769, April 1979.
29. Hitch, H.P.Y., "Comment on 'Flutter Analysis of NACA 64A006 Airfoil in Small Disturbance Transonic Flow'", and Yang, T.Y., Guruswamy, P., Striz, A.G., and Olsen, J.J., "Reply by Authors to H.P.Y. Hitch", Journal of Aircraft, Vol. 18, No. 2, February 1981, pp. 158-160.
30. Eastep, F.E. and Olsen, J.J., "Transonic Flutter Analysis of a Rectangular Wing with Conventional Airfoil Sections", AIAA Journal, Vol. 18, No. 10, October 1980, pp. 1159-1164.

DATE  
FILMED  
-8